Synthesis of Novel Amphiphilic Polymers and Investigation of Their Aggregation Behavior in Solution by Small-Angle Scattering

1998

Minoru Nakano

Synthesis of Novel Amphiphilic Polymers and Investigation of Their Aggregation Behavior in Solution by Small-Angle Scattering

1998

Minoru Nakano

Contents

Part I

Micellization Behavior of Amphiphilic Polymers of Vinyl Ethers

Chapter 4.

Characterization of Micellization Behavior of Amphiphilic Polymer Having Octadecyl Group by Small-Angle X-ray and Neutron Scattering ——————— 45

Part II

Synthesis and Aggregation Behavior of Carbosilane Block Copolymers

Chapter 5.

Synthesis of Carbosilane Block Copolymers by Means of a Living Anionic Polymerization of 1,1-Diethylsilacyclobutane ———————————— 73

Chapter 6.

Self-Assembly of Poly(1,1-diethylsilabutane)-*block*-poly(2-hydroxyethyl methacrylate) Block Copolymer.   1.   Micelle Formation and Micelle–Unimer–Reversed Micelle Transition by Solvent Composition

Chapter 7.

Self-Assembly of Poly(1,1-diethylsilabutane)-*block*-poly(2-hydroxyethyl methacrylate) Block Copolymer.   2.   Monolayer at Air–Water Interface

Chapter 1

General Introduction

1.1. Historical Backgrounds

Amphiphiles are molecules consisting of two parts, one polar and the other one nonpolar. They self-assemble in the presence of selective medium, such as selective solvents and selective surface, causing micellization and adsorption, respectively. These specific behaviors of amphiphiles have attracted the attention of many research groups for a few decades.[1-6]

Theoretical analysis of amphiphilic polymer solution originated from the study of the end-adsorbed polymer on a flat surface by Alexander in 1977.[7] It was proceeded by Cantor to apply for a block copolymer between two immiscible solvents.[8] The model for star polymers proposed by Daoud and Cotton extend Alexander model toward curved interfaces, which enable to apply for polymeric micellar systems.[9] Moreover, computer simulations have been also performed.[10]

On the other hand, experimental evolution in this field has been rather slow since Krause performed the light scattering and the viscosity measurements for styrene–methyl methacrylate block copolymer in selective solvent in 1964.[11] It was mainly due to the difficulty to obtain the samples satisfying a prior condition which the theory requests, i.e., the samples with well controlled structure, and due to the lack of appropriate method to investigate the details of aggregate state.

1.2. Purpose of This Thesis

As mentioned above, the two most important things which comply with theorists' demand are precise preparation and precise characterization of the samples. Based on these concepts, a series of studies in the present thesis has been done mainly used by the techniques as described below. The aim of this thesis is to obtain important aspects of amphiphile association by the quantitative evaluation of aggregation properties, which will give a basis for many theoretical works. In addition, it is shown throughout this thesis that the self-association of amphiphilic polymers can give aggregates of very different size and geometries, which is precious aspect for understanding of intermolecular interactions, such as hydrophilic and hydrophobic interactions.

1.2.1. Preparation of Amphiphilic Polymers of Well-defined Structure.

Living polymerization is the most important and powerful technique to obtain polymers with narrow molecular weight distribution and controlled molecular weight. Most nonionic amphiphilic block copolymers which are used for many researches and in industrial fields have poly(ethyleneoxyde) as a hydrophilic segment, and can be synthesized by living anionic polymerization.[12] In this thesis, amphiphilic block copolymers having poly(2-hydroxyethyl vinyl ether) or poly(2-hydroxyethyl methacrylate) are presented as novel amphiphiles, synthesized by living cationic[13] or anionic polymerization, respectively.

1.2.2. Scattering Methods.

Small-angle scattering[14] is a method to measure the angle dependence of the scattered intensity of incident rays on sample, that allows dimensions to be measured in the range 10 to 500 Å. It supplies us with the information regarding the size, shape, and their distribution as well as the spatial arrangement and surface appearance when it is applied for

micellar systems. Historically, the first application was the small-angle X-ray scattering (SAXS)[15,16] for the micellar solutions of sodium dodecyl sulfate, cetyltrimethylammonium chloride, cetyltrimethylammonium bromide and four different soaps, which was performed by Reiss-Husson and Luzzati in 1964.[17] For neutron scattering (SANS), Cabos and Delord performed the first systematic studies of octyl benzene sulfonate micelles in water in 1977.[18] As regarding polymer micelles, SAXS measurements were performed for polystyrene–polybutadiene–polystyrene triblock copolymer in ethyl methyl ketone in 1973,[19] and SANS were adopted for micelles of polystyrene–poly(ethylene oxide) graft copolymer in 1979.[20] These powerful methods have been contributing to the development in colloid and surface chemistry.[21]

Concerning SANS,[22,23] contrast variation method is available, which enables to investigate the heterogeneity of the internal structure of the micelle by use of deuterated compounds, i.e., isotopic labeling. This is due to the fact that the difference of the scattering length between hydrogen and deuterium is one of the largest that can be obtained.

In Part I of this thesis, internal structure of polymer micelles has been analyzed by contrast variation method of SANS, or by combination of SAXS and SANS measurements.

X-ray reflectivity (XR)[24] which is described in the final chapter in the present thesis extracts plenty of information from planar interface. Although it differs from scattering methods from the point of view that the former observes a reflected image and the latter does a diffraction figure, the XR is also an outstanding and rather new technique that contribute to the surface chemistry.[25]

1.3. Outline of This Thesis

This thesis consists of an introductory chapter and two parts. Part I contains Chapters 2, 3 and 4, in which micelles formed by amphiphilic polymers of vinyl ethers are dealt with. In Chapter 2, partially deuterated copolymers at ether substituent parts of poly(2-hydroxyethyl vinyl ether)-*block*-poly(*n*-butyl vinyl ether) (poly(HOVE-*b*-NBVE)) were especially prepared for SANS experiments.[26] The micelle structure of the amphiphilic block copolymers formed in water was investigated by the contrast variation method of SANS. A sphere to rod transition in the shape of the micelles was observed as the mole fraction of hydrophobic segments in the copolymers increased.

The sphere to rod transition is quantitatively analyzed by systematic SANS investigation in Chapter 3.[27] Poly(HOVE-*b*-NBVE) with the same hydrophilic length but different hydrophobic lengths were prepared. By the contrast variation method, the hydration effect in the micellar shell was quantitatively estimated. SANS profiles of polymer micelles were well described by a sphere–rod coexistence model. Hydrophobic chain length dependence could be understood as changes of both micellar size and the volume fraction of rodlike micelle.

Chapter 4 treats micellization behavior of amphiphilic polymers having an octadecyl group as a hydrophobic segment (ODVE–poly(HOVE)) which was investigated by SAXS and SANS measurements.[28] The increase in hydrophilic chain length reduced the aggregation number, but had little effect on the size of overall micelle. A sphere to disk transition with decreasing temperature was found, and was explained relating to the crystallization behavior of alkyl chains.

Part II presents novel amphiphilic block copolymer, poly(1,1-diethylsilabutane)-*block*-poly(2-hydroxyethyl methacrylate) (poly(SB-*b*-HEMA)). In Chapter 5, block polymerization of 1,1-diethylsilacyclobutane with styrene derivatives and methacrylate

derivatives was investigated.[29] Poly(1,1-diethylsilabutane)-*block*-poly(2-(*tert*-butyldimethylsiloxy)ethyl methacrylate) was led to poly(SB-*b*-HEMA) by hydrolysis, which showed amphiphilic character.

In Chapter 6, SAXS measurements were performed for poly(SB-*b*-HEMA) in methanol, which is a good solvent for HEMA and a poor solvent for SB.[30] The aggregation number of the micelle was found to strongly depend on the polymer composition, while total micellar size was almost independent of the degree of polymerization of HEMA. The reduction of the solvent polarity by addition of toluene induced the morphological change from micelle to reversed micelle via unimer state.

Chapter 7 deals with the spread monolayer of poly(SB-*b*-HEMA) at air–water interface.[31] XR measurements showed the copolymer forms monolayer with uniform thickness and smooth surface. The two layer model consisting of a melt of SB chains and hydrated HEMA chains reasonably explained the XR data, and suggested the enhancement of the thickness of the monolayer with increasing surface pressure.

References

(1) Halperin, A.; Tirrell, M.; Lodge, T. P. *Adv. Polym. Sci.* **1992**, *100*, 31.

(2) Degiorgio, V., Corti, M., Eds., *Physics of Amphiphiles: Micelles, Vesicles and Microemulsions*; North-Holland: Amsterdam, 1985.

(3) Zana, R., Ed., *Surfactant Solutions: New Methods of Investigation*; Marcel Dekker: New York, 1987; Vol. 22.

(4) Tuzar, Z.; Kratochvil, P. *Advances in Colloid and Interface Science*; Elsevier: Amsterdam, 1976.

(5) Chu, B. *Langmuir* **1995**, *11*, 414.

(6) Zana, R. *Colloid and Surfaces A: Physicochem. Eng. Aspects* **1997**, *123–124*, 27.

(7) Alexander, S. *J. Phys. (Paris)* **1977**, *38*, 977.

(8) Cantor, R. *Macromolecules* **1981**, *14*, 1186.

(9) Daoud, M.; Cotton, J. P. *J. Phys. (Paris)* **1982**, *43*, 531.

(10) Rodrigues, K.; Mattice, W. L. *J. Chem. Phys.* **1991**, *94*, 761.

(11) Krause, S. *J. Phys. Chem.* **1964**, *68*, 1948.

(12) Grubbs, R. H.; Tumas, W. *Science* **1989**, *243*, 907.

(13) Miyamoto, M.; Sawamoto, M.; Higashimura, T. *Macromolecules* **1984**, *17*, 265.

(14) Cabane, B. in reference 3.

(15) Guinier, A.; Fournet, G. *Small-Angle Scattering of X-rays*; John Wiley: New York, 1955.

(16) Glatter, O.; Kratky, O. *Small Angle X-ray Scattering*; Academic Press: London, 1982.

(17) Reiss-Husson, F.; Luzzati, V. *J. Phys. Chem.* **1964**, *68*, 3504.

(18) Cabos, C.; Delord, P. *J. Phys. (Paris) Lett.* **1977**, *38*, L365.

(19) Plestil, J.; Baldrian, J. *Makromol. Chem.* **1973**, *174*, 183.

(20) Candau, F.; Guenet, J. M.; Boutillier, J.; Picot, C. *Polymer* **1979**, *20*, 1227.

(21) Riess, G.; Hurtrez, G.; Bahadur, P. in *Encyclopedia of Polymer Science and Engineering. 2nd Edition*: Mark, H.F., Bikales, N.M., Overberger, Ch.G., Menges, G., Eds.; John Wiley: New York, 1985.

(22) Hayter, J. P. in reference 2.

(23) Higgins, J. S.; Benoit, H. C. *Polymers and Neutron Scattering*; Oxford: New York, 1994.

(24) Kiessig, H. *Ann. Phys.* **1931**, *10*, 769.

(25) Matsuoka, H.; Yamaoka, H. *Proceedings of Risø International Symposium on Material Science* **1997**, *18*, 437.

(26) Nakano, M.; Matsuoka, H.; Yamaoka, H.; Poppe, A.; Richter, D. *Physica B* **1998**, *241–243*, 1038.

(27) Nakano, M.; Matsuoka, H.; Yamaoka, H.; Poppe, A.; Richter, D. *Macromolecules*, in press.

(28) Nakano, M.; Matsumoto, K.; Matsuoka, H.; Yamaoka, H. *Macromolecules*, submitted.

(29) Matsumoto, K.; Deguchi, M.; Nakano, M.; Yamaoka, H. *J. Polym. Sci., Part A: Polym. Chem.* **1998**, *36*, 2699.

(30) Nakano, M.; Deguchi, M.; Matsumoto, K.; Matsuoka, H.; Yamaoka, H. *Macromolecules*, submitted.

(31) Nakano, M.; Deguchi, M.; Endo, H.; Matsumoto, K.; Matsuoka, H.; Yamaoka, H. *Macromolecules* submitted.

Part I

Micellization Behavior of Amphiphilic Polymers
of Vinyl Ethers

Chapter 2

Micellization of Vinyl Ether Amphiphilic Block Copolymers as Studied by Small-Angle Neutron Scattering

Abstract

Several amphiphilic block copolymers based on vinyl ether derivatives were synthesized by living cationic polymerization. Different compositions of hydrophilic and hydrophobic segments in the copolymers were achieved by changing the monomer ratios of vinyl ether derivatives. Partially deuterated copolymers at ether substituent parts were especially prepared for small-angle neutron scattering (SANS) experiments. These copolymers formed micelles of core–shell structure in water. SANS measurements for aqueous solutions of various copolymers were performed by using a contrast variation method. The morphology of these micelles was studied as a function of chemical composition of the copolymers.

2.1. Introduction

Amphiphilic block copolymers, which consist of hydrophilic and hydrophobic segments connected by a covalent linkage, are typical polymeric surfactants. Although the physical properties of commercially available polyoxyalkylene block copolymers have been widely studied in the past few years,[1] little is known about the behavior of other amphiphilic block copolymers in solution. For example, no detailed research is available on the mechanism of their micellization, as well as the structure and properties of the micelles.

As part of the studies of the synthesis and properties of amphiphilic block polymers,[2-4] the micellar structure formed by vinyl ether amphiphilic block copolymers in aqueous solution and the effect of segment composition are descrived in this chapter by means of a small-angle neutron scattering (SANS) method.

2.2. Experimental Section

In order to synthesize the partially deuterated block copolymers for SANS experiments, n-butyl-d_9 vinyl ether (NBVE-d_9) was used as a comonomer. The sequential living cationic polymerization of 2-acetoxyethyl vinyl ether (AcOVE) and NBVE-d_9 was carried out by the HCl adduct of AcOVE and zinc chloride initiating system in dichloromethane solution.[5] The segments of AcOVE in the copolymers were hydrolyzed by sodium hydroxide in dioxane, and converted to 2-hydroxyethyl vinyl ether (HOVE) segments. The resulting poly(HOVE-b-NBVE-d_9) exhibited an amphiphilic character. These were completely purified by dialysis with deionized water. The characteristics of the copolymers obtained are listed in Table 2.1.

Table 2.1.   Characteristics of Poly(HOVE-b-NBVE-d_9) Used for SANS Measurements.

Sample	$m : n^a$	$M_w/M_n{}^b$	$\phi_{NBVE}{}^c$
D-1	50 : 10	1.10	0.17
D-2	39 : 21	1.17	0.35
D-3	65 : 40	1.25	0.38

^{a} Determined by ^{1}H NMR. ^{b} Determined by GPC using polystyrene standard. ^{c} Molar fraction of NBVE in a polymer, given by $n/(m+n)$.

SANS measurements were performed by using SANS-U of Institute for Solid State Physics, The University of Tokyo, Tokai, Japan, and also carried out by KWS1-spectrometer at Institut für Festkörperforschung, Forschungszentrum Jülich, Germany. For the measurements at SANS-U, the wavelength (λ) of neutron source was chosen to be 7 Å ($\Delta\lambda/\lambda = 10\%$). Two different sample–detector distance (2 and 8 m) were selected. At KWS1, λ of 7 Å ($\Delta\lambda/\lambda = 20\%$) and three different sample–detector distance (2, 8 and 20 m) were used. Scattering data collected by 2D-detector were circular averaged to be 1D-form scattering data, and were transformed to absolute cross sections using the Lupolen$^®$ standard.

2.3. Results and discussion

SANS measurements for aqueous solutions of the copolymers were carried out by using a contrast variation method in a mixed solvent system of H_2O and D_2O. The scattering profiles were strongly dependent on the change in the solvent ratios, reflecting core-shell structure of micelles. Figure 2.1 shows SANS profiles of three different samples in D_2O. The data do not cover the same q range because of the difference in micellar sizes. The scattering curves of D-1 at several contrasts were well reproduced by the theoretical curves of a core-shell spherical model. In the case of D-2, which has higher value of ϕ_{NBVE} than D-1 as listed in Table 2.1, the scattering profiles were coincident with the theoretical curves of a core-shell ellipsoidal model, an anisotropic factor of which is 2. Concerning D-3 which has the highest ϕ_{NBVE}, the scattering profiles at lower q region is quite different from the others, where the intensity is proportional to $1/q$ as shown in Figure 2.1(c). This behavior indicates the formation of rodlike micelles.

Figure 2.2 schematically shows the change in the shape of micelles that are formed in the aqueous solution of the block copolymers on increasing the hydrophobicity. The spherical micelle first becomes ellipsoidal one. On further increasing the hydrophobicity, the ellipsoidal structure is converted to a rodlike shape. It is quite difficult to clarify the transition of micellar shape quantitatively because a lot of factors affect the micellization behavior and the shape of micelles, e.g. the surface tension of core, the interaction of hydrophilic segments with water molecules, the interaction among hydrophobic segments and so on. However, the qualitative tendency that the micellar shape is influenced by the change in ϕ_{NBVE}, as a measure of hydrophobicity, was apparently observed.
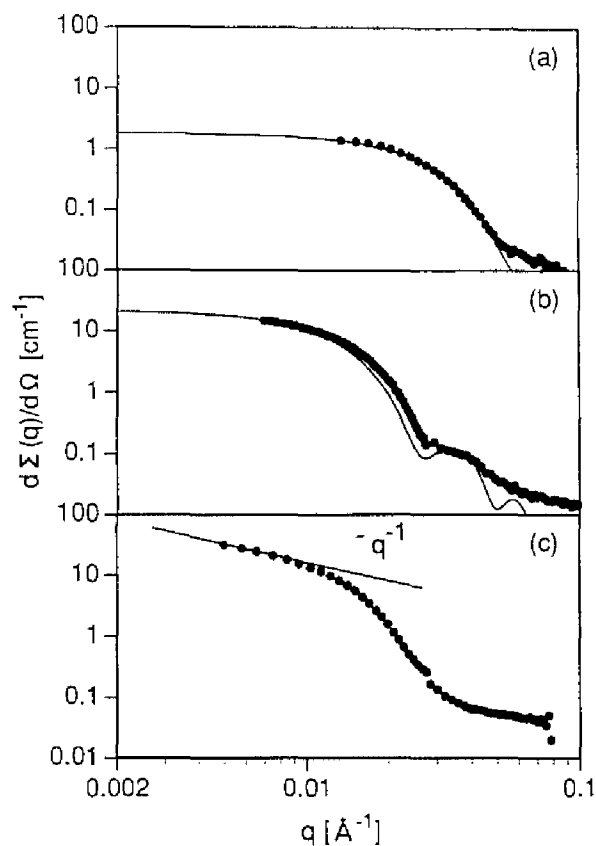
Figure 2.1. SANS profiles of poly(HOVE-b-NBVE-d_9) in D_2O. (a) D-1 (the solid line is theoretical curve of core–shell sphere.); (b) D-2 (the solid line is theoretical curve of core–shell ellipsoid.); (c) D-3 (the initial slope at lower q region where the intensity is proportional to $1/q$ indicates the formation of rodlike micelles.)
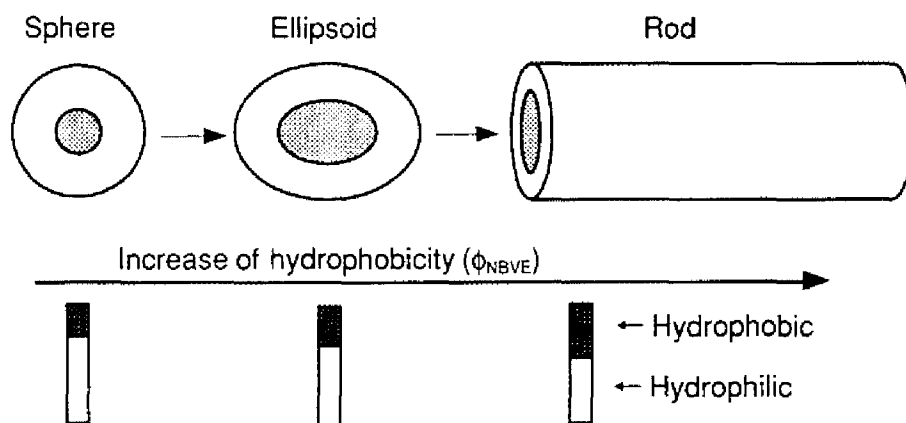
Figure 2.2. Schematic diagram of the relationship between the fraction of hydrophobic segments in a block copolymer and the shape of micelles estimated from SANS profiles.

-15-

2.4. Conclusions

SANS measurements of poly(HOVE-b-NBVE-d_9) in aqueous solution were performed by using a contrast variation method. The shape of micelles formed was found to be largely dependent on the segment composition of the copolymers. The SANS data revealed a sphere to rod transition in the shape of the micelles with increasing the ratios of hydrophobic segments to hydrophilic ones in the copolymers. This transition behavior of the copolymers in aqueous solution will be discussed in detail in the next chapter.

References

(1) Chu, B.; Zhou, Z. *Surfactant Science Series, vol. 60, Nonionic Surfactants: Polyoxyalkylene Block Copolymers* p. 67; Marcel Dekker, New York, 1996.

(2) Yamaoka, H.; Matsuoka, H.; Sawamoto, M. *Polym. Preprints* **1994**, *35*, 574.

(3) Yamaoka, H.; Matsuoka, H.; Sumaru, K.; Hanada, S.; Imai, M.; Wignall, G. D. *Physica B* **1995**, *213&214*, 700.

(4) Matsumoto, K.; Miyagawa, K.; Yamaoka, H. *Macromolecules* **1997**, *30*, 2524.

(5) Sawamoto, M. *Prog. Polym. Sci.* **1991**, *16*, 111.

Chapter 3

Sphere to Rod Transition of Micelles Formed by Amphiphilic Diblock Copolymers of Vinyl Ethers in Aqueous Solution

Abstract

Amphiphilic block copolymers of vinyl ethers containing 2-hydroxyethyl vinyl ether (HOVE) and partially deuterated n-butyl vinyl ether (NBVE) were synthesized by living cationic polymerization. Four block copolymers with the same hydrophilic length but different hydrophobic lengths were prepared. The internal structures of the micelles formed by these copolymers in aqueous solution were investigated by the contrast variation method of small-angle neutron scattering (SANS) measurement. The molar volume of HOVE was estimated to be quite small from the dependence of the forward scattering intensity on the contrast, which comes from the hydration effect in the micellar shell. The SANS data were well described by the theoretical form factor of a core–shell model. The micellar shape was strongly dependent on the hydrophobic chain length of the block copolymer. The polymer with the shortest hydrophobic chain was suggested to form spherical micelles, whereas the scattering curves of the longer hydrophobic chain polymers showed the q^{-1} dependence, reflecting the formation of rodlike micelles. These scattering curves could be well described by a sphere–rod coexistence model. The volume fraction of the rodlike micelle was found to increase with increasing hydrophobic chain length.

3.1. Introduction

Amphiphilic copolymers which are widely used in industrial fields are also important materials in many fields of natural science such as colloid science and biology. Many groups have studied the specific behavior of amphiphilic polymers such as micellar formation and adsorption in selective solvents during the past few decades.[1-4]

Quantitative theoretical approaches demand the synthesis of amphiphilic polymers with a well-defined structure. Living polymerization is the most important and powerful technique for this purpose. Indeed, most nonionic amphiphilic block copolymers, which have an oxyethylene chain as a hydrophilic segment, are synthesized by living anionic polymerization[5] in order to obtain narrow molecular weight distribution and controlled molecular weight.

Sawamoto et al. have reported the living cationic polymerization of alkyl vinyl ethers,[6,7] and they synthesized an amphiphilic block copolymer with 2-hydroxyethyl vinyl ether as a hydrophilic part. This new polyalcohol-type amphiphile can be a valuable sample along with the oxyethylene-type nonionic block copolymer for investigation of its specific phenomena, since it can be prepared with a precise control of molecular weight using relatively simple equipment.

Small-angle neutron scattering (SANS), which has been reported by many groups,[2,8-13] is a valuable method for evaluation of the internal structure of micelles. Since the neutron is scattered by the density fluctuation of scattering length inherent for each atom, and an atom (proton, for example) has a different scattering length from its isotope (deuterium), SANS measurement makes it possible to investigate the heterogeneity of the internal structure of the micelle by use of a hydrogenated/deuterated mixture. This so-called contrast variation method[14,15] is applicable to the system with enough contrast inside the particle, which means that, in the case of a micellar system, partial deuteration is needed to ob-

tain a large contrast of the scattering length density (SLD) between the core and the shell of the micelle. An alkyl vinyl ether monomer with a deuterated alkyl group can be prepared by the palladium-catalyzed ether exchange reaction with deuterated alcohol.[10] Thus, amphiphilic block copolymers of vinyl ethers are quite useful materials for the investigation of their micellar structure by means of SANS.[11]
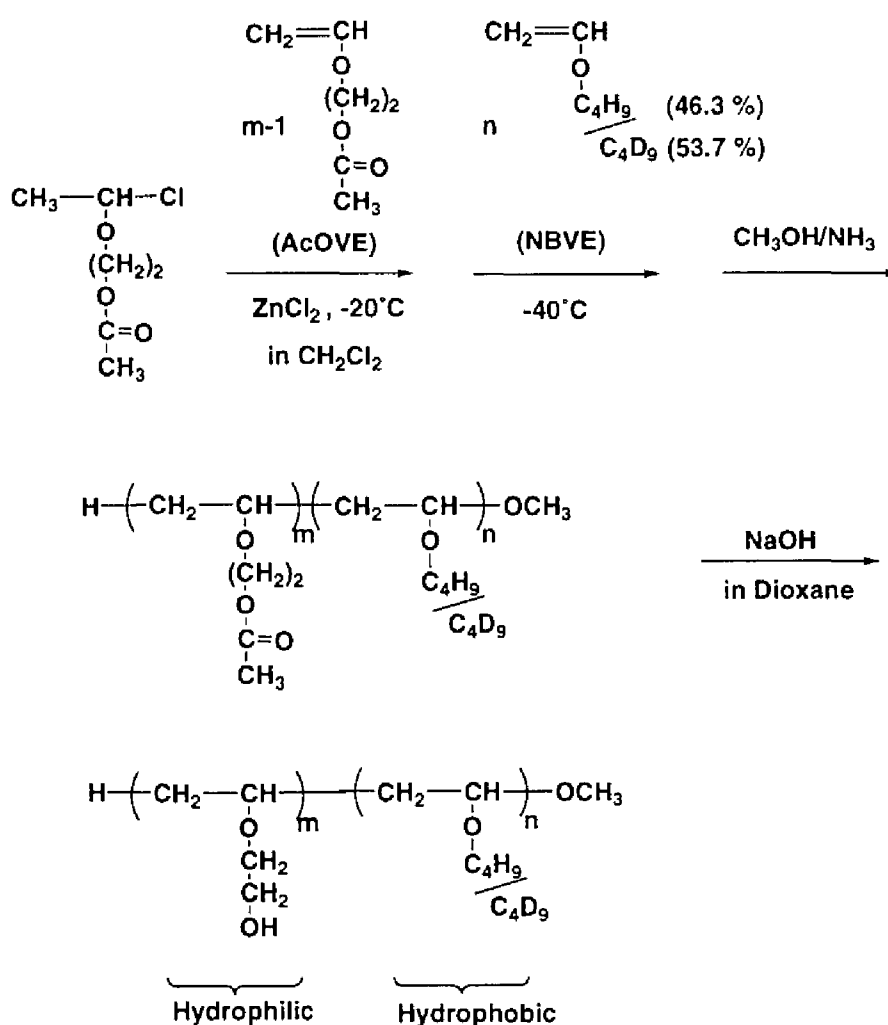
Here, we have investigated the behavior of amphiphilic block copolymers synthesized by living cationic polymerization in aqueous solution and have determined the size and shape of the micelles by the SANS technique. We report the transition of the micellar shape from sphere to rod with increasing molar fraction of hydrophobic part in a polymer.

3.2. Experimental Section

3.2.1. Synthesis of Amphiphilic Diblock Copolymers.

Block copolymers were synthesized by living cationic polymerization with two kinds of monomers, 2-acetoxyethyl vinyl ether (AcOVE) and n-butyl vinyl ether (NBVE), as shown in Scheme 3.1. AcOVE can be led to water-soluble 2-hydroxyethyl vinyl ether (HOVE) by hydrolysis of the protective group after polymerization. The AcOVE monomer was synthesized from sodium acetate (98.5%, Nacalai tesque, Kyoto) and 2-chloroethyl vinyl ether (99%, Aldrich, Milwaukee) at 90 °C. As a hydrophobic segment, a mixture of n-butyl-d_9 vinyl ether and n-butyl-h_9 vinyl ether was used for two purposes. One was to obtain enough contrast between hydrophilic and hydrophobic segments for neutron scattering, and the other was to achieve high accuracy for determination of the polymer composition by ^{1}H NMR spectroscopy. n-Butyl-d_9 vinyl ether was synthesized from octadecyl vinyl ether (Tokyo Kasei, Tokyo) and n-butanol-d_{10} (99.5 at. % D, C/D/N Isotopes, Quebec) by the ether exchange reaction with 1,10-phenanthroline palladium diacetate as a catalyst. This

monomer and commercial NBVE (Nacalai tesque) were mixed and then distilled before polymerization. The molar fraction of the deuterated monomer in the NBVE mixture was determined to be 0.537 by ^{1}H NMR. The hydrogen chloride adduct of AcOVE was obtained by bubbling the hydrogen chloride gas into a hexane solution of AcOVE. Commercial zinc chloride as diethyl ether solution (Aldrich) was used without further purification.

$$CH_2{=}CH \qquad CH_2{=}CH$$

For AcOVE:

$$CH_3{-}CH{-}Cl$$
$$O$$
$$(CH_2)_2$$
$$O$$
$$C{=}O$$
$$CH_3$$

AcOVE monomer:
$$CH_2{=}CH$$
$$O$$
$$(CH_2)_2$$
$$_{m-1} \;\; O$$
$$C{=}O$$
$$CH_3$$
(AcOVE)

NBVE monomer:
$$CH_2{=}CH$$
$$O$$
$$_n \;\; C_4H_9 \;\; (46.3\%)$$
$$C_4D_9 \;\; (53.7\%)$$
(NBVE)

$$\xrightarrow[\text{in } CH_2Cl_2]{ZnCl_2,\,-20^\circ C} \qquad \xrightarrow{-40^\circ C} \qquad \xrightarrow{CH_3OH/NH_3}$$

$$H{-}(CH_2{-}CH)_m(CH_2{-}CH)_n{-}OCH_3$$
$$O \qquad\qquad O$$
$$(CH_2)_2 \qquad\quad C_4H_9$$
$$O \qquad\qquad\quad C_4D_9$$
$$C{=}O$$
$$CH_3$$

$$\xrightarrow[\text{in Dioxane}]{NaOH}$$

$$H{-}(CH_2{-}CH)_m{-}(CH_2{-}CH)_n{-}OCH_3$$
$$O \qquad\qquad O$$
$$CH_2 \qquad\quad C_4H_9$$
$$CH_2 \qquad\quad C_4D_9$$
$$OH$$

$$\underbrace{\qquad\qquad}_{\text{Hydrophilic}} \qquad \underbrace{\qquad\qquad}_{\text{Hydrophobic}}$$

Scheme 3.1. Synthesis of Poly(HOVE-b-NBVE)

Polymerization was performed in a dried flask with a three-stopcock under nitrogen. We started five batches simultaneously, to prepare four block copolymers with the same hydrophilic length and a different hydrophobic length. The hydrogen chloride adduct of AcOVE and zinc chloride was injected as an initiator system into the dichloromethane solution of AcOVE at -20 °C. When the AcOVE monomer conversion determined by gas chromatography reached 95%, one batch was quenched by ammoniacal methanol; simultaneously, a different amount of NBVE monomer was added to the other four reaction solutions at -40 °C. The copolymerization was terminated by injection of ammoniacal methanol.

The copolymers were hydrolyzed by sodium hydroxide in dioxane and led to HOVE–NBVE block copolymers. These were purified by dialysis with deionized water, and their aqueous solutions were passed through a filter with a pore size of 0.22 μm.

3.2.2. Molecular Characterization.

The values of M_w/M_n were determined by GPC (solvent: chloroform) with a polystyrene standard calibration for AcOVE–NBVE block copolymers, where M_w and M_n are the weight- and number-averaged molecular weights, respectively. We obtained the number-averaged degree of polymerization of AcOVE (m) to be 84.5 from the mass spectrum of the homopolymer and assumed that four block copolymers synthesized simultaneously have the same value of m. The degree of polymerization of NBVE (n) was evaluated by comparing the area of methyl peaks of both acetoxyl and butyl groups obtained by ^{1}H NMR. These values are listed in Table 3.1. Although they were evaluated for poly(AcOVE-b-NBVE) precursor polymers, they can be applied for poly(HOVE-b-NBVE) polymers as well, since we confirmed by ^{1}H NMR that no subreaction had taken place during hydrolysis, such as polymer degradation process. The ^{1}H NMR spectrum of poly(HOVE-b-NBVE) with $m = 85$ and $n = 15$ (N8515) in D_2O is shown in Figure 3.1. It shows no acetoxy peak, indicating

that the protective groups were completely hydrolyzed and removed by purification. In addition, a relatively broad peak derived from the methyl protons of butyl groups is observed at 0.8 ppm, reflecting the fact that the hydrophobic part tends to avoid contact with water molecules, which is evidence of micelle formation in water.

Table 3.1. Molecular Characteristics of Poly(HOVE-_b_-NBVE)

	m^a	n^b	M_w/M_n^c
homopolymer	84.5		1.08
N8515	84.5	15.1	1.15
N8530	84.5	31.1	1.18
N8545	84.5	44.5	1.21
N8560	84.5	60.1	1.23

^{a} Obtained by mass spectrum for the homopolymer, and assumed to have the same value as for the block copolymers. ^{b} ^{1}H NMR. ^{c} GPC.
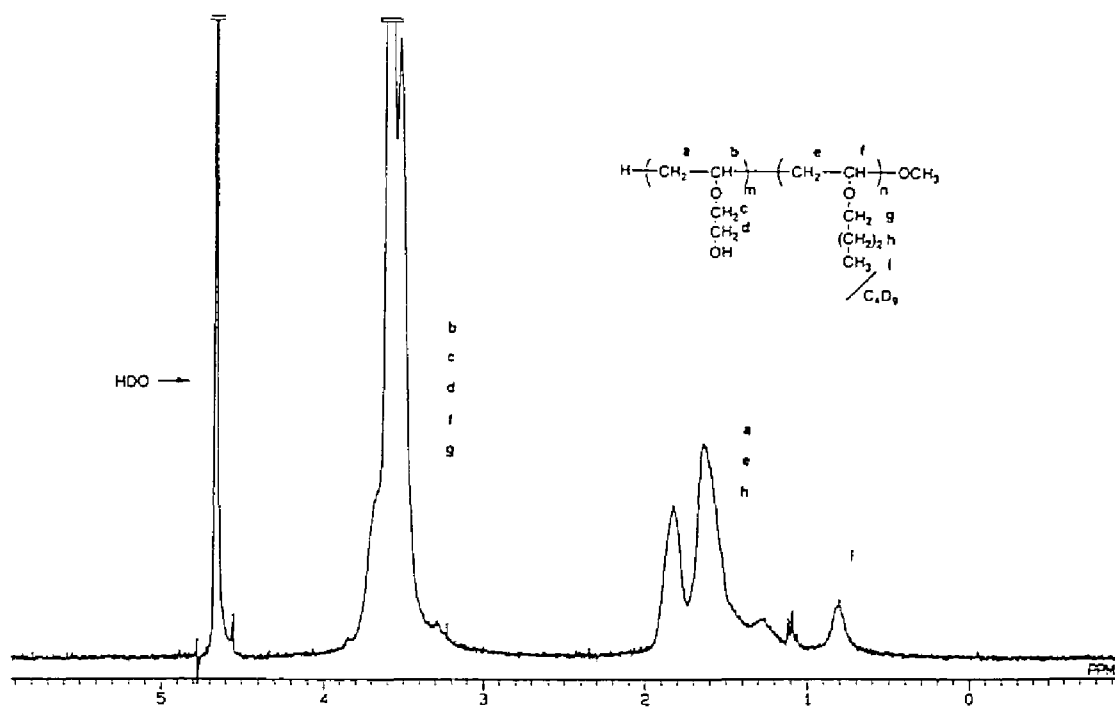
Figure 3.1. ^{1}H NMR spectrum of poly(HOVE-*b*-NBVE) in D_2O.

3.2.3. Small-Angle Neutron Scattering.

The SANS measurements were performed by the KWS1 spectrometer at the research reactor FRJ2 at the Forschungszentrum Jülich GmbH. The wavelength (λ) of neutron source was chosen to be 7 Å ($\Delta\lambda/\lambda = 20\%$). Solutions were measured in quartz cells with a path length of 1 and 2 mm. The SANS experiments were carried out at a sample to detector distance of 2, 4, 8, and 20 m, covering a range of the scattering vector of $0.002 \leq q \leq 0.1$ Å^{-1}. Scattering data measured by a 2D detector were circular averaged to be 1D form scattering data and then corrected for electronic background, and the scattering of the empty cell was subtracted. The data were transformed to absolute cross sections using the Lupolen$^®$ standard. For all scattering data of samples, the scattering of solvent and the calculated incoherent scattering of the protonated portion of the polymer were subtracted.

For measurements by the contrast variation method, we used D_2O/H_2O solvent mixtures. Four different volume fractions of D_2O (ϕ_{D2O}) were chosen for each polymer solution to obtain various contrasts:

$\phi_{D2O} = 0$ (H_2O contrast)

$\phi_{D2O} = 0.199$ (core contrast, where $\rho_0 = \rho_{HOVE}$)

$\phi_{D2O} = 0.350$ (intermediate contrast)

$\phi_{D2O} = 0.500$ (shell contrast, where $\rho_0 = \rho_{NBVE}$)

For the calculation of the core and the shell contrasts, the molar volumes of NBVE (105.54 cm^3/mol) and HOVE (75.56 cm^3/mol) corresponding to the measured densities of homopolymers NBVE (0.949 g/cm^3) and HOVE (1.166 g/cm^3) were used. The volume fraction of polymer was chosen to be 1% for all measurements, except for the investigation of the concentration dependence.

3.3. Theoretical Background

If the contribution of interparticle interaction is negligible, the neutron scattering cross section can be given by the equation

$$d\Sigma(q)/d\Omega = n_p P(q) \tag{3.1}$$

where n_p is the number density of particles and $P(q)$ is the particle form factor. The scattering vector q is given by $q = 4\pi \sin\theta/\lambda$, where 2θ is the scattering angle and λ is the neutron wavelength. $P(q)$ depends on the size, shape, and density distribution inside the scattering particles.

Here we deal with two models for describing the SANS data, spherical and cylindrical ones. In both cases, we assumed that the micelles consist of a core–shell structure. The form factor of a spherical core–shell model with the radii of the core R_C and of the overall micelle R_S can be written as follows:[17]

$$P(q)_{sphere} = \{(\rho_C - \rho_S)V_C F_C(q)_{sphere} + (\rho_S - \rho_0)V_S F_S(q)_{sphere}\}^2 \tag{3.2}$$

$$F_C(q)_{sphere} = 3(\sin(qR_C) - qR_C \cos(qR_C))/(qR_C)^3 \tag{3.3}$$

$$F_S(q)_{sphere} = 3(\sin(qR_S) - qR_S \cos(qR_S))/(qR_S)^3 \tag{3.4}$$

where ρ_C, ρ_S, and ρ_0 are the SLDs of the core, the shell, and the solvent. V_C and V_S are given as $4\pi R_C^3/3$ and $4\pi R_S^3/3$, respectively. The aggregation number (N_{agg}) is calculated from V_C, n, and the volume of NBVE repeat unit (v_{NBVE}):

$$N_{agg} = \phi_p V_C / (n\, v_{NBVE}) \tag{3.5}$$

where ϕ_p is the volume fraction of polymer in the core, and is equal to 1 for the close-packed core. The volume occupied by hydrophilic parts of polymers in the shell of a micelle is given by ($N_{agg}\, m\, v_{HOVE}$), where v_{HOVE} is the volume of the HOVE repeat unit. Thus, the volume

fraction of polymer in the shell (ϕ_s) is calculated as

$$\phi_s = N_{agg} m \, v_{HOVE}/(V_s - V_c) \tag{3.6}$$

then ρ_0, ρ_c, and ρ_s are given by the SLDs of D_2O (ρ_{D2O}), H_2O (ρ_{H2O}), NBVE (ρ_{NBVE}), and HOVE (ρ_{HOVE}):

$$\rho_0 = \phi_{D2O}\rho_{D2O} + (1 - \phi_{D2O})\rho_{H2O} \tag{3.7}$$

$$\rho_c = \phi_p\rho_{NBVE} + (1 - \phi_p)\rho_0 \tag{3.8}$$

$$\rho_s = \phi_s\rho_{HOVE} + (1 - \phi_s)\rho_0 \tag{3.9}$$

where ϕ_{D2O} is the volume fraction of D_2O in solvent. Here the SLDs of repeat units and pure solvents can be calculated as

$$\rho_i = \sum b_z/v_i \tag{3.10}$$

where subscript i refers to D_2O, H_2O, NBVE, or HOVE. b_z is the scattering length of atom z in the repeat unit or solvent molecule, and v_i is the corresponding volume. Thus, ρ_{D2O} = 6.406×10^{10} and $\rho_{H2O} = -5.617 \times 10^9$ cm^{-2} can be obtained. One can obtain the values of ρ_{NBVE} and ρ_{HOVE} if the densities of NBVE and HOVE are determined. For the calculation of ρ_{HOVE}, the isotopic exchange of the hydrogen in the OH group of HOVE should be taken into account, by assuming that this hydrogen is occupied by a deuterium or hydrogen in proportion to ϕ_{D2O}.

In the case of a core–shell cylinder with the radii of the core R_c and the overall micelle R_s and the length L, its form factor is given by[17]

$$P(q)_{cylinder} = (1/2)\int_0^\pi \{(\rho_c - \rho_s)V_c F_c(q)_{cylinder} + (\rho_s - \rho_0)V_s F_s(q)_{cylinder}\}^2 \sin\beta \, d\beta$$

$$(3.11)$$

$$F_c(q)_{cylinder} = \{(\sin(q(L/2)\cos\beta)/(q(L/2)\cos\beta)\}\{2J_1(qR_c \sin\beta)/(qR_c \sin\beta)\}$$

$$(3.12)$$

$$F_s(q)_{cylinder} = \{(\sin(q(L/2)\cos\beta)/(q(L/2)\cos\beta)\}\{2J_1(qR_s \sin\beta)/(qR_s \sin\beta)\}$$

$$(3.13)$$

where β is the angle between the axis of symmetry of cylinder and the scattering vector q, and J_1 denotes the Bessel function of the first kind and of order 1. V_c and V_s are the volumes of cylinders with radii R_c and R_s, respectively, and length L.

On the condition that $q \gg 2\pi/L$ and $L \gg R_s$, the form factor of cylinder can be modified to a simpler form:

$$P(q)_{cylinder} = (\pi/qL)\{(\rho_c - \rho_s)V_c 2J_1(qR_c)/(qR_c) + (\rho_s - \rho_0)V_s 2J_1(qR_s)/(qR_s)\}^2$$

$$(3.14)$$

The same equation as eqs 3.5–9 can apply to the cylinder for calculation of N_{agg}, ϕ_s, and the SLDs. The neutron wavelength distribution ($\Delta\lambda/\lambda = 20\%$) and collimation of the SANS machine were taken into account in the data evaluation.[18]

3.4. Results and Discussion

Figure 3.2 shows the SANS profiles of aqueous solutions of N8515 and N8560 at several contrasts. As shown in Figure 3.2a, the profiles for N8515 which has the shortest hydrophobic length exhibited a plateau at a smaller angle that is typical for spherical particles. For N8560 having the longest NBVE chain, the profiles were quite different from those of N8515 as shown in Figure 3.2b. Notice that the y axis in Figure 3.2b is the absolute scattering intensity multiplied by q. The q^{-1} dependence of the scattering intensities can be clearly found at a smaller angle, which is characteristic of rodlike particles. This q^{-1} dependence was observed for N8545 as well. A tendency that the SANS profile depends on the polymer composition has been also observed previously.[19]

It is clear experimentally from the scattering profiles and also theoretically from eq 3.2 that the forward scattering intensity $(d\Sigma(q=0)/d\Omega)$ depends on the SLD of solvent (ρ_0) and that the square root of the forward scattering intensity is proportional to ϕ_{D2O}.[20] For N8515 and N8530, the determination of the forward scattering intensity for each contrast was possible by a linear extrapolation of a Guinier plot[17] $(\ln(d\Sigma(q)/d\Omega) \sim q^2$ plot). The plots of the square root of these forward scattering intensities against ϕ_{D2O} gave a good linear relationship as can be seen in Figure 3.3. For N8545 and N8560, however, it is impossible to determine the forward scattering intensity because of the q^{-1} dependence at a small angle as described above. However, the value of $d\Sigma(q=0)/d\Omega \times q$ can be obtained instead of $d\Sigma(q=0)/d\Omega$ by linear extrapolation of $\ln(d\Sigma(q)/d\Omega \times q) \sim q^2$ plot,[10] and similarly, a good linear relationship between $(d\Sigma(q=0)/d\Omega \times q)^{1/2}$ and ϕ_{D2O} was found as shown in Figure 3.3.
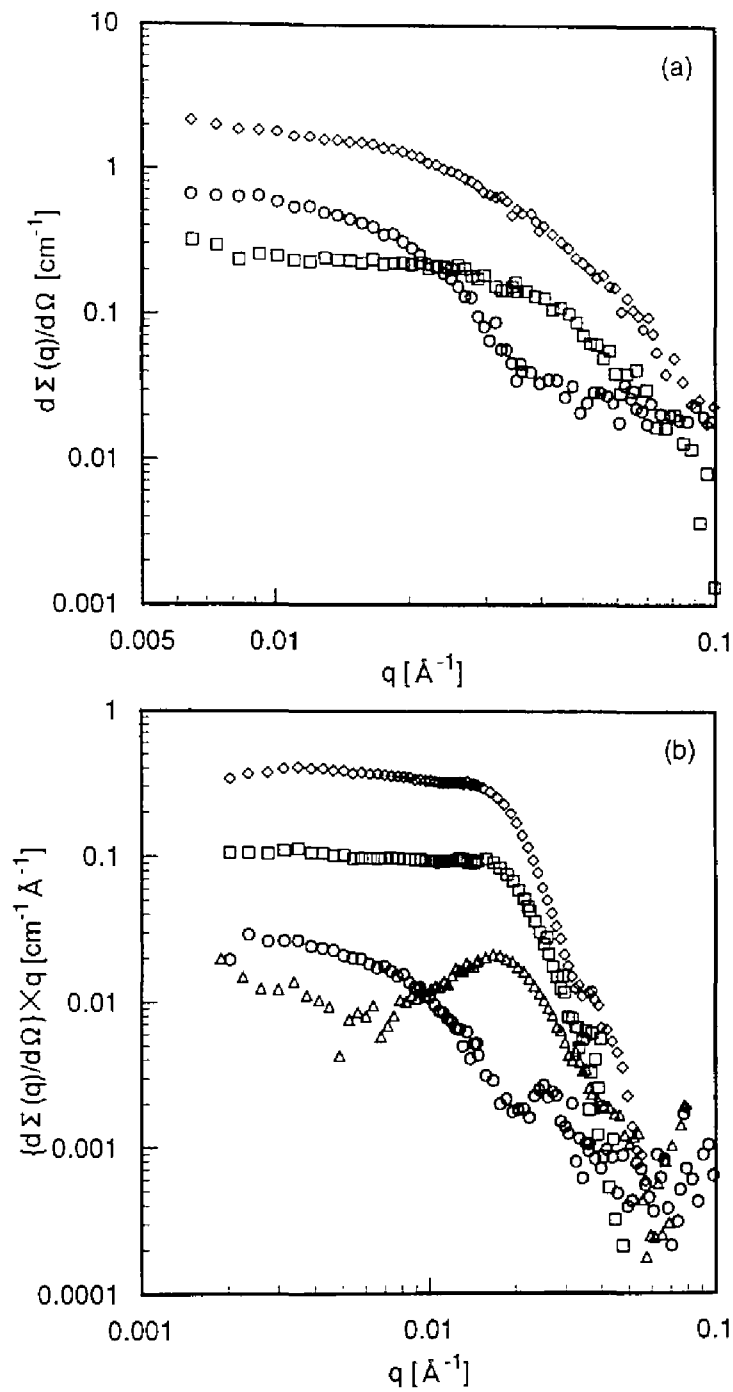
Figure 3.2. (a) Scattering cross sections of N8515 and (b) Holtzer plots of N8560 under several contrast conditions: H_2O ($\Diamond$), core ($\square$), intermediate ($\triangle$), and shell contrast ($\bigcirc$).
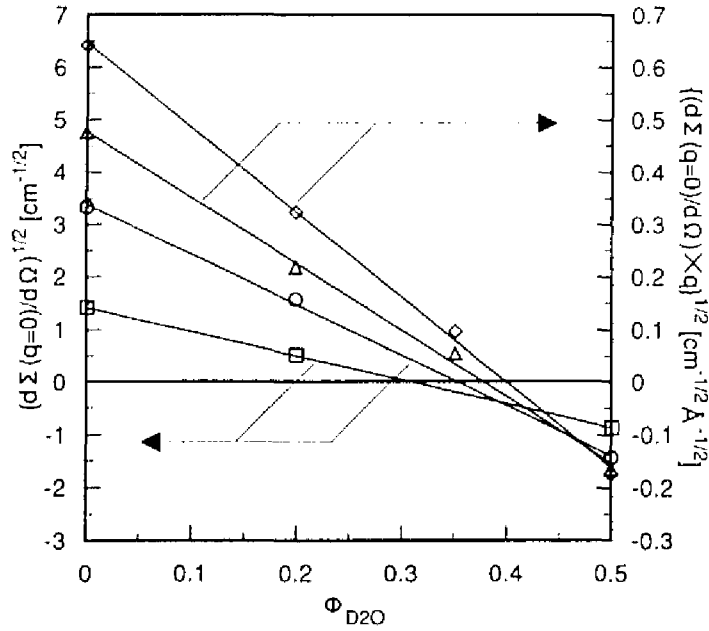
Figure 3.3. Square root of forward scattering intensity plotted against the volume fraction of D_2O: N8515 ($\square$), N8530 ($\bigcirc$), N8545 ($\triangle$), and N8560 ($\diamondsuit$). For the latter two cases, $\{(d\Sigma(q{=}0)/d\Omega) \times q\}^{1/2}$ is plotted instead of forward scattering intensity. The solid lines are due to least-squares fits, and the crossing point with $y = 0$ is zero average contrast (ϕ_{ZAC}).
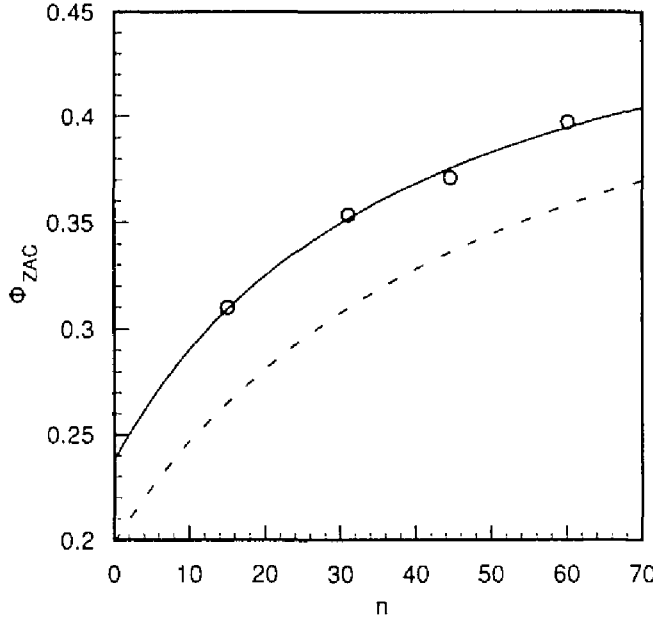
Figure 3.4. Dependence of ϕ_{ZAC} obtained from Figure 3.3 on hydrophobic chain length. The broken line is due to eq 16 with the values of $v_{NBVE} = 105.54$ and $v_{HOVE} = 75.56$ cm^3/mol. The solid line shows the fitted results obtained by changing v_{NBVE} and v_{HOVE} as fitting parameters.

The volume fraction of D_2O at $d\Sigma(q=0)/d\Omega = 0$ or $d\Sigma(q=0)/d\Omega \times q = 0$ (ϕ_{ZAC}) was determined for each polymer by least-squares fits and is plotted against n (NBVE length) in Figure 3.4. At the zero average contrast condition $\phi_{D2O} = \phi_{ZAC}$, the SLD of solvent mixture coincides with the averaged SLD of the copolymer:

$$\phi_{ZAC}\rho_{D2O} + (1 - \phi_{ZAC})\rho_{H2O} = (mb_{HOVE} + nb_{NBVE})/(mv_{HOVE} + nv_{NBVE}) \quad (3.15)$$

where b_{HOVE} and b_{NBVE} are the scattering lengths of HOVE and NBVE, respectively. Modifying eq 3.15, ϕ_{ZAC} can be represented as a function of n:

$$\phi_{ZAC}(n) = \{(mb_{HOVE} + nb_{NBVE})/(mv_{HOVE} + nv_{NBVE}) - \rho_{H2O}\}/(\rho_{D2O} - \rho_{H2O})$$

$$(3.16)$$

Note that the value of b_{HOVE} depends on the solvent composition due to the isotopic exchange of the hydrogen as described above. The broken line in Figure 3.4 is derived from eq 3.16 with the values of 105.54 and 75.56 cm^3/mol as the molar volumes of NBVE and HOVE, respectively. A large discrepancy was observed between the broken line and experimental data. Then, we tried to fit the experimental data by eq 3.16 changing v_{NBVE} and v_{HOVE} as fitting parameters. As a result, we obtained the molar volumes of NBVE of 105.62 and HOVE of 59.13 cm^3/mol and found good agreement with experimental data as shown by the solid line in Figure 3.4. For NBVE, nearly the same molar volume was obtained as expected. On the other hand, the molar volume of 59.13 cm^3/mol for HOVE, which corresponds to the density 1.490 g/cm^3, is considerably small. This means that the partial molar volume of HOVE in water is smaller than the molar volume of its own molar volume in bulk state. It is well-known that when a hydrophobic substance is put in water, water forms a highly structurized "iceberg" surrounding the hydrophobic molecule.[21] The decrease of the partial molar volume can be explained as apparent deletion of the volume of methylene groups which are located in the main chain or side chain of HOVE, by movement of the

methylene into a vacancy inside of the iceberg. This phenomenon, for example, is also observed as the decrease of total volume when water and ethanol are mixed. This hydration effect is important and must be taken into account to describe the data.[12]

We used the calculated molar volumes (105.62 and 59.13 cm^3/mol for NBVE and HOVE, respectively) and fitted the data for all contrast conditions, simultaneously. For N8515, using the spherical core–shell model, we found good agreement between experimental and theoretical data as can be seen in Figure 3.5. However, we had to introduce the value of $\phi_p = 0.72$ to describe the data, suggesting the existence of water in the micellar core; otherwise, we could not fit the data on an absolute scale. It can be concluded that NBVE which has an ether bonding may permit the penetration of water into the core to some extent. The obtained values of the micellar structure parameters are listed in Table 3.2.

Table 3.2.   Parameters of Sphere–Rod Coexistence Model

	R_c [Å]	R_s [Å]	ϕ_{rod}	sphere		rod	
				N_{agg}	ϕ_s	N_{agg}/L [Å^{-1}]^a	ϕ_s
N8515	36	98	0	53	0.12		
N8530	68	145	0.05	174	0.13	1.92	0.30
N8545	88	170	0.15	263	0.12	2.24	0.27
N8560	110	200	0.30	381	0.11	2.60	0.23

^{a} The aggregation number of rodlike micelles per unit length.
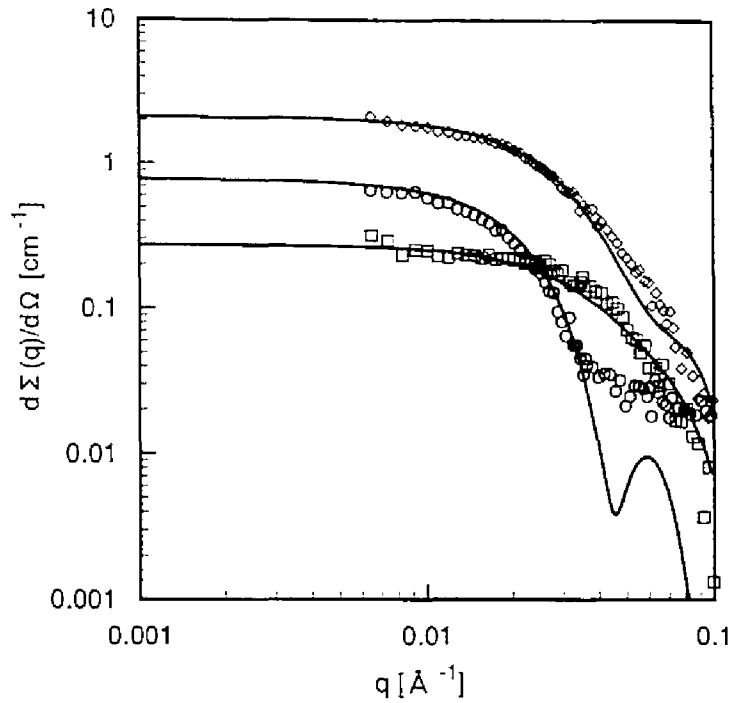
Figure 3.5. Scattering cross sections of N8515. The same symbols are used as in Figure 3.2. The solid lines represent the theoretical curves of the core-shell spherical model.
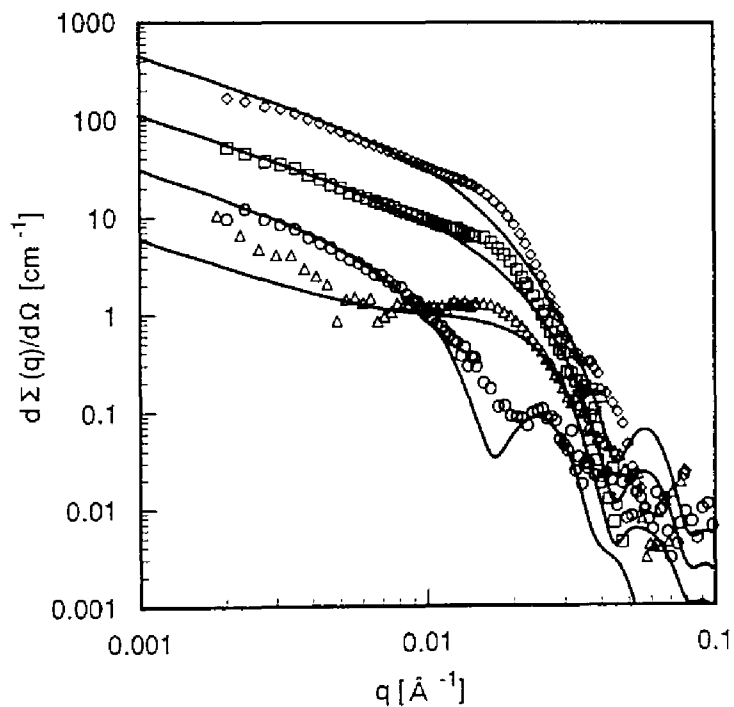
Figure 3.6. Scattering cross sections of N8560. The same symbols are used as in Figure 3.2. The solid lines represent the theoretical curves of the core-shell cylindrical model.

Since the q^{-1} dependence of the scattering intensities was clearly observed for N8560, the core–shell cylindrical model was first applied. It is impossible to determine the length or total volume of the rod, because it is possible only when the deviation from the q^{-1} slope and so-called Guinier region are observed. Then eq 3.14 is sufficient and was used for fitting the data. However, the agreement between experimental and theoretical profiles was not satisfactory as shown in Figure 3.6. The theoretical curves of the cylinder properly showed the q^{-1} dependence and was consistent with the experimental data at a smaller angle. However, in the region $q \approx 0.02$ Å^{-1} where the scattering intensity deviates from the straight line with a slope of -1, the two curves did not fit each other.

Then, we introduced a new assumption that not only the rodlike micelles but also the spherical micelles coexist in the solution of N8560. This sphere–rod coexistence model can be satisfied by this form factor with eqs 3.2 and 3.14:

$$P(q)_{\text{mix}} = \phi_{\text{Nrod}} P(q)_{\text{cylinder}} + (1 - \phi_{\text{Nrod}}) P(q)_{\text{sphere}} \qquad (3.17)$$

where ϕ_{Nrod} is the number fraction of the rodlike micelles in the total number of micelles in the solution. It is more convenient to use the volume fraction of the rodlike micelles ϕ_{rod} which relates to ϕ_{Nrod}:

$$\phi_{\text{Nrod}} = \phi_{\text{rod}} / \{ \phi_{\text{rod}} + (1 - \phi_{\text{rod}})(N_{\text{agg, rod}} / N_{\text{agg, sphere}}) \} \qquad (3.18)$$

Here $N_{\text{agg, rod}}$ and $N_{\text{agg, sphere}}$ are the aggregation numbers of the rodlike micelles and the spherical micelles, respectively. If all the polymers in the solution can be assumed to participate in the micelles, i.e., the critical micellar concentration is considerably low, ϕ_{rod} is identical to the number fraction of polymers contributing to the formation of the rodlike micelles. In this model, radial dimensions are identical for the spherical and the rodlike micelles, that is, $R_{\text{C, rod}} = R_{\text{C, sphere}}$ and $R_{\text{S, rod}} = R_{\text{S, sphere}}$.

The fitting results for N8560 with the coexistence model are shown in Figure 3.7. A marked improvement of fitting quality was obtained compared with the core–shell cylindrical model. The obtained model parameters are listed in Table 3.2.

Using the same model, the scattering curves of N8530 and N8545 micelles were fitted as shown in Figures 3.8 and 3.9. In all cases, the value of $\phi_p = 0.72$ was fixed, and good agreement was achieved on an absolute scale. The obtained model parameters are listed in Table 3.2. As a result, we found an increase of micellar size (R_C, R_S, or N_{agg}) with increasing hydrophobic chain length of block copolymer. In addition, rodlike aggregates started to form, and their volume fraction increased by the elongation of the hydrophobic chain. The rodlike micelles could have a broad distribution of lengths, but the averaged length should be quite large (at least 5000 Å) from the fact that the Guinier region could not be observed in the experimental q range. We were not able to determine the length distribution of rod since the consideration of the length distribution of the rod made no change on SANS profiles in the experimental q range. It should be also noticed that at least 70% of molecules contribute to the formation of spherical micelle. It means that a large number of spherical micelles coexist with a small number of rodlike micelles which have extremely large dimensions and a broad distribution of lengths. Other models such as pure cylinder or ellipsoid with the length distribution reproduce neither the micellization tendency nor the experimental SANS profiles. Other approaches such as electron microscopy will provide this information and prove the coexistence model.

Although there have been many examples of sphere to rod transition for the triblock copolymer system such as poly(ethylene oxide)–poly(propylene oxide)–poly(ethylene oxide) (PEO–PPO–PEO) in water at elevated temperatures,[13,22] the rodlike micelle formation of diblock copolymers at a low concentration and low temperature in water which we presented here should be noted. Zhang and Eisenberg have used electron microscopy and found the "crew-cut" micelles of multiple morphologies of polystyrene-block-poly(acrylic acid) includ-

ing rodlike structure.[23] Zhao et al. have also reported the rodlike micelle of polystyrene-block-poly(p-hydroxystyrene) formed in toluene by a combination of both static and dynamic light scattering studies.[24] These are rare examples of the rodlike micelles of diblock copolymer, and the methods that they used for the investigation could be applicable to our system and might be complementary to the SANS data.

The transition behavior can be qualitatively understood from the concept of "critical packing parameter" introduced by Israelachvili[25] for low molecular weight surfactants. If the hydrophobic chain length keeps on increasing in the spherical micelle, the area occupied by the polymer at the core-shell interface increases. However, there is an upper limit to the area that can be covered by a hydrophilic chain with a certain length. Therefore, transition to a rod shape will occur when the interfacial area per molecule of the spherical micelle exceeds this limit by the increase of the hydrophobic chain length.
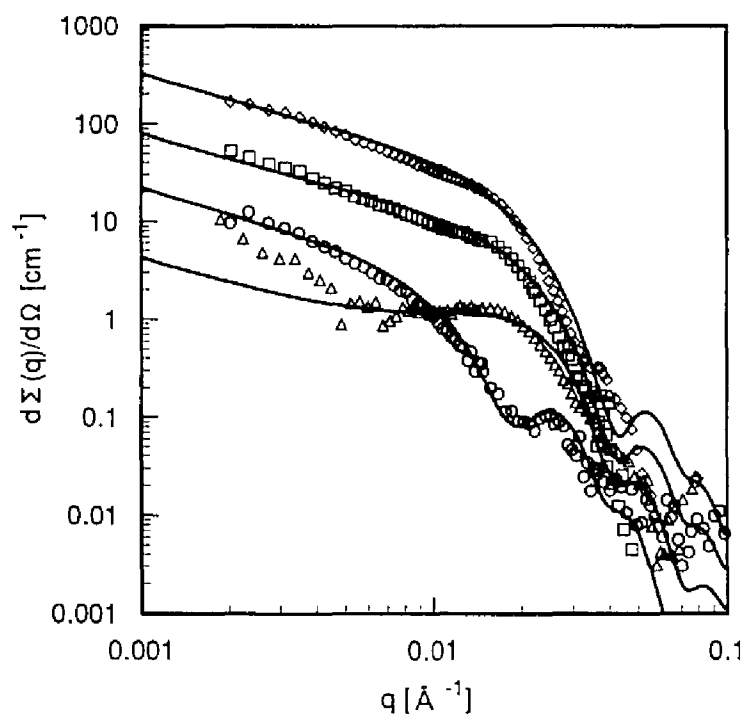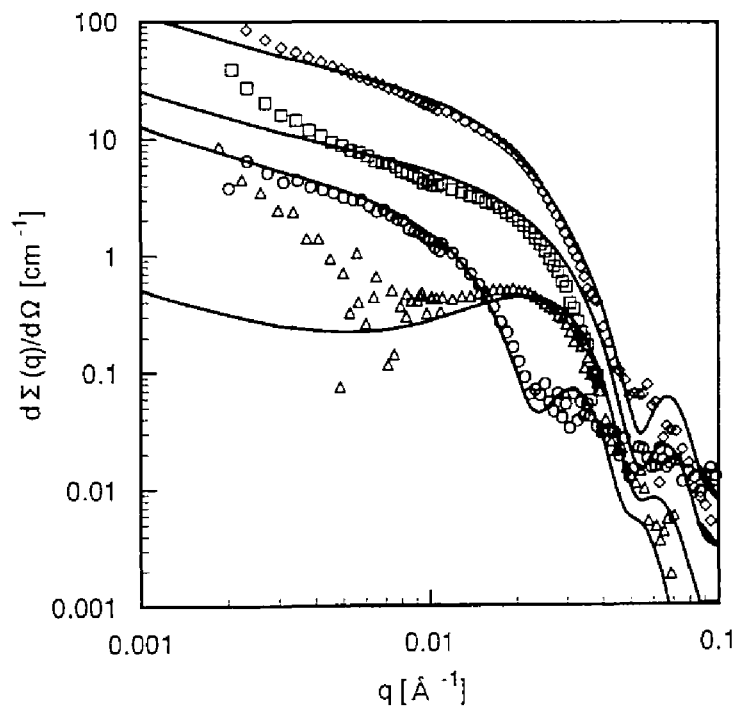

Figure 3.7. Scattering cross sections of N8560 with the fitted curve using coexisting model.
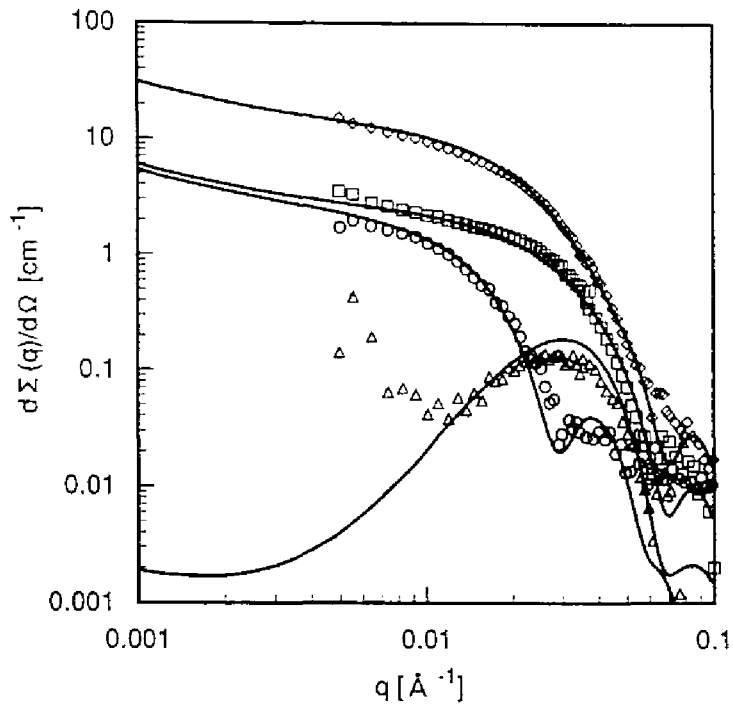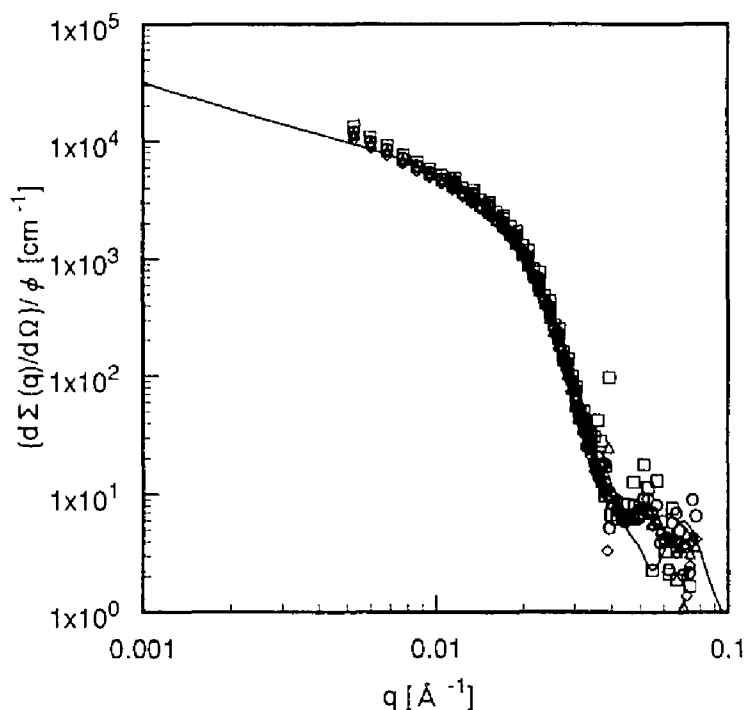
Figure 3.8. Scattering cross sections of N8530 with the fitted curve using coexisting model.

Figure 3.9. Scattering cross sections of N8545 with the fitted curve using coexisting model.

The concentration dependence of the SANS profile was investigated for N8545. To obtain the highest intensity (contrast), D_2O was used as a solvent, and the polymer volume fraction was varied from 0.05 to 0.5%. The data were normalized by the polymer volume fraction. We expected that the decrease in the concentration would shorten the length of the rodlike micelle, thereby making the total micellar size detectable, or reduce the volume fraction of the rod, but the SANS data were independent of the concentration as can be seen in Figure 3.10. The normalized data were reproduced by the calculated curve with the same parameters as used in Figure 3.9. This suggests that the rodlike micelle with an extremely long dimension already exists at a considerably low concentration and that the volume fraction of rod does not change at least up to 1%.

Figure 3.10. Scattering cross sections of N8545 in D_2O normalized by polymer concentration: 0.05% (□), 0.1% (○), 0.2% (△), and 0.5% (◇). The solid line is the theoretical curve with the same parameters as used in Figure 3.9.

No cloud point for the 1% solution of these copolymers was observed when we increased the temperature up to 90 °C. In the case of the PEO–PPO–PEO triblock copolymer, a strong temperature dependence of the phase behavior such as sphere to rod transition or phase separation has been observed.[13,22,26] Since the copolymers we used have OH groups at the side chains of the hydrophilic chain, which can effectively interact with the solvent, the hydrogen bond may not be broken even by frequent thermal motion of the polymer, and phase separation may not occur even at a high temperature. However, further studies are required on the dependence of rodlike aggregates on temperature or concentration. Moreover, a theoretical approach[26,27] is necessary to interpret the phenomena experimentally observed.

3.5. Conclusions

Amphiphilic diblock copolymers poly(HOVE-b-NBVE) with a partially deuterated hydrophobic segment were synthesized by living cationic polymerization and subsequent hydrolysis. These copolymers formed micelles in an aqueous solution. The internal structure of the micelles was investigated by the contrast variation method of SANS measurements. The molar volume of HOVE obtained by calculation of zero average contrast was quite small, which results from the hydration effect in the micellar shell. The SANS curves were described by the core–shell model. The micellar shape was strongly dependent on the hydrophobic chain length of the polymer. The polymer with the shortest hydrophobic chain was suggested to form spherical micelles. With increasing hydrophobic chain length, rodlike micelles started to form, and their volume fraction was increased.

References

(1) Halperin, A.; Tirrell, M.; Lodge, T. P. *Adv. Polym. Sci.* **1992**, *100*, 31.

(2) Chu, B. *Langmuir* **1995**, *11*, 414.

(3) Tuzar, Z.; Kratochvil, P. *Advances in Colloid and Interface Science*; Elsevier: Amsterdam, 1976.

(4) Zana, R. *Colloid and Surf. A: Physicochem. Eng. Aspects* **1997**, *123–124*, 27.

(5) Grubbs, R. H.; Tumas, W. *Science* **1989**, *243*, 907.

(6) Miyamoto, M.; Sawamoto, M.; Higashimura, T. *Macromolecules* **1984**, *17*, 265.

(7) Sawamoto, M. *Prog. Polym. Sci.* **1991**, *16*, 111.

(8) Mortensen, K.; Brown, W. *Macromolecules* **1993**, *26*, 4128.

(9) Magid, L. J. *Nonionic Surfactants*; Marcel Dekker: New York, 1987; Vol. 23.

(10) Herbst, L.; Kalus, J.; Schmelzer, U. *J. Phys. Chem.* **1993**, *97*, 7774.

(11) Yamaoka, H.; Matsuoka, H.; Sumaru, K.; Hanada, S.; Imai, M.; Wignall, G. D. *Physica B* **1995**, *213&214*, 700.

(12) Poppe, A.; Willner, L.; Allgaier, J.; Stellbrink, J.; Richter, D. *Macromolecules* **1997**, *30*, 7462.

(13) Mortensen, K. *J. Phys.: Condens. Matter* **1996**, *8*, A103.

(14) Cantor, C. R.; Schimmel, P. R. *Biophysical Chemistry, Part II: Techniques for the Study of Biological Structure and Function*; W. H. Freeman and Co.: San Francisco, 1980.

(15) Higgins, J. S.; Benoit, H. C. *Polymers and Neutron Scattering*; Oxford: New York, 1996.

(16) McKeon, J. E.; Fitton, P. *Tetrahedron* **1972**, *28*, 233.

(17) Guinier, A.; Fournet, G. *Small-Angle Scattering of X-rays*; John Wiley: New York,

1955.

(18) Pedersen, J. S.; Posselt, D.; Mortensen, K. *J. Appl. Crystallogr.* **1990**, *23*, 321.

(19) Nakano, M.; Matsuoka, H.; Yamaoka, H.; Poppe, A.; Richter, D. *Physica B* **1998**, *241–243*, 1038.

(20) Ibel, K.; Stuhrmann, H. B.; *J. Mol. Biol.* **1975**, *93*, 255.

(21) Frank, H. S.; Evans, M. W. *J. Chem. Phys.* **1945**, *13*, 507.

(22) Schillén, K.; Brown, W.; Johnsen, R. M. *Macromolecules* **1994**, *27*, 4825.

(23) Zhang, L.; Eisenberg, A. *Science* **1995**, *268*, 1728.

(24) Zhao, J. Q.; Pearce, E. M.; Kwei, T. K.; Jeon, H. S.; Kesani, P. K.; Balsara, N. P. *Macromolecules* **1995**, *28*, 1972.

(25) Israelachvili, J. N. *Intermolecular and Surface Forces*, 2nd ed.; Academic Press: London, 1985.

(26) Linse, P. *J. Phys. Chem.* **1993**, *97*, 13896.

(27) Munch, M. R.; Gast, A. P. *Macromolecules* **1988**, *21*, 1360.

Chapter 4

Characterization of Micellization Behavior of Amphiphilic Polymer Having Octadecyl Group by Small-Angle X-ray and Neutron Scattering

Abstract

Amphiphilic polymers having an octadecyl group as a hydrophobic segment with different degrees of polymerization were synthesized by living cationic polymerization. Matrix-assisted laser-desorption-ionization time-of-flight mass spectrometry (MALDI TOF MS) was performed to determine the molecular weight. Differential scanning calorimetry (DSC) measurements for polymer solid samples showed the melting point depending on the degree of polymerization. The size and shape of micelles formed by the polymers in water were investigated by small-angle X-ray scattering (SAXS) and neutron scattering (SANS) measurements. The aggregation number reduced with increasing degree of polymerization, while the overall micelle size was almost independent. The SAXS and SANS data revealed the sphere to disk transition on changing temperature for the polymer with the shortest hydrophilic chain. Below the melting point of hydrophobic chain, the polymer formed disklike aggregates with a crystallized core of octadecyl groups surrounded by swollen shell. With increasing temperature, octadecyl groups melted and the spherical micelle were formed.

4.1. Introduction

Amphiphiles, which show specific behavior such as micelle formation and adsorption in selective solvents, have attracted the attention of many research groups for a few decades.[1,2] Amphiphiles can be roughly divided into two groups, i.e., low molecular weight surfactants and polymer amphiphiles. For low molecular weight surfactants,[3] characterization of their self-assembly system is relatively simple because of no molecular weight distribution. However, since it is difficult to change the size of ionic head group of molecules, investigations of the effects of head groups can be fulfilled only by changing the apparent size by variation of ionic strength in the system. On the other hand, the hydrophilic-lipophilic-balance (HLB) of amphiphilic block copolymers[4-7] can be changed by control of the degrees of polymerization of both hydrophilic and hydrophobic segments, while molecular weight distribution yields ambiguity of phenomena, and enhances the difficulty of characterization such as the determination of critical micellar concentration or micellar size.

Here, we introduce a new type of polymer amphiphile, which is synthesized by homopolymerization with an initiator having an octadecyl group. A constant length of hydrophobic chain is attainable by the initiator method, and the control of degree of polymerization corresponds to the control of head group size of the surfactant. Thus, this polymer has merits of both low molecular weight surfactants and polymer amphiphiles.

We have reported the micellization behavior of amphiphilic block copolymers having poly(2-hydroxyethyl vinyl ether (HOVE)) as a hydrophilic segment, and formation of the anisotropic micelle.[8-10] The polymer which we present here has the same hydrophilic chain, and the degree of polymerization of HOVE can be precisely controlled by living cationic polymerization.[11,12]

Micelles of the surfactant with an octadecyl group have been little studied[13-16] because of the crystallinity with high melting point and poor solubility in water. However,

sufficient hydrophilicity for dissolution can be supplied by an increase of the degree of polymerization. Moreover, such polymer surfactants must have an interesting micellization behavior near the melting point.

Herein, we studied the size and shape of the micelles formed by the amphiphilic polymer with an octadecyl group in water by the small-angle X-ray scattering (SAXS)[17,18] and neutron scattering (SANS)[19] techniques. The micellar shape was found to change from sphere to disk. This phenomenon is discussed along with differential scanning calorimetry (DSC) data.

4.2. Experimental Section

4.2.1. Synthesis.

The amphiphilic polymers were prepared as shown in Scheme 4.1. The initiator having an octadecyl group was synthesized by bubbling the hydrogen chloride gas into a hexane solution of octadecyl vinyl ether (ODVE, Tokyo Kasei, Tokyo). 2-Acetoxyethyl vinyl ether (AcOVE) was synthesized from sodium acetate (98.5%, Nacalai Tesque, Kyoto) and 2-chloroethyl vinyl ether (99%, Aldrich, Milwaukee) at 90 °C. Commercial zinc chloride as diethylether solution (Aldrich) was used without further purification.

Living cationic polymerization was performed in a dried flask with a three-stop cock under nitrogen. The hydrogen chloride adduct of ODVE and zinc chloride were injected as an initiator system in dichloromethane solution of AcOVE at –20 °C. The initial monomer/initiator molar ratio was changed to obtain four different molecular weight polymers (OD10, 20, 30, and 40, see Table 4.1). The polymerization was terminated by the addition of ammoniacal methanol.

After polymerization, AcOVE was led to water soluble 2-hydroxyethyl vinyl ether

(HOVE) by hydrolysis of the protective group with sodium hydroxide in dioxane. The obtained amphiphilic polymer ODVE-poly(HOVE) was purified by dialysis with deionized water. Their aqueous solutions were prepared by their direct dissolution into water and heated at 50 °C for 1 h. Then, they were passed through a filter with a pore size of 0.22 µm.

$$CH_2{=}CH$$
$$|$$
$$O$$
$$|$$
$$(CH_2)_2$$
$$m \quad O$$
$$|$$
$$C{=}O$$
$$|$$
$$CH_3$$

$$CH_3{-}CH{-}Cl$$
$$|$$
$$O$$
$$|$$
$$(CH_2)_{17}$$
$$|$$
$$CH_3$$

(AcOVE)

$$\xrightarrow[\text{in } CH_2Cl_2]{ZnCl_2, -20°C}$$

$$CH_3OH/NH_3 \longrightarrow$$

$$CH_3{-}(CH_2)_{17}{-}O{-}CH{-}\!\!\left(CH_2{-}CH\right)_{\!m}\!OCH_3$$
$$|\qquad\qquad\qquad |$$
$$CH_3 \qquad\qquad\quad O$$
$$|$$
$$(CH_2)_2$$
$$|$$
$$O$$
$$|$$
$$C{=}O$$
$$|$$
$$CH_3$$

$$\xrightarrow[\text{in Dioxane}]{NaOH}$$

$$CH_3{-}(CH_2)_{17}{-}O{-}CH{-}\!\!\left(CH_2{-}CH\right)_{\!m}\!OCH_3$$
$$|\qquad\qquad\qquad |$$
$$CH_3 \qquad\qquad\quad O$$
$$|$$
$$(CH_2)_2$$
$$|$$
$$OH$$
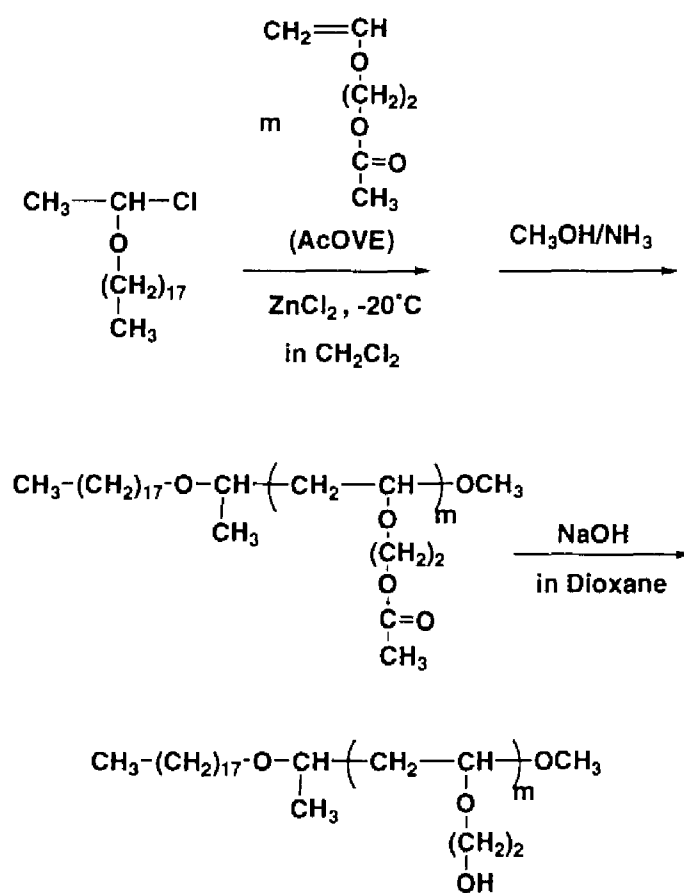
Scheme 4.1.   Synthesis of ODVE-poly(HOVE)

4.2.2. Molecular Characterization.

Gel permeation chromatography (GPC) was carried out in chloroform on a Jasco 880–PU chromatograph equipped with four polystyrene gel columns (Shodex K–802, K–803, K–804, and K–805) and a Jasco 830–RI refractive index detector. ^{1}H NMR spectra were obtained on a JEOL GSX 270 spectrometer. Matrix-assisted laser-desorption-ionization time-of-flight mass spectrometry (MALDI TOF MS) was performed on a Shimadzu KOMPACT MALDI IV mass spectrometer using 3,5-dimethoxy-4-hydroxycinnamic acid (98%, Aldrich) as a matrix compound.

4.2.3. Differential Scanning Calorimetry (DSC).

The DSC measurements were performed on a Thermal analyzer system WS002 (MAC Science, Tokyo) equipped with a TAPS1000S control unit and a DSC3100S module. Polymer solid samples (ca. 8 mg) were measured in an aluminum container under a dry nitrogen flow at a heating or cooling rate of 10 °C/min. α-Alumina was used as a standard.

4.2.4. Small-Angle X-ray Scattering (SAXS).

The SAXS measurements were performed using a Kratky type camera (Rigaku Corporation, Tokyo) equipped with a rotating anode X-ray generator and a position sensitive proportional counter (PSPC). The SAXS instrument has been described in detail elsewhere.[20] Sample solutions were measured in glass capillaries (Mark, Berlin) with a diameter of 2 mm.

4.2.5. Small-Angle Neutron Scattering (SANS).

The SANS measurements were performed by SANS-U of Institute for Solid State Physics, The University of Tokyo, at the research reactor JRR–3, Tokai, Japan. We used the wavelength (λ) of neutron source of 7 Å ($\Delta\lambda/\lambda = 10\%$). Solutions were measured in

quartz cells (Nippon Silica Glass Co., Tokyo) with a pass length of 4 mm. Scattering data measured by 2D-detector were corrected for electronic background and circular averaged to be 1D-form scattering data; then, the scattering of empty cell was subtracted. The data were transformed to absolute cross sections using the Lupolen® standard. From all scattering data of samples, we subtracted the scattering of solvent and the calculated incoherent scattering of the protonated portion of the polymer.

The SANS experiments for OD10 solution were carried out at sample to detector distances of 1, 4 and 12 m, covering a range of the scattering vector (q) of $0.003 \leq q \leq 0.28$ Å^{-1}. For OD20 and OD30, the distance of 2 m was chosen to cover the range of $0.02 \leq q \leq$ 0.15 Å^{-1}. We used D_2O as a solvent, and a volume fraction of polymer of 1 vol % for all measurements.

4.3. Data Analysis of SAXS and SANS Measurements

The similar basic principle can be applied for both SAXS and SANS. The main difference is that the neutron is scattered by the density fluctuation of scattering length inherent for each atom, while the scattering of X-ray occurs by the electron density fluctuation.

When the contribution of interparticle interaction is negligible, the neutron scattering cross section can be given by the equation:

$$d\Sigma(q)/d\Omega = n_p P(q) \tag{4.1}$$

where n_p is the number density of particles and $P(q)$ is the particle form factor including particle volume and density fluctuation terms. The scattering vector q is given by $q = 4\pi$ $\sin\theta/\lambda$, where 2θ is the scattering angle and λ is the neutron wavelength.

Here we deal with the micelles in a core-shell structure. The particle form factor of a core-shell model can be written as follows:

$$P(q) = (1/2)\int_0^\pi \{(\rho_C - \rho_S)V_C F_C(q) + (\rho_S - \rho_0)V_S F_S(q)\}^2 \sin\beta \, d\beta \qquad (4.2)$$

where ρ_C, ρ_S and ρ_0 are the scattering length densities (for SANS) or electron densities (for SAXS) of the core, the shell and the solvent. V_C and V_S are the volumes of the core and overall micelle, respectively. The scattering amplitude $F_i(q)$ ($i = c, s$) depends on the size and shape of the scattering particles.[17] For a core-shell sphere with a core radius of R_C and overall micelle size R_S (see Figure 4.10), $F_i(q)$ is given by

$$F_i(q) = 3 \, (\sin(qR_i) - qR_i \cos(qR_i)) / (qR_i)^3 \qquad (4.3)$$

For a core-shell cylinder with a core radius of R_C, and overall micelle size R_S and length L:

$$F_i(q) = \{(\sin(q(L/2)\cos\beta) / (q(L/2)\cos\beta)\}\{2J_1(qR_i\sin\beta) / (qR_i\sin\beta)\} \qquad (4.4)$$

For a disklike structure with a core thickness of L_C, overall micelle size L_S and radius R (see Figure 4.10):

$$F_i(q) = \{(\sin(q(L_i/2)\cos\beta) / (q(L_i/2)\cos\beta)\}\{2J_1(qR\sin\beta) / (qR\sin\beta)\} \qquad (4.5)$$

β is the angle between the axis of symmetry of particle and the scattering vector q, and J_1 denotes the Bessel function of the first kind and of the order 1.

4.4. Results

4.4.1. Characterization of Amphiphilic Polymers.

The number-averaged degree of polymerization of HOVE (m) was obtained by MALDI TOF MS. The polydispersity index M_w/M_n was determined for ODVE–poly(AcOVE) (before the hydrolysis) by GPC with polystyrene standard calibration, where M_w and M_n are the weight- and number-averaged molecular weights, respectively, since ODVE–poly(HOVE) was not soluble in chloroform. These values are listed in Table 4.1. Figure 4.1 shows MALDI TOF spectra of OD40 and its precursor polymer as typical examples. Observed peaks were quite sharp as can be seen in Figure 4.1, and the peak interval corresponded to the molecular weight of monomers (88 for ODVE–poly(HOVE) and 130 for ODVE–poly(AcOVE)). MALDI TOF MS is a quite effective technique to obtain the
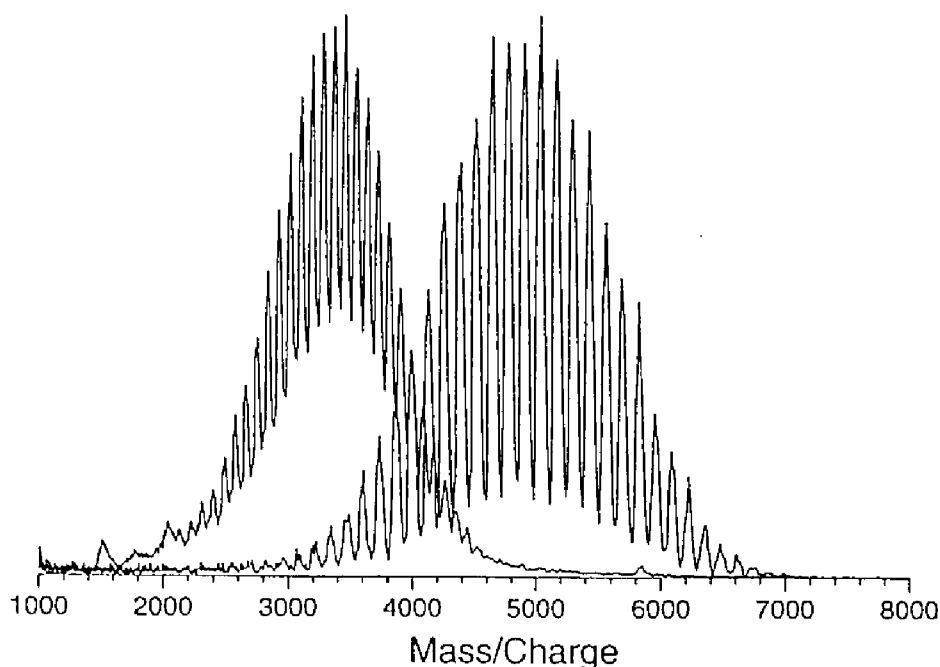
Figure 4.1. MALDI TOF spectra of OD40 and its precursor polymer.

absolute molecular weight, but in the case of a diblock copolymer, it is not possible to obtain sharp peaks because of the chain length distributions of both segments. For the amphiphilic polymers we used, however, peaks were clearly found and the molecular weight determination was possible, since these polymers had a hydrophobic chain with a fixed length introduced by the initiator method of living cationic polymerization. The obtained number-averaged degree of polymerization of both HOVE and AcOVE were in agreement within 5% for all cases. This suggests that the hydrolysis was completed without any sub-reaction such as polymer degradation process. We also confirmed by ^{1}H NMR that the octadecyl group was stable under the basic condition of hydrolysis.

4.4.1. DSC.

The DSC curves of OD10, 20, 30, and 40 are shown in Figures 4.2(a)–(d). In all cases, two endothermic peaks were observed in the heating curves. One peak which appeared at ca. 10 °C is probably due to the glass transition of poly(HOVE), and will not be discussed here. The other peak is more characteristic: It was observed at ca. 42 °C, and it became smaller with increasing hydrophilic chain length. This peak had a counterpart in the cooling curve, but the corresponding exothermic peak shifted to a lower temperature as the hydrophilic chain of the polymer became longer, and disappeared as for OD30 and 40. This peak was attributed to the melting point of octadecyl group. The increase of the hydrophilic chain length was considered to lower the degree of crystallinity, and the long hydrophilic chain prevents the octadecyl group from crystallizing during the cooling process. This thermal behavior of the polymers in a solid state is related with the properties of their micelles in an aqueous solution, which will be discussed later.
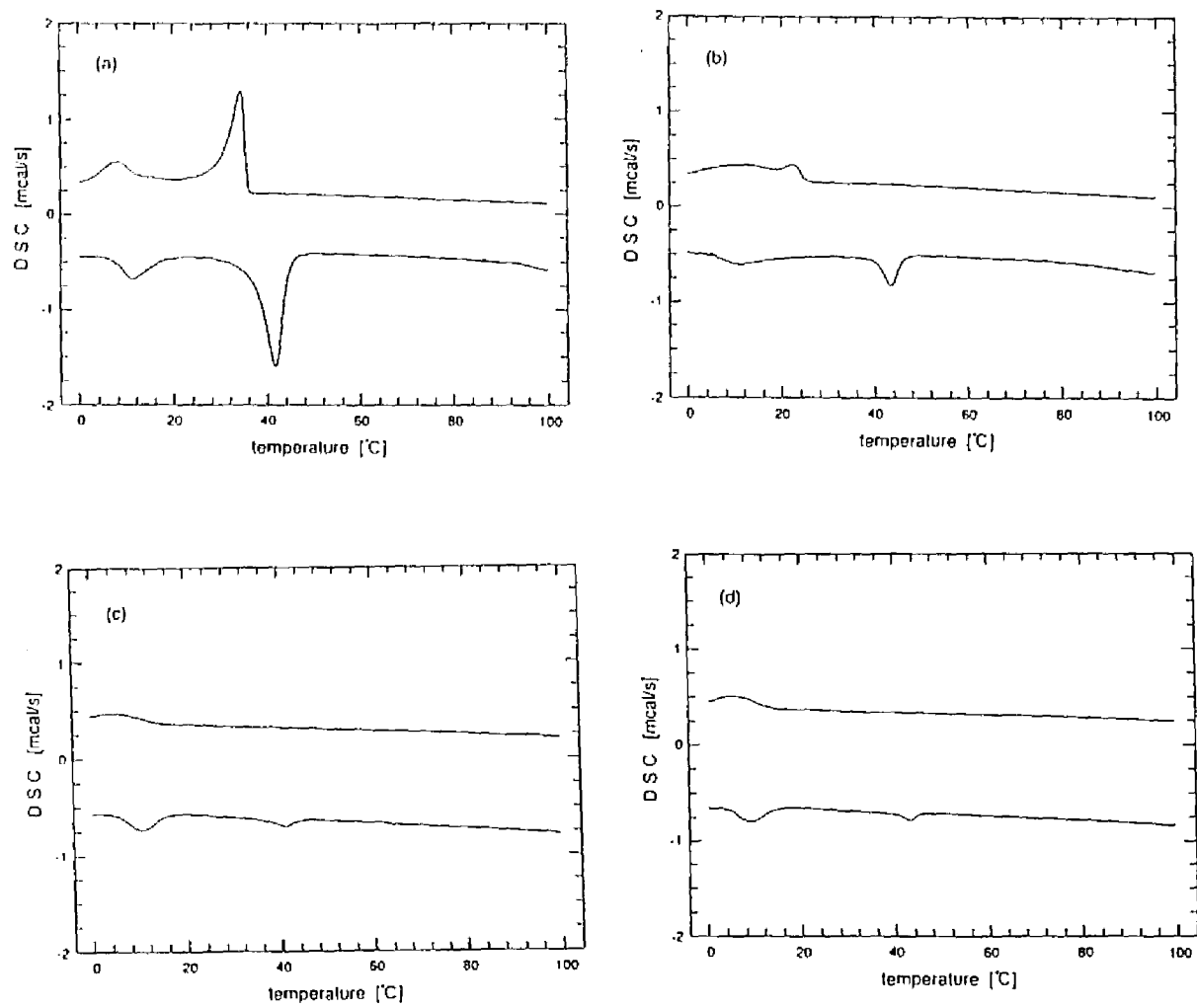
Figure 4.2. DSC curves of OD10 (a), OD20 (b), OD30 (c), and OD40 (d).

4.4.3. SAXS and SANS.

The amphiphilic polymers OD20, 30 and 40 were dissolved into H_2O to prepare 1 wt % solutions for SAXS measurements. Direct dissolution with a smaller HOVE content made slightly turbid suspensions. However, they changed to transparent solutions by heating at 50 °C. These solutions were stable and kept their transparency at room temperature even after 1 month. For SANS measurements, a 1 vol % D_2O solution was prepared.

The SAXS profiles of the aqueous solutions of OD20–40 at room temperature are shown in Figures 4.3(a)–(c). In all cases, a strong scattering was observed at small angles, indicating the formation of large aggregates. In addition, a secondary maximum can be seen at $q \approx 0.1$ [$Å^{-1}$], implying a relatively narrow size distribution of micelles.
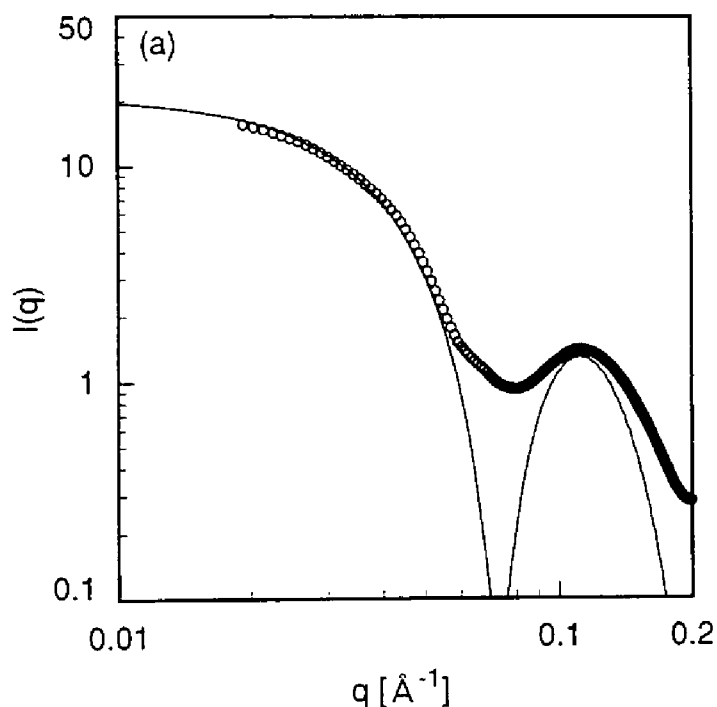
Figure 4.3. SAXS profiles of amphiphilic polymers in H_2O at 25 °C: OD20 (a), OD30 (b), and OD40 (c). Solid lines are theoretical curves of spherical core-shell model.
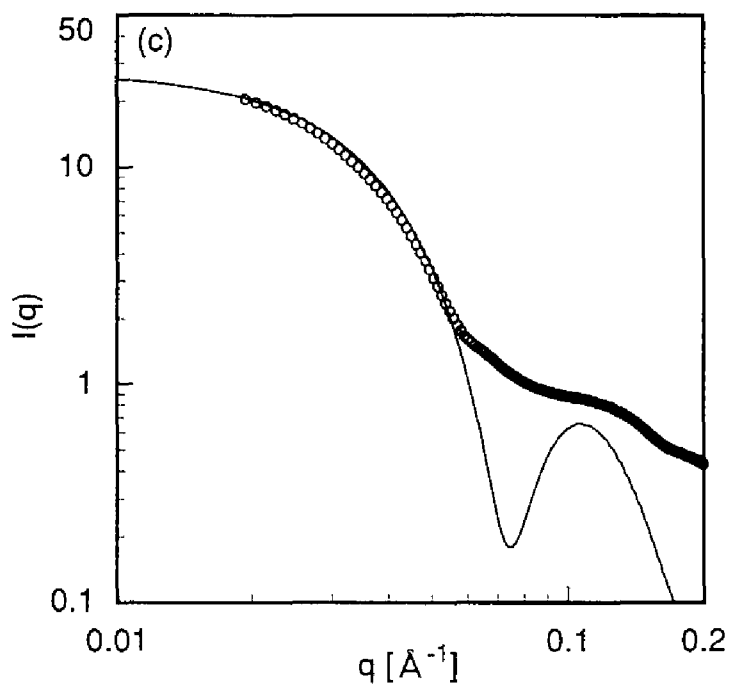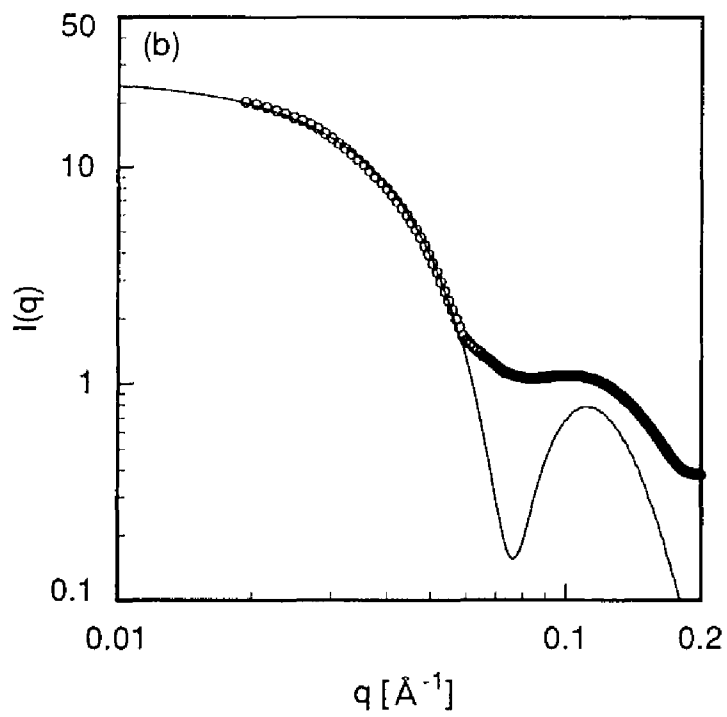
Figure 4.3. Continued.

The SANS profiles of D_2O solutions of OD20 and OD30 at room temperature are shown in Figures 4.4(a), (b). The secondary maximum near $q = 0.1$ was not observed in SANS curves. The difference of the scattering profiles between SAXS and SANS is evidence that micelles consist of the core–shell structure. In SANS experiments, the contrast between the core and the shell is considerably low compared with that between the shell and solvent. Then the scattering profile is similar to that of the homogeneous sphere. On the contrary, the electron density of the shell is higher than that of the core or the solvent, which yields the secondary maximum in SAXS profile.

These scattering profiles were fitted by the form factor of spherical core–shell model with R_C and R_S as fitting parameters. By fitting the SANS profiles in an absolute scale we obtained the aggregation number of micelles, under the assumption of a close-packed core consisting of the hydrophobic initiator part of the polymer chain. The SAXS profiles in which the intensity is given on a relative scale were fitted by introduction of a shift factor. The value of the shift factor was kept constant while all the SAXS profiles were fitted. The fitting curves are shown in Figures 4.3 and 4.4 with the experimental data, and the results in Table 4.1. The scattering at smaller angles and the position of secondary maximum were excellently reproduced by the fitting curve in all cases. The slight discrepancy for sharpness of the secondary maximum may be due to the polydispersity of micellar size. The deviation at larger angles is due to the low accuracy of the measured curves in this range, and due to the fact that the scattering at larger angles is dominated by individual fluctuation of polymer chains in the shell (blobs), which was not considered in the core–shell model.
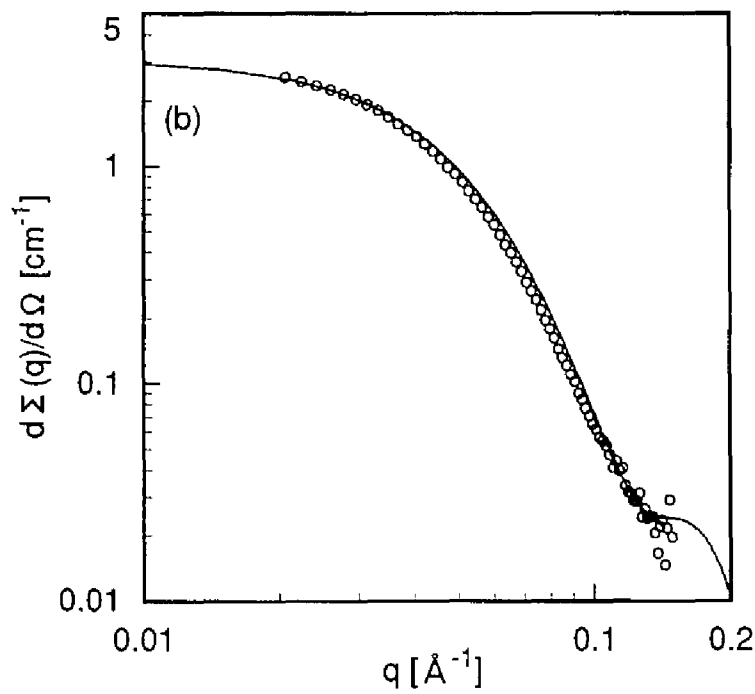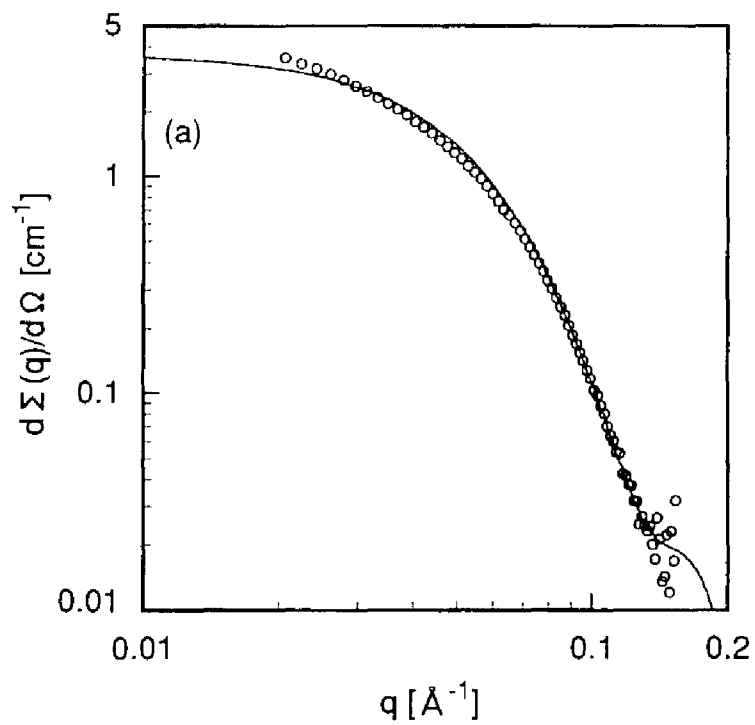
Figure 4.4. SANS profiles of D_2O solutions of OD20 (a) and OD30 (b). Solid lines are theoretical curves of spherical core-shell model.

The aqueous solution of OD20 was also investigated at 45 °C by SAXS. The SAXS profiles at both room temperature and 45 °C show good agreement as can be seen in Figure 4.5, suggesting no temperature dependence of micellar shape and size in the temperature range studied here.
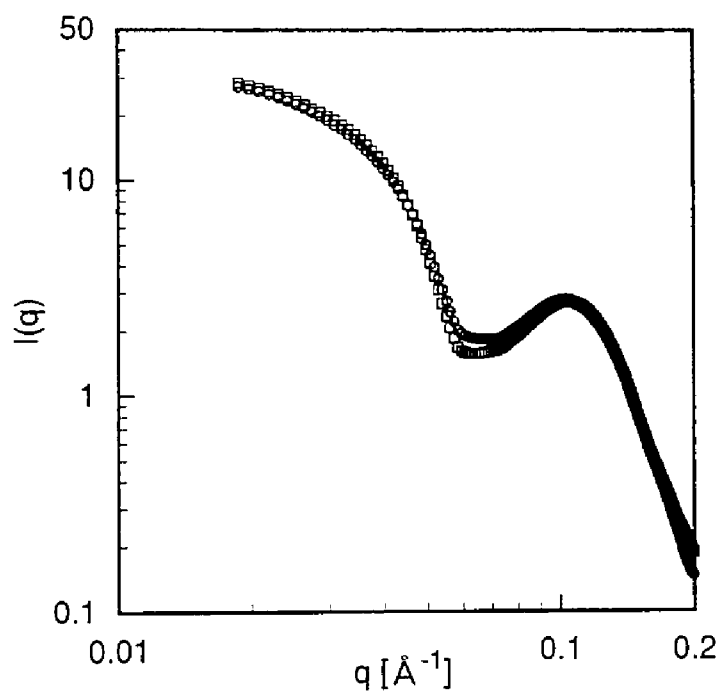

Figure 4.5. SAXS profiles of OD20 in H_2O at 25 °C ($\square$) and 45 °C (O).

Different from OD20–40, the 1 wt % aqueous solution of OD10 was slightly turbid at room temperature, and reversibly changed to transparent at a high temperature. Its SAXS profile at room temperature also exhibited a different tendency as shown in Figure 4.6. Although the position of the secondary maximum did not differ so much from that of the other polymer solutions, the intensity at smaller angles decreased more abruptly with the increase of q, indicating the existence of larger aggregates. Figure 4.6 shows the qualitatively fitted results of the SAXS profile of OD10 by lines. The SAXS profile was first fitted by the form factor of a spherical core–shell model. However, the secondary maximum peak was not reproduced when a lower q region was fitted. A core–shell cylinder model shifted the peak position to a higher q, but it was still inadequate. Finally, the agreement of both peak and a lower q region was achieved by introduction of a core–shell disk (or better to say sandwich-like) model. Thus, the existence of disklike aggregates was qualitatively proved, but quantitative fitting will be performed later.
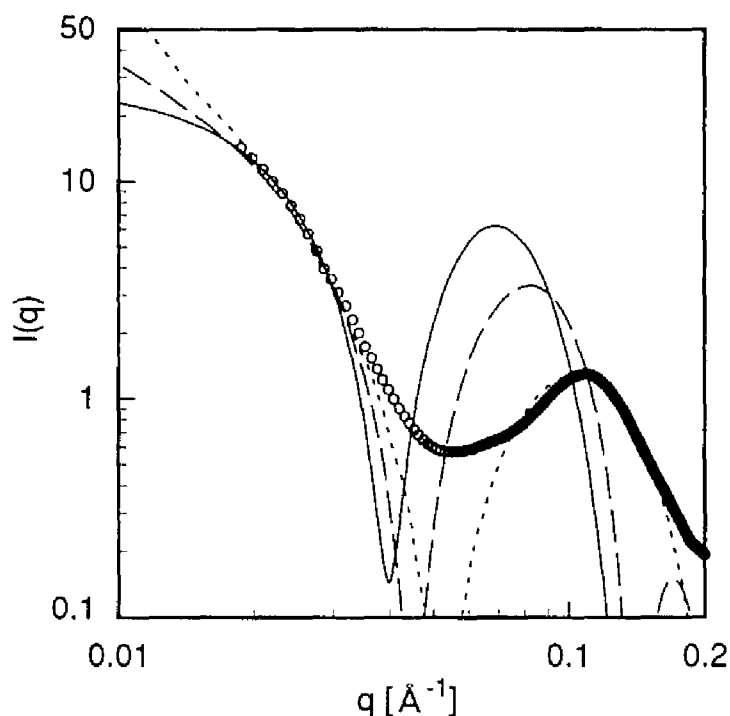

Figure 4.6. SAXS profile of OD10 in H_2O at 25 °C. Solid, broken, and dotted lines are theoretical curves of sphere, rod, and disk with a core–shell structure, respectively.

The scattering intensity of disklike particles is proportional to q^{-2} at small angles.[17] This scattering behavior could not be observed in the SAXS profile of OD10, since it was beyond the measurable q range. On the other hand, this behavior could be observed by SANS, which provides more information of smaller angle regions. Figure 4.7 shows the SANS profile of 1 vol % D_2O solution of OD10 at room temperature. A linear region of the intensity was observed at q < 0.06 [Å^{-1}], which is a quite different profile from the form factor of sphere. However, the slope of the linear region was about 5/3, which was smaller than that of disk (2). This profile may indicate the other shapes such as flexible rods (threadlike), branch or network of rods, but it is more reasonable to consider that the disklike aggregates coexist with spherical micelles, if one takes into account the crystallization of octadecyl groups below the melting point.
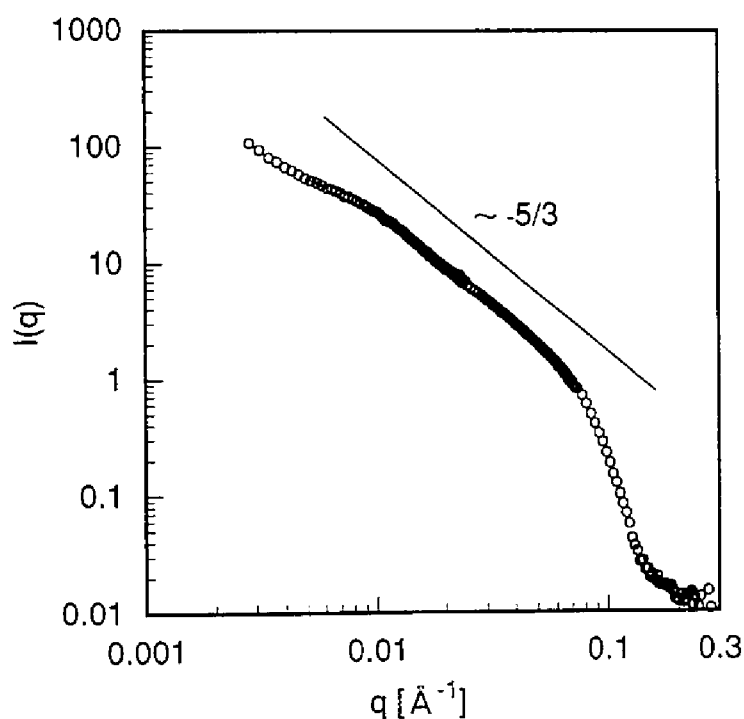

Figure 4.7. SANS profile of OD10 in D_2O at 25 °C. A linear region of the intensity with a slope of about 5/3 was observed.

The SANS measurement of D_2O solution of OD10 was also performed at 45 °C, which is higher than the melting point. A marked difference of the profiles between 25 and 45 °C can be seen in Figure 4.8. The profile of 45 °C resembled that of spherical micelles, since a flat region was observed at middle angle regions. Indeed, this profile could be fitted by the form factor of a sphere with a core-shell structure as shown by the solid line in Figure 4.8. Deviation at a smaller angle might be due to a trace of large aggregates. The parameters are listed in Table 4.1. The solution was cooled to room temperature, and then SANS was performed again at 25 °C. The result was the same as obtained before heating, indicating the reversible change of the SANS profile, and hence the reversible change of micelle structure.
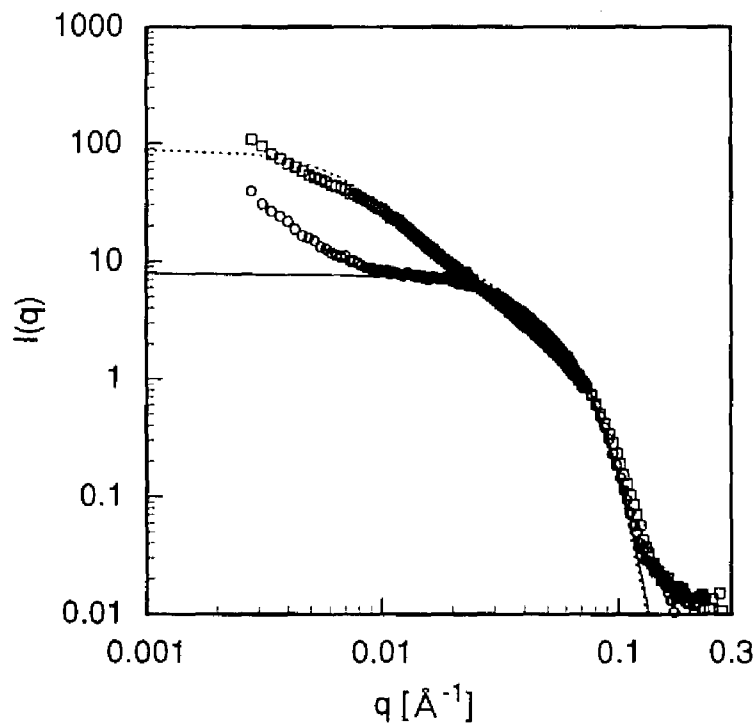
Figure 4.8. SANS profiles of OD10 in D_2O at 25 °C (□) and 45 °C (○). The solid line is the theoretical curve of the spherical core-shell model. The dotted line is based on the assumption of coexistence of spherical micelles and disklike aggregates with the volume fraction of disk of 0.2.

Using both eqs (4.3) and (4.5), with introduction of the volume fraction of disklike aggregates ϕ_{disk}, the SANS curve of 25 °C was well fitted as shown by the dotted line in Figure 4.8. The structure of the spherical micelles involved in the solution at 25 °C was assumed to be the same as that at 45 °C, and the volume fraction of disklike aggregates was determined to be 0.2 (20% disk and 80% sphere in volume). The values of L_C and L_S are also listed in Table 4.1. Although the value of the overall radius R of 300 Å was used, it is the smallest possible value and exact size of the disklike aggregates could not be determined, since the information about the total size is provided from a smaller q region than that covered in this experiment. With the same structure parameters as used for describing the SANS data of OD10, the SAXS curves was also well reproduced as shown in Figure 4.9.
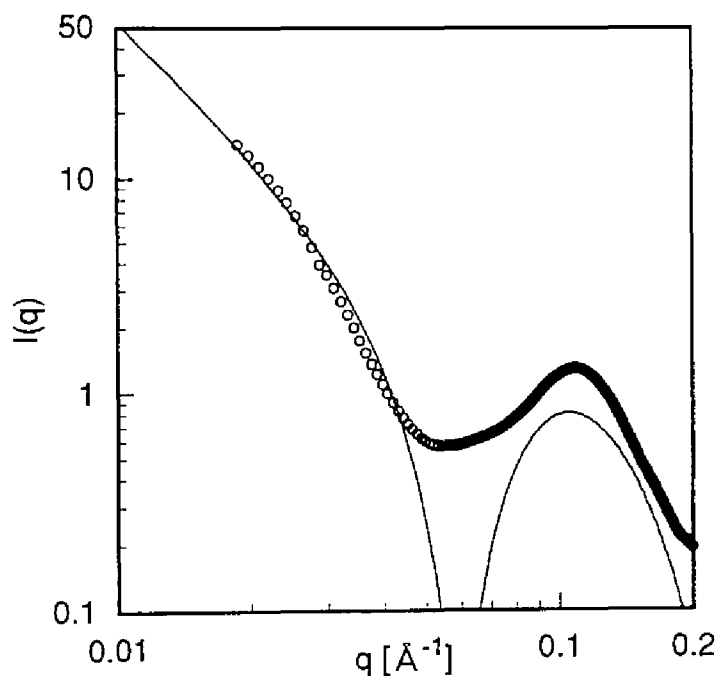
Figure 4.9. SAXS profiles of OD10 in H_2O at 25 °C, fitted by the same model as used for SANS.

4.5. Discussion

4.5.1. Spherical Micelle.

The relationship between molecular architecture and structure of micelles can be clarified from SAXS and SANS results. If the structure of the spherical micelles is assumed to be independent of temperature, the four different spherical micelles can be compared (Table 4.1). The polymer with a shorter hydrophilic chain forms micelles having a larger value of R_C (or N_{agg}), while R_S seems to be independent of the degree of polymerization (m). From the values listed in Table 4.1, we obtained the relation of $N_{agg} \propto m^{-1.31}$. The higher hydrophilicity given by the increase of m reduced the aggregation number. On the contrary, the size of overall micelle was little affected by the total length of polymer.

Table 4.1.   Characterization of ODVE–poly(HOVE)s and Their Micelles

	m_0/I_0 [a]	m [b]	M_w/M_n [c]	shape	R_C	R_S	ϕ_{disk}	N_{agg}
OD10	10	7.9	1.15	disk (25 °C)	$L_C = 20$	$L_S = 62$	0.2	—
				sphere (45 °C)	28	50		167
OD20	20	16	1.18	sphere	20	50		61
OD30	30	28	1.21	sphere	16.5	53		34
OD40	40	34	1.23	sphere	15.5	56		28

[a] The initial monomer/initiator ratio. [b] Obtained by MALDI TOF MS. [c] By GPC before hydrolysis.

4.5.2. Sphere to Disk Transition.

OD10, which is the polymer with the shortest hydrophilic chain, showed properties different from the others. It formed disklike aggregates at room temperature, and reversibly changed into spherical micelles with increasing temperature. This transitional behavior can be interpreted by the DSC result. For OD10, the exothermic peak corresponding to the melting point observed on cooling was higher than that at room temperature (25 °C), in contrast with the other polymers which had exothermic peaks lower than those at room temperature, or no peaks. From these results, we concluded that the structural transition of micelles is induced by the crystallization or melting of alkyl chains. Below the melting point, the polymer forms disklike aggregates with a crystallized core of octadecyl groups surrounded by a swollen HOVE shell, and spherical micelles are formed by the melting of the crystallized core at temperatures higher than the melting point.

The sphere to disk transition has been reported for octadecyltrimethyammonium bromide ($C_{18}TAB$) micelles with increasing salt concentration, and disklike micelles coexisting with globular micelles at a certain salt concentration have been observed by cryo–TEM measurements.[14] This surfactant has an alkyl chain of the same length as the polymer we used. The increase of salt concentration shields the electrostatic repulsion between charged headgroups of $C_{18}TAB$ globular micelles, which induces the transition to disklike structures. The same effect, i.e., a decrease of "effective" area of head group can be introduced by reduction of hydrophilic chain length in the case of our polymer surfactants. Indeed, we observed the sphere to disk transition at room temperature when the degree of polymerization of HOVE was decreased.

The internal structures of disk and spherical micelles predicted by the present systematic study are schematically shown in Figure 4.10. The polymers with a longer hydrophilic chain favor the spherical micelle formation because of the larger repulsion between hydrophilic chains. On the other hand, the disklike structure is favored for shorter chain

polymers. For the disklike structure of C_{18}TAB, the core is considered to consist of a bilayer of octadecyl chains.[15] ODIO, however, is supposed to have a crystallized monolayer core where octadecyl groups penetrate from both sides of the planar core as shown in Figure 4.10, if the relatively small value of L_c (20 Å) determined by SANS and SAXS is taken into account.

Disk   Sphere
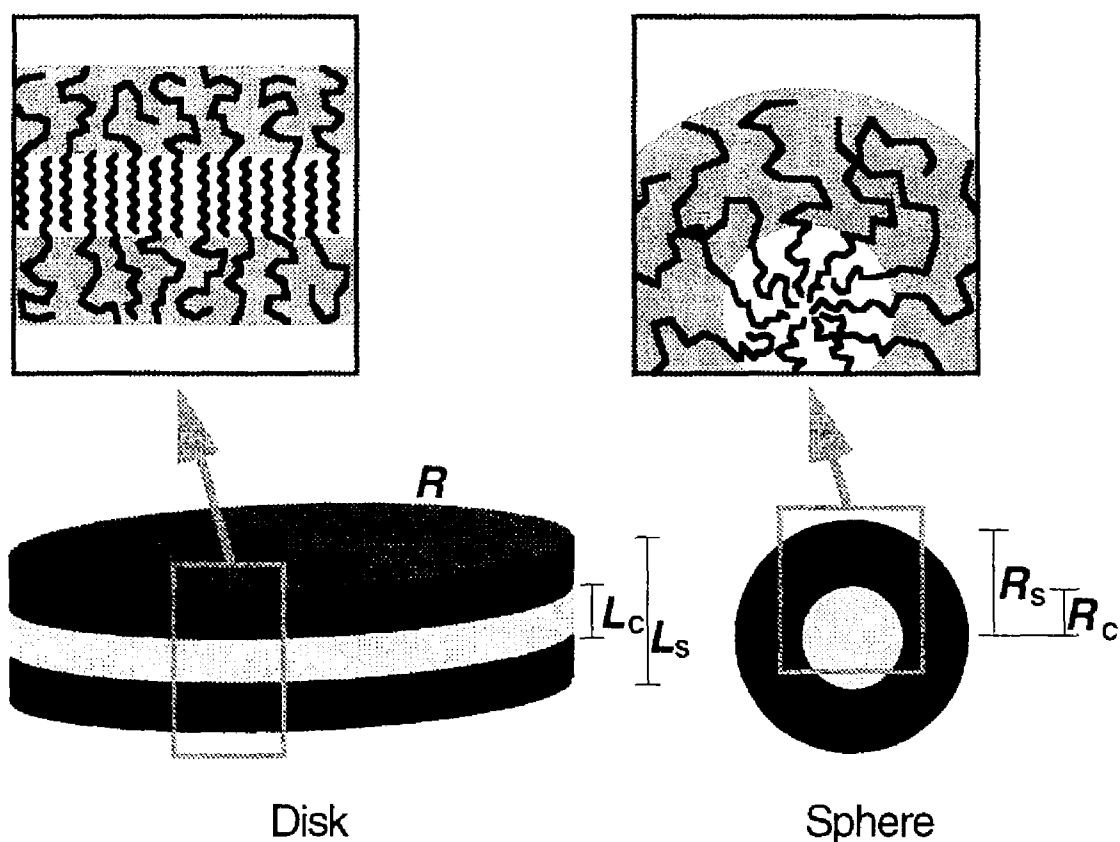
Figure 4.10.   Schematic representation of the structures of spherical micelle and disklike aggregate. The crystallized alkyl chains form the core of a disk surrounded by swollen HOVE chains.

4.6. Conclusions

The amphiphilic polymers ODVE-poly(HOVE) were synthesized by living cationic polymerization and subsequent hydrolysis. The molecular weight determination by MALDI TOF MS was possible because of the fixed length of the hydrophobic chain. The size and shape of micelles formed by these polymers in water were investigated by SAXS and SANS measurements. The aggregation number was reduced with the increase in hydrophilic chain length, while the size of overall micelle was almost independent of the total length of polymer. In addition, the SAXS and SANS data showed a transition from disk to sphere with decreasing temperature for the polymer with the shortest hydrophilic chain. This transition can be explained by the DSC data of the polymer in a solid state, which shows the melting point. We conclude that the disklike aggregates with crystallized core change into the spherical micelles by the melting of octadecyl groups with increasing temperature.

References

(1) Shah, O. D. *Micelles, Microemulsions, and Monolayers*; Marcel Dekker: New York, 1998.

(2) Tanford, C. *The Hydrophobic Effect: Formation of Micelles and Biological Membranes*, 2nd Ed.; John Wiley: New York, 1980.

(3) Tadros, T. F. *Surfactants*; Academic Press: London, 1984.

(4) Halperin, A.; Tirrell, M.; Lodge, T. P. *Adv. Polym. Sci.* **1992**, *100*, 31.

(5) Chu, B. *Langmuir* **1995**, *11*, 414.

(6) Tuzar, Z.; Kratochvil, P. *Advances in Colloid and Interface Science*; Elsevier: Amsterdam, 1976.

(7) Zana, R. *Colloid and Surfaces A: Physicochem. Eng. Aspects* **1997**, *123–124*, 27.

(8) Yamaoka, H.; Matsuoka, H.; Sumaru, K.; Hanada, S.; Imai, M.; Wignall, G. D. *Physica B* **1995**, *213&214*, 700.

(9) Nakano, M.; Matsuoka, H.; Yamaoka, H.; Poppe, A.; Richter, D. *Physica B* **1998**, *241–243*, 1038.

(10) Nakano, M.; Matsuoka, H.; Yamaoka, H.; Poppe, A.; Richter, D. *Macromolecules*, in press.

(11) Sawamoto, M. *Prog. Polym, Sci.* **1991**, *16*, 111.

(12) Minoda, M.; Sawamoto, M.; Higashimura, T. *Macromolecules* **1987**, *20*, 2045.

(13) Kodama, M.; Seki, S. *Adv. Colloid Interface Sci.* **1991**, *35*, 1.

(14) Swanson-Vethamuthu, M.; Feitosa, E.; Brown, W. *Langmuir* **1998**, *14*, 1590.

(15) Kodama, M.; Tsujii, K.; Seki, S. *J. Phys. Chem.* **1990**, *94*, 815.

(16) von Berlepsch, H.; Mittelbach, R.; Hoinkis, E.; Schnablegger, H. *Langmuir* **1997**, *13*, 6032.

(17) Guinier, A.; Fournet, G. *Small-Angle Scattering of X-rays*; John Wiley: New York, 1955.

(18) Glatter, O.; Kratky, O. *Small Angle X-ray Scattering*; Academic Press: London, 1982.

(19) Higgins, J. S.; Benoit, H. C. *Polymers and Neutron Scattering*; Oxford: New York, 1994.

(20) Ise, N.; Okubo, T.; Kunugi, S.; Matsuoka, H.; Yamamoto, K.; Ishii, Y. *J. Chem. Phys.* **1984**, *81*, 3294.

Part II

Synthesis and Aggregation Behavior of Carbosilane Block Copolymers

Chapter 5

Synthesis of Carbosilane Block Copolymers by Means of a

Living Anionic Polymerization of 1,1-Diethylsilacyclobutane

Abstract

Block polymerization of 1,1-diethylsilacyclobutane with styrene derivatives and methacrylate derivatives was investigated. Sequential addition of styrene to a living poly(1,1-diethylsilabutane), which was prepared from phenyllithium and 1,1-diethylsilacyclobutane in THF–hexane at –48 °C, gave poly(1,1-diethylsilabutane)-*block*-polystyrene. Similarly, addition of 4-(*tert*-butyldimethylsiloxy)styrene to the living poly(1,1-diethylsilabutane) provided poly(1,1-diethylsilabutane)-*block*-poly(4-(*tert*-butyldimethylsiloxy)styrene). Poly(1,1-diethylsilabutane)-*block*-poly(methyl methacrylate) was obtained by treatment of living poly(1,1-diethylsilabutane) with 1,1-diphenylethylene followed by an addition of methyl methacrylate. Poly(1,1-diethylsilabutane)-*block*-poly(2-(*tert*-butyldimethylsiloxy)ethyl methacrylate) was also synthesized by adding 2-(*tert*-butyldimethylsiloxy)ethyl methacrylate to the living poly(1,1-diethylsilabutane) which was end-capped with 1,1-diphenylethylene in the presence of lithium chloride.

5.1. Introduction

Polycarbosilanes have been the subject of much interest and were widely studied in the last three decades,[1] since they have quite unique characteristics compared to polysiloxanes and usual hydrocarbon polymers. Applications of polycarbosilanes to advanced materials such as ceramic precursors or heat-resistant polymers have been investigated by many workers.[2] A number of synthetic methods are known for preparation of polycarbosilanes.[3] Despite these developments, little was known about carbosilane block copolymers because of the lack of appropriate synthetic methods to obtain them. Recently, we have reported living anionic ring-opening polymerization of 1,1-dialkyl-substituted silacyclobutanes. Polysilabutanes with well-defined molecular weights and molecular weight distributions can be synthesized by using that technique[4] (Scheme 5.1).
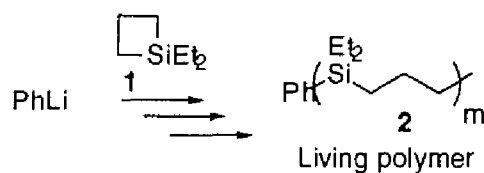
Scheme 5.1.

In this chapter, we report an efficient method to obtain carbosilane block copolymers by using the living polymerization of 1,1-diethylsilacyclobutane (1). Applications to the synthesis of amphiphilic block copolymers containing polycarbosilane as a hydrophobic segment are also described.

5.2. Experimental Section

5.2.1. Materials.

1,1-Diethylsilacyclobutane was prepared by treatment of 1,1-dichlorosilacyclobutane and ethylmagnesium bromide in THF at 0 °C and purified by distillation under re-

duced pressure over lithium aluminum hydride. 1,1-Dichlorosilacyclobutane was purchased from Tisso and used as delivered. Styrene and methyl methacrylate were washed three times with 1M NaOH, three times with water, dried over Na$_2$SO$_4$, and then distilled twice over calcium hydride under reduced pressure. 4-(tert-Butyldimethylsiloxy)styrene[5] and 2-(tert-butyldimethylsiloxy)ethyl methacrylate[6] were prepared according to the reported procedure, and purified by distillation under reduced pressure over calcium hydride. Phenyllithium diethyl ether solution was purchased from Kanto Chemical Co. and used as delivered. Lithium naphthalene was prepared by treatment of lithium metal with naphthalene in THF at room temperature for 3 h. Diphenylethylene was purified by distillation from butyllithium in vacuum. Hexane and tetrahydrofuran (THF) were freshly distilled over sodium benzophenone ketyl under an argon atmosphere before use.

5.2.2. Measurements.

Gel permeation chromatography was carried out in chloroform on a Jasco 880-PU chromatograph equipped with four polystyrene gel columns (Shodex K-802, K-803, K-804, and K-805) and a Jasco 830-RI refractive index detector. ^{1}H NMR spectra were obtained on Varian GEMINI 300 or JEOL GSX 270 spectrometers.

5.2.3. Block Polymerization of 1,1-Diethylsilacyclobutane (1) with Styrene Derivatives.

Block polymerization with 4-(tert-butyldimethylsiloxy)styrene is representative. In a 50-mL round-bottomed flask equipped with a Teflon-covered magnetic stirring bar and a rubber septum were placed THF (5 mL) and hexane (5 mL) under an argon atmosphere. The solvents were titrated with a THF solution of lithium naphthalene to eliminate all reactive impurities. The mixture was cooled to –48 °C and a phenyllithium diethyl ether solution (1.0 M, 0.25 mL, 0.25 mmol) was added, and then 1,1-diethylsilacyclobutane (0.64 g, 0.76 mL,

5.0 mmol) was added. The reaction mixture was stirred at –48°C for 1 h to provide living poly(1,1-diethylsilabutane) (2). 4-(tert-Butyldimethylsiloxy)styrene (1.16 g, 1.05 mL, 5.0 mmol) was added and stirred for another 1 h. Then methanol (0.5 mL) was added to terminate the polymerization. The resulting mixture was poured into brine and extracted with toluene (50 mL). The organic layer was separated, washed with water (50 mL), and dried over anhydrous sodium sulfate. The volatile fractions were removed by evaporation. The resulting product was dissolved in a small amount of toluene and precipitated into excess methanol, filtered out, and dried to give poly(1,1-diethylsilabutane)-block-poly(4-(tert-butyldimethylsiloxy)styrene) (4, 1.35 g). ^{1}H NMR (CDCl$_3$): δ 0.06–0.22 (s, 139H), 0.45–0.61 (m, 194H), 0.77–1.02 (m, 366H), 1.24–1.38 (m, 50 H), 6.18–6.80 (m, 91H), 7.30–7.38 (m, 3H), 7.45–7.52 (m, 2H). M_n = 8600 (determined by ^{1}H NMR), and M_w/M_n = 1.15 (determined by GPC using polystyrene as a standard and CHCl$_3$ as an eluent).

5.2.4. Poly(1,1-diethylsilabutane)-block-polystyrene (3).

^{1}H NMR (CDCl$_3$): δ 0.38–0.65 (m, 182H), 0.76–1.02 (m, 138H), 1.22–1.41 (m, 48H), 6.30–7.24 (m, 119H), 7.31–7.38 (m, 3H), 7.45–7.52 (m, 2H). M_n = 5400 (determined by ^{1}H NMR), and M_w/M_n = 1.09 (determined by GPC).

5.2.5. Deprotection of Poly(1,1-diethylsilabutane)-block-poly(4-(tert-butyldimethylsiloxy)styrene) (4).

Deprotection of tert-butyldimethylsilyl groups was carried out according to the reported procedure.[6] To a solution of polymer 4 (1.35 g) in 1,4-dioxane (40 mL) was added hydrochloric acid (35 wt %, 8 mL). The mixture was heated at 50°C for 3 h. The resulting product was precipitated into water, filtered out, and dried in vacuo to give poly(1,1-diethylsilabutane)-block-poly(4-hydroxystyrene) (5, 0.86 g) in 91% yield. ^{1}H NMR

(CD$_3$OD): δ 0.20–0.66 (m, 194H), 0.67–0.97 (m, 160H), 1.05–1.58 (m, 50H), 6.09–6.81 (m, 90H), 7.10–7.21 (m, 3H), 7.29–7.38 (m, 2H).

5.2.6. End-Capping Experiment of Living Poly(1,1-diethylsilabutane) with Diphenylethylene.

To a living polymer solution prepared from 1 (0.76 mL, 5.0 mmol) and phenyl-lithium (1.00 M, 0.25 mL, 0.25 mmol) in THF (5 mL) and hexane (5 mL) at –48°C for 1 h was added 1,1-diphenylethylene (0.088 mL, 0.50 mmol). The color of the solution turned dark red. After the mixture was stirred for 30 min, methanol (0.5 mL) was added. The resulting mixture was poured into brine and extracted with toluene (30 mL). The organic layer was separated, washed with water (30 mL), and dried over anhydrous sodium sulfate. The volatile fractions were removed under reduced pressure. The product was reprecipitated (toluene/methanol) and dried in vacuo to provide a mixture of polymers 6 and 7 (0.45 g).

^{1}H NMR (CDCl$_3$): δ 0.42–0.61 (m, 182H), 0.74–0.98 (m, 150H), 1.24–1.40 (m, 50H), 2.03 (q, $J = 7.0$ Hz, 2H), 3.85 (t, $J = 7.0$ Hz, 1H), 7.06–7.29 (m, 10H), 7.30–7.37 (m, 3H), 7.42–7.52 (m, 2H). M_n = 3200 (determined by ^{1}H NMR), and M_w/M_n = 1.08 (determined by GPC).

5.2.7. Block Polymerization of 1,1-Diethylsilacyclobutane (1) with Methyl Methacrylate.

To a living polymer solution prepared from 1 (0.64 g, 0.76 mL, 5.0 mmol) and phenyllithium (1.00 M, 0.25 mL, 0.25 mmol) in THF (5 mL) and hexane (5 mL) at –48°C for 1 h was added 1,1-diphenylethylene (0.088 mL, 0.50 mmol). The color of the solution turned dark red. After the solution was stirred for 30 min, methyl methacrylate (0.50 g, 0.54 mL, 5.0 mmol) was introduced, and the whole reaction was stirred for another 1 h. Then,

methanol (0.5 mL) was added to terminate the polymerization, and the resulting mixture was poured into brine and extracted with toluene (50 mL). The organic layer was separated, washed with water (50 mL), and dried over anhydrous sodium sulfate. The volatile fractions were removed by evaporation. The resulting product was dissolved in a small amount of toluene and precipitated into excess methanol, filtered out, and dried to give poly(1,1-diethylsilabutane)-*block*-poly(methyl methacrylate) (9, 0.93 g). ^{1}H NMR (CDCl$_3$): δ 0.39–0.62 (m, 175H), 0.73–1.09 (m, 197H), 1.18–1.40 (m, 49H), 1.75–2.10 (s, 37H), 3.51–3.69 (s, 62H), 7.05–7.25 (m, 10H), 7.30–7.39 (m, 3H), 7.42–7.53 (m, 2H). M_n = 5300 (determined by ^{1}H NMR), and M_w/M_n = 1.19 (determined by GPC).

5.2.8. Block Polymerization of 1,1-Diethylsilacyclobutane (1) with 2-(*tert*-Butyldimethylsiloxy)ethyl Methacrylate.

Lithium chloride (0.35M THF solution, 1.0 mL, 0.35 mmol), THF (5 mL), and hexane (4 mL) were introduced to a reaction flask under an argon atmosphere. Then the solvents were titrated with a THF solution of lithium naphthalene to eliminate reactive impurities. The mixture was cooled to –48°C and a phenyllithium diethyl ether solution (1.0 M, 0.25 mL, 0.25 mmol) and 1,1-diethylsilacyclobutane (0.64 g, 0.76 mL, 5.0 mmol) were added. The reaction mixture was stirred at –48°C for 1 h. To the solution thus prepared, 1,1-diphenylethylene (0.088 mL, 0.50 mmol) was added. The color of the solution turned dark red. After the solution was stirred for 30 min, 2-(*tert*-butyldimethylsiloxy)ethyl methacrylate (1.22 g, 1.30 mL, 5.0 mmol) was introduced, and the whole reaction was stirred for another 1 h. Then, methanol (0.5 mL) was added, and the resulting mixture was poured into brine and extracted with toluene (50 mL). The organic layer was separated, washed with water (50 mL), and dried over anhydrous sodium sulfate. The volatile fractions were removed by evaporation. The resulting product was dissolved in a small amount of toluene and precipitated into excess methanol, filtered out, and dried to give poly(1,1-

diethylsilabutane)-*block*-poly(2-(*tert*-butyldimethylsiloxyethyl methacrylate) (**10**, 1.33 g).

^{1}H NMR (CDCl$_3$): δ -0.10 to 0.17 (s, 146H), 0.27–0.70 (m, 201H), 0.71–1.18 (m, 449H), 1.20–1.49 (m, 53H), 1.70–2.10 (s, 33H), 3.63–3.86 (m, 47H), 3.64–4.17 (m, 47H), 7.05–7.25 (m, 10H), 7.30–7.38 (m, 3H), 7.42–7.52 (m, 2H). M_n = 9400 (determined by ^{1}H NMR), and M_w/M_n = 1.20 (determined by GPC).

5.2.9. Deprotection of Poly(1,1-diethylsilabutane)-*block*-poly(2-(*tert*-butyldimethylsiloxy)ethyl methacrylate) (10).

To a solution of polymer **10** (0.30 g) in 1,4-dioxane (12 mL) was added diluted hydrochloric acid (3 M, 1.0 mL). The mixture was stirred at room temperature for 24 h. Dialysis of the product in water using Spectra MWCO 2000 gave a white precipitate, which was filtered out, and dried *in vacuo* to afford poly(1,1-diethylsilabutane)-*block*-poly(2-hydroxyethyl methacrylate) (**11**, 0.14 g) in 68% yield. ^{1}H NMR (CD$_3$OD): δ 0.20–0.69 (m, 175H), 0.70–1.14 (m, 189H), 1.15–1.63 (m, 60H), 1.69–2.36 (s, 17H), 3.45–4.25 (m, 52 H), 6.88–7.13 (m, 10H), 7.14–7.24 (m, 3H), 7.30–7.41 (m, 2H).

5.3. Results and Discussion

5.3.1. Block Polymerization of 1,1-Diethylsilacyclobutane with Styrene Derivatives.

In a previous paper, we have reported that organolithium-initiated polymerization of 1,1-diethylsilacylobutane (**1**) proceeded in accordance with a living mechanism in THF–hexane (1 : 1) at –48°C.[4b] Here, initially, we examined block polymerization of **1** with styrene. To a solution of living poly(1,1-diethylsilabutane) which was prepared from **1** (5.0

mmol) and phenyllithium (0.25 mmol) in THF–hexane, styrene (5.0 mmol) was added. Polymerization of styrene readily started, and the block copolymer was obtained after termination with methanol (Scheme 5.2, Table 5.1, run 1).
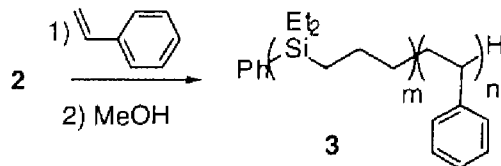
Scheme 5.2.

The formation of the block copolymer was confirmed by GPC measurement. Figure 5.1 shows GPC charts for poly(1,1-diethylsilabutane) homopolymer (**A**) and the obtained polymer (**B**). The GPC curves shifted to a higher molecular weight region with narrow molecular weight distribution (M_w/M_n = 1.09). This indicates clean formation of poly(1,1-diethylsilabutane)-*block*-polystyrene (**3**). The number average molecular weight (M_n) and the composition of the obtained block copolymer (m : n) were determined by ^{1}H NMR integral ratios of signals corresponding to the initiation end group and each polymer segments. The molecular weight of the obtained polymer (M_n = 5400) was in good agreement with M_n calculated from the initial concentration ratio of phenyllithium and the sum of two monomers (M_n = 4700). The composite m : n of the obtained polymer was also in good agreement with the ratio of the initial concentration of each monomer.

This polymerization was applied to synthesis of a functionalized block copolymer consisting of a polystyrene derivative.[5] Addition of 4-(*tert*-butyldimethylsiloxy)styrene (5.0 mmol) to a solution of living polymer prepared from **1** (5.0 mmol) and phenyllithium (0.25mmol) gave poly(1,1-diethylsilabutane)-*block*-poly(4-(*tert*-butyldimethylsiloxy)styrene) (**4**) (Scheme 5.3, Table 5.1, run 2). GPC curves (**A** and **C**) revealed formation of the block copolymer (Figure 5.1), although a contamination of a small amount of silabutane homopolymer was observed.

Table 5.1.   Block Polymerization of 1,1-Diethylsilacyclobutane with Various
Monomers[a]

Run	Second Monomer	Conditions	Polysilabutane		Block Copolymer		
			M_n^b	M_w/M_n^c	M_n^b	$m:n^b$	M_w/M_n^c
1	St[d]	X	3000	1.09	5400	24 : 22	1.09
2	SiOSt[e]	X	3700	1.09	8700	25 : 23	1.15
3	MMA[f]	Y	3200[h]	1.09	5300	23 : 21	1.19
4	SiHEMA[g]	Z	3800[h]	1.07	9400	26 : 27	1.20

[a] Conditions: homopolymerization of 1,1-diethylsilacyclobutane (5.0 mmol) with PhLi (0.25 mmol); X, second monomer (5.0 mmol) was added; Y, 1,1-diphenylethylene (0.5 mmol) and second monomer (5.0 mmol) were added; Z, LiCl (0.35 mmol), 1,1-diphenylethylene (0.5 mmol), and second monomer (5.0 mmol) were added.

[b] Determined by ^{1}H NMR. [c] Determined by GPC using polystyrene as a standard. [d] styrene. [e] 4-(tert-butyldimethylsiloxy)styrene. [f] methyl methacrylate. [g] 2-(tert-butyldimethylsiloxy)ethyl methacrylate. [h] M_n of end-capped polymer.
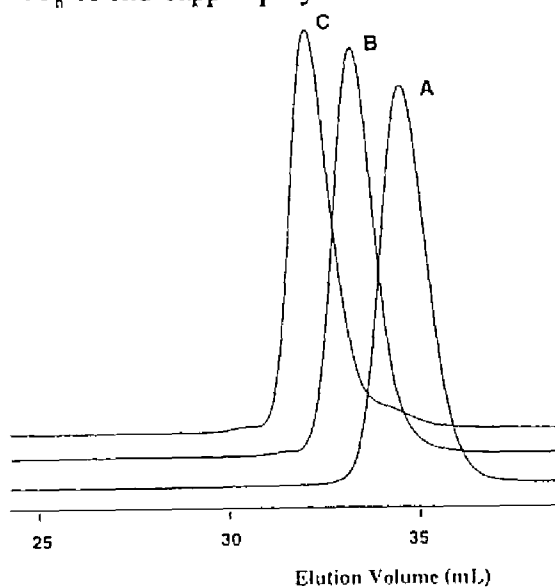
Figure 5.1.   GPC charts: (A) poly(1,1-diethylsilabutane); (B) poly(1,1-diethylsilabutane)-block-polystyrene (3); (C) poly(1,1-diethylsilabutane)-block-poly(4-(tert-butyldimethylsiloxy)styrene) (4).
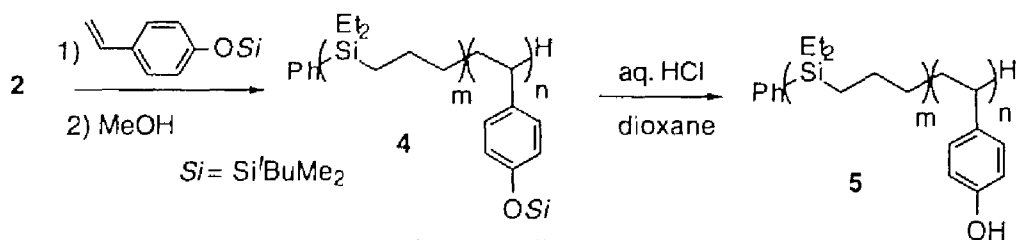
Scheme 5.3.

Hydrolysis of the *tert*-butyldimethylsilyl groups of the polymer 4 was easily achieved by adding hydrochloric acid in dioxane and gave poly(1,1-diethylsilabutane)-*block*-poly(4-hydroxystyrene) (5). Figure 5.2 shows the ^{1}H NMR spectra of the polymer 5. Signals ascribed to poly(1,1-diethylsilabutane), which cannot normally be observed in CD$_3$OD, could be detected in this case. This fact also suggested the formation of a block copolymer. Polymer 5 thus obtained can be considered as an amphiphilic block copolymer because it is soluble in not only a nonpolar solvent such as chloroform but also a polar solvent such as methanol.
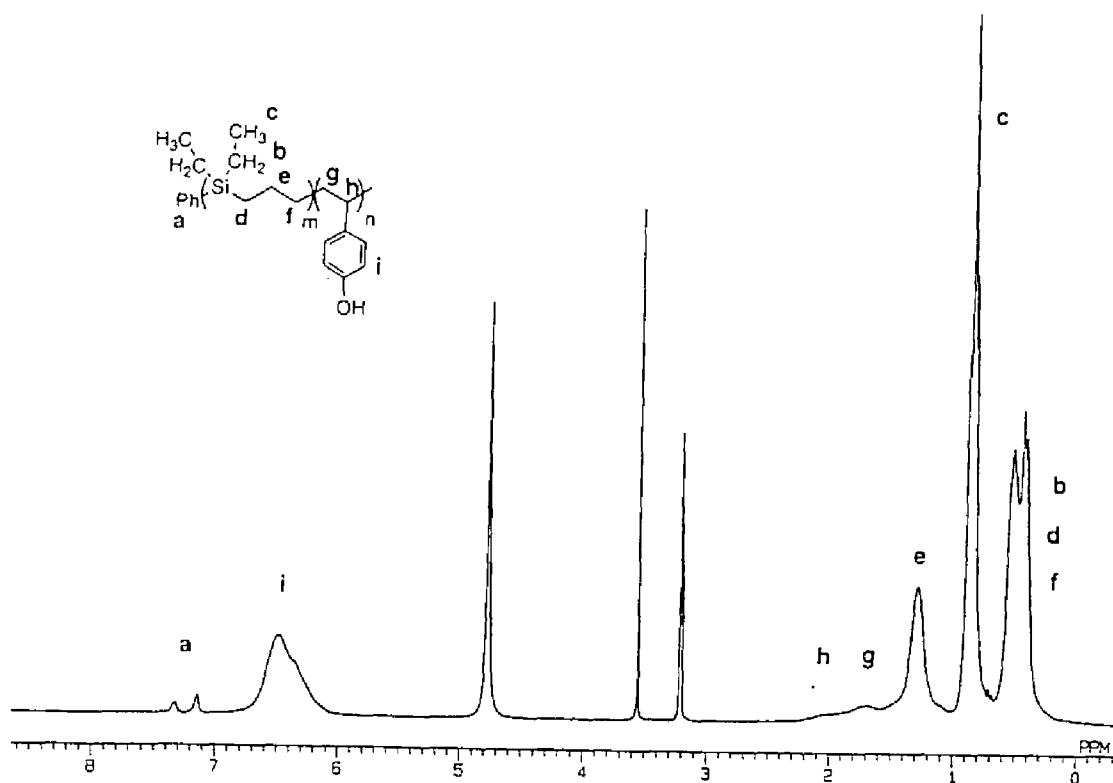
Figure 5.2. 270 MHz ^{1}H NMR spectrum of poly(1,1-diethylsilabutane)-*block*-poly(4-hydroxystyrene) (5) in CD$_3$OD.

5.3.2. Block Polymerization of 1,1-Diethylsilacyclobutane with Methyl Methacrylate.

To explore block polymerization with monomers other than styrene derivatives, polymerization with methacrylate esters was studied. However, direct addition of methyl methacrylate to a living poly(1,1-diethylsilabutane) did not give poly(1,1-diethylsilabutane)-block-poly(methyl methacrylate) selectively, probably because the propagating center of the living poly(1,1-diethylsilabutane) is too reactive to polymerize methyl methacrylate in a controlled manner.

To decrease reactivity of the living center, end-capping of the living anion with 1,1-diphenylethylene[7] was performed. On addition of 1,1-diphenylethylene (0.5 mmol) to the living polymer, the color of the solution immediately turned red, and 30 min after the addition, the reaction was quenched with methanol and the product purified by precipitation (Scheme 5.4). Figure 5.3 shows the ^{1}H NMR spectrum of the obtained polymer. The polymer end was successfully capped with 1,1-diphenylethylene. The efficiency of the end-capping ($6/(6 + 7)$) was 0.95, which was determined from the integral ratio of phenyl group absorption at d 7.30–7.52 (initiation end) and d 7.06–7.29 (termination end).
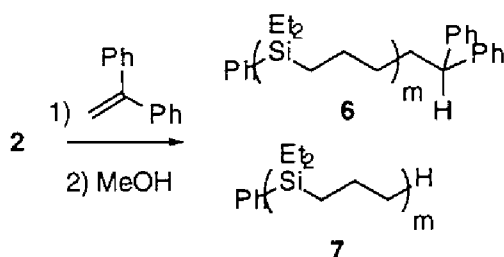
Scheme 5.4

It is well-known that (1,1-diphenylalkyl)lithium can polymerize methacrylate esters to provide poly(methacrylate esters) with controlled molecular weights and sufficiently narrow molecular weight distributions.[7a,8] Therefore, polymerization of methyl methacrylate by using living poly(1,1-diethylsilabutane) end-capped with 1,1-diphenylethylene was reexamined. As a result, poly(1,1-diethylsilabutane)-block-poly(methyl methacrylate) (9) was ob-

tained efficiently by an addition of methyl methacrylate to the end-capped living polymer **8** (Scheme 5.5, Table 5.1, run 3). GPC curves (**A** and **B**) in Figure 5.4 indicate the formation of the block copolymer. The number average molecular weight (M_n = 5300) and the composition of the obtained block copolymer ($m : n$ = 23 : 21) determined by ^{1}H NMR were in good agreement with the value calculated from the initial concentration ratio of phenyllithium, **1**, and methyl methacrylate.

Scheme 5 5.
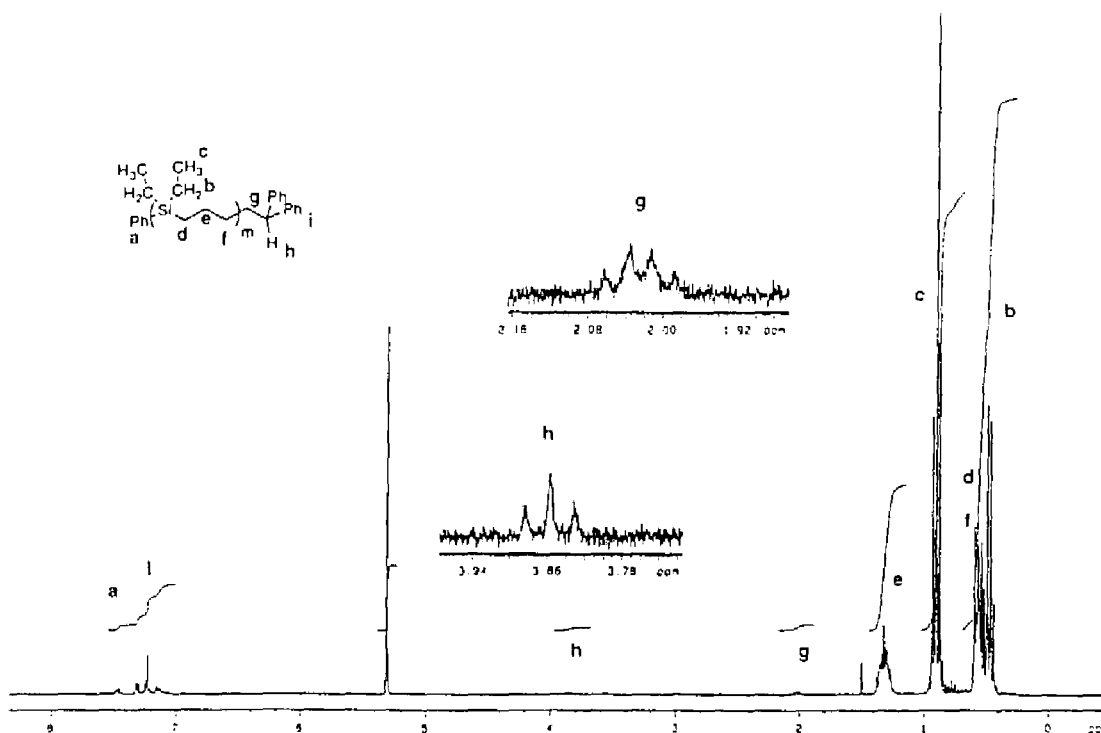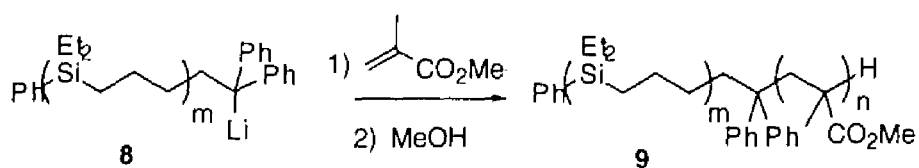
Figure 5.3. 300 MHz ^{1}H NMR spectrum of the product obtained by end-capping reaction in CD_2Cl_2.

-84-

5.3.3. Block Polymerization of 1,1-Diethylsilacyclobutane with 2-(*tert*-Butyldimethylsiloxy)ethyl Methacrylate.

Hirao and Nakahama reported that living polystyrene end-capped with 1,1-diphenylethylene could polymerize functionalized methacrylates such as 2-(trimethylsiloxy)ethyl methacrylate or 2-(*tert*-buthyldimethylsiloxy)ethyl methacrylate smoothly in the presence of lithium chloride.[6] Accordingly, block polymerization of 1,1-diethylsilacyclobutane with 2-(*tert*-butyldimethylsiloxy)ethyl methacrylate was examined. Addition of 2-(*tert*-butyldimethylsiloxy)ethyl methacrylate (5.0 mmol) to a living poly(1,1-diethylsilabutane) end-capped with 1,1-diphenylethylene (8) in the presence of lithium chloride (0.35 mmol) gave poly(1,1-diethylsilabutane)-*block*-poly(2-(*tert*-butyldimethylsiloxy)ethyl methacrylate) (10) (Scheme 5.6, Table 5.1, run 4). The GPC charts for the block polymerization are shown in Figure 5.4. The GPC curves (A and C) showed the formation of the block copolymer. The small tailing peak of the chart C in lower molecular weight region is considered as that of silabutane homopolymer, and the small leading peak in higher
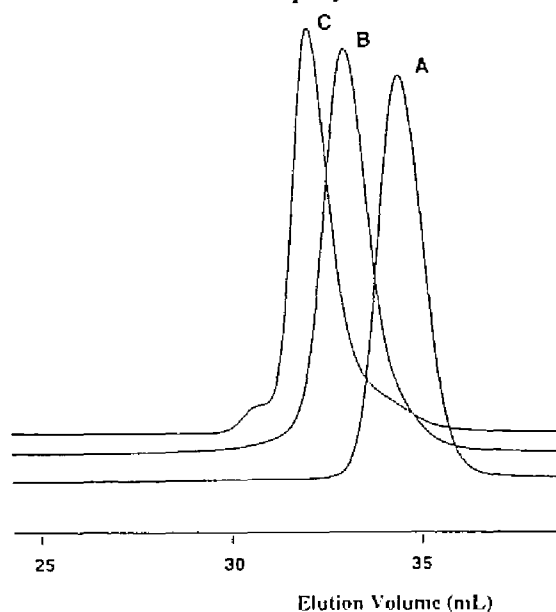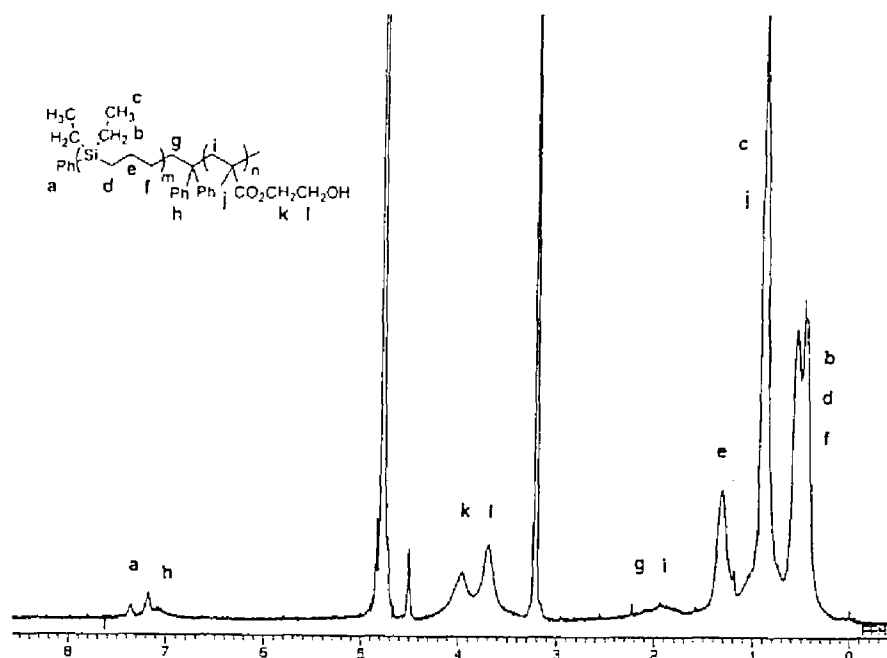

Figure 5.4. GPC charts: (A) poly(1,1-diethylsilabutane) end-capped with 1,1-diphenylethylene; (B) poly(1,1-diethylsilabutane)-*block*-poly(methyl methacrylate) (9); (C): poly(1,1-diethylsilabutane)-*block*-poly(2-(*tert*-butyldimethylsiloxy)ethyl methacrylate) (10).

molecular weight region might be ascribed to oxidatively coupled block copolymer which was produced at the termination procedure.

Scheme 5. 6.
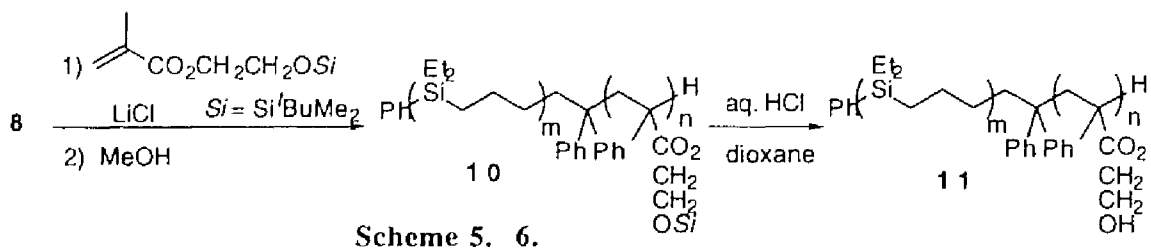
The *tert*-butyldimethylsilyl groups were easily hydrolyzed with $3M$ HCl in dioxane, and poly(1,1-diethylsilabutane)-*block*-poly(2-hydoxyethyl methacrylate) (**11**) was obtained. Figure 5.5 shows the ^{1}H NMR spectrum of polymer **11** in CD_3OD. It is noteworthy that signals ascribed to poly(1,1-diethylsilabutane), which is insoluble in methanol, could be observed. This result provides another evidence for the formation of the block copolymer. Because polymer **11** (1 wt %) was soluble in a polar solvent such as methanol or even in a methanol−water (1 : 5) mixture as well as in a nonpolar solvent such as chloroform, it can be considered as a nonionic amphiphilic block copolymer.

Figure 5.5. 270 MHz ^{1}H NMR spectrum of poly(1,1-diethylsilabutane)-*block*-poly(2-hydroxyethyl methacrylate) (**11**) in CD_3OD.

5.4. Conclusions

An anionic polymerization of 1,1-diethylsilacyclobutane was successfully applied to block copolymer synthesis. Block copolymers consisting of polysilabutane and polystyrenes were obtained by sequential addition of a styrene monomer to the living polysilabutane. On the other hand, block copolymers consisting of polysilabutane and poly(methacrylate ester)s were obtained by an addition of methacrylate ester monomers to living polysilabutane end-capped with 1,1-diphenylethylene. It is noteworthy that polysilabutane-*block*-poly(4-hydroxystyrene) and polysilabutane-*block*-poly(2-hydroxyethyl methacrylate) have amphiphilic character. These polymers are expected to be new functional materials such as polymer surfactants. Physical properties of the latter block copolymer will be reported in the following two chapters.

References

(1) (a) Zeldin, M.; Wynne, K. J.; Allcock, H. R. *Inorganic and Organometallic Polymers.*
ACS Symposium Series 360; American Chemical Society: Washington, DC, 1988. (b)
Zeigher, J. M.; Fearon, F. W. G. *Silicon-Based Polymer Science, Advances in Chemis-
try Series 224*; American Chemical Society: Washington, DC, 1990. (c) Richard, G. J.,
Ed., *Silicon-Containing Polymers*; The Royal Society of Chemistry: Cambridge, 1995. (d)
Kricheldorf, H. R., Ed., *Silicon in Polymer Synthesis*; Springer: Berlin, 1996.

(2) (a) Yajima, S.; Hayashi, J.; Omori, M. *Chem. Lett.* **1975**, 931. (b) Yajima, S.;
Hayashi, J.; Omori, M. *Chem. Lett.* **1975**, 1209. (c) Itoh, M.; Mitsuzuka, M.; Iwaka, K.;
Inoue, K. *Macromolecules* **1994**, *27*, 7917. (d) Ohshita, J.; Ishii, M.; Ueno, Y.;
Yamashita, A.; Ishikawa, M. *Macromolecules* **1994**, *27*, 5583.

(3) For example, see the following.

synthesis of polysilabutanes: (a) Matsumoto, K.; Miyagawa, K.; Yamaoka, H. *Macromole-
cules* **1997**, *30*, 2524. (b) Matsumoto, K.; Shimazu, H.; Yamaoka, H. *J. Polym. Sci.,
Part A: Polym. Chem.* **1998**, *36*, 225. (c) Nametkin, N. S.; Vdvin, V. M.; Zav'yalov, V.
I. *Dokl. Akad. Nauk, SSSR* **1965**, *162*, 824. (d) Nametkin, N. S.; Poletaev, V. A.;
Zav'yalov, V. I.; Vdovin, V. M. *Dokl. Akad. Nauk, SSSR* **1971**, *198*, 1096. (e) Nametkin,
N. S.; Bespalova, N. B.; Ushakov, N. V.; Vdovin, V. M. *Dokl. Akad. Nauk, SSSR* **1973**,
209, 621.

Synthesis of polysilamethylenes: (f) Weyenberg, D. R. *J. Org. Chem.* **1965**, *30*, 2168. (g)
Koopmann, F.; Frey, H. *Macromolecules* **1996**, *29*, 3071. (h) Rushkin, I. L.; Interrante,
L. V. *Macromolecules* **1996**, *29*, 5784.

Synthesis of polysilapent-3-enes: (i) Zhang, X.; Zhou, Q.; Weber, W. P.; Horvath, R. F.;
Chan, T. H.; Manuel, G. *Macromolecules* **1998**, *21*, 1563.

Synthesis of other polycarbosilanes: (j) Dunnavant, W. R. *Inorg. Macromol. Rev.* **1971**, *1*, 165. (k) Noltes, J. G.; van der Kerk, G. J. M. *Rec. Trav. Chim.* **1962**, *81*, 565. (l) Birot, M.; Pillot, J.; Dunogues, J. *Chem. Rev.* **1995**, *95*, 1443. (m) Yamashita, H.; Tanaka, M. *Bull. Chem. Soc. Jpn.* **1995**, *68*, 403.

(4) (a) Matsumoto, K.; Yamaoka, H. *Macromolecules* **1995**, *28*, 7029. (b) Matsumoto, K.; Shimazu, H.; Deguchi, M.; Yamaoka, H. *J. Polym. Sci., Part A: Polym. Chem.* **1997**, *35*, 3207.

(5) Hirao, A.; Takenaka, K.; Packirisamy, S.; Yamaguchi, K.; Nakahama, S. *Macromol. Chem.* **1985**, *186*, 1157.

(6) Mori, H.; Wakisaka, O.; Hirao, A.; Nakahama, S. *Macromol. Chem. Phys.* **1994**, 195, 3213.

(7) (a) Ramireddy, C.; Tuzar, Z.; Prochazka, K.; Webber, S. E.; Munk, P. *Macromolecules* **1992**, *25*, 2541. (b) Gauthier, S.; Eisenberg, A. *Macromolecules* **1987**, *20*, 760.

(8) (a) Anderson, B. C.; Andrews, G. D.; Arthur, J. P.; Jacobson, H. W.; Playtis, A. J.; Sharkey, W. H. *Macromolecules* **1981**, *14*, 1599. (b) Luts, P.; Masso, P.; Beinert, G.; Rempp, P. *Polym. Bull.* **1986**, *15*, 127.

Chapter 6

Self-Assembly of Poly(1,1-diethylsilabutane)-*block*-poly(2-hydroxyethyl methacrylate) Block Copolymer.

1. Micelle Formation and Micelle–Unimer–Reversed Micelle Transition by Solvent Composition

Abstract

Amphiphilic block copolymer poly(1,1-diethylsilabutane)-*block*-poly(2-hydroxy-ethyl methacrylate) (poly(SB-*b*-HEMA)) was synthesized by living anionic polymerization of 1,1-diethylsilacyclobutane with 2-(*tert*-butyldimethylsiloxy)ethyl methacrylate, and subsequent hydrolysis of silyl-protecting groups. These copolymers formed spherical micelles in methanol. Small-angle X-ray scattering (SAXS) measurements revealed that the aggregation number of the micelle strongly depends on the polymer composition, while total micellar size is almost independent of the degree of polymerization of HEMA. SAXS measurements were also performed for the polymer with the highest degree of polymerization of SB in methanol/toluene mixed solvents. The polymer in the solution was found to have different morphology depending on the mixing ratio of the solvent; i.e., micelle–unimer–reversed micelle transition with increasing toluene content was clearly observed.

6.1. Introduction

Block copolymers self-assemble in selective solvents. They form micelles in bulk consisting of an inner core composed of solely insoluble segments and outer shell of soluble segments swollen by the solvent. They are also adsorbed at the surface when insoluble segments favorably interact to the surface. Many groups have studied these specific behavior of amphiphilic polymers during the past few decades.[1-4]

Copolymers with narrow molecular weight distribution (MWD) must be obtained to analyze the properties of their self-assembly systems. We have been trying to create novel amphiphilic polymers with narrow MWD and investigate their properties.[5-8] Previously, we have reported the living anionic ring-opening polymerization of 1,1-diethylsilacyclobutane, and block polymerization with methacrylate derivatives,[9] which was also descrived in Chapter 5. Since 1,1-diethylsilabutane (SB) is a typical nonpolar segment and 2-hydroxyethyl methacrylate (HEMA) has high polarity, the block copolymer having both segments is expected to behave as an amphiphile. Nakahama et al. have reported that the surface of amphiphilic copolymer films contain HEMA as a hydrophilic segment changes to hydrophilic one when it is exposed to water and reverts to hydrophobic by annealing.[10] The copolymers which we present here can also show interesting environment responses.

In this chapter, the micellar structure of amphiphilic block copolymers poly(1,1-diethylsilabutane)-*block*-poly(2-hydroxyethyl methacrylate) (poly(SB-*b*-HEMA)) in methanol and methanol/toluene mixed solvents has been investigated by small-angle X-ray scattering[11,12] (SAXS) technique. It was clearly confirmed that the micelle shape relates to the polymer composition and the solvent composition.

6.2. Experimental Section

6.2.1. Synthesis and Characterization of the Poly(SB-b-HEMA) Block Copolymers.

Block   copolymers,   poly(1,1-diethylsilabutane)-block-poly(2-(tert-butyldimethylsiloxy)ethyl methacrylate) were synthesized by living anionic polymerization. The resulting polymers were hydrolyzed by diluted hydrochloric acid for the deprotection of tert-butyldimethylsilyl groups and lead to amphiphilic block copolymers, poly(SB-b-HEMA) (see Figure 6.1). These procedures have been described in detail in Chapter 5.
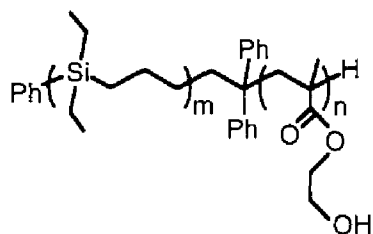
Figure 6.1. Chemical structure of poly(SB-b-HEMA) block copolymer.

For characterization of polymers, gel permeation chromatography (GPC) was carried out on a Jasco 880-PU chromatograph equipped with four polystyrene gel columns (Shodex K-802, K-803, K-804, and K-805) and a Jasco 830-RI refractive index detector. ^{1}H NMR spectra were obtained on a JEOL GSX 270 spectrometer. Molecular characterization of the copolymers were performed before hydrolysis, since chloroform which is the eluent of GPC was not a good solvent for HEMA, while the precursor polymers were molecularly dissolved in chloroform. In addition, we confirmed by ^{1}H NMR that no sub-reaction had taken place during hydrolysis, such as polymer degradation process.

Three copolymers with different compositions were prepared by changing the monomer/initiator ratio on polymerization, whose characteristics are tabulated in Table 6.1. The number-averaged degree of polymerization of SB (m) and HEMA (n) were determined

by ^{1}H NMR, and M_w/M_n were determined by GPC, where M_w and M_n are the weight- and number-averaged molecular weights, respectively. Polymer A has nearly the same length of polar segment and longer nonpolar segment than polymer B, and polymer C has the same value of m and larger n than polymer B. Then, polymer A is the copolymer with the highest hydrophobicity.

6.2.2. Small-Angle X-ray Scattering (SAXS).

The SAXS measurements were performed using a Kratky type camera (Rigaku Corporation, Tokyo) equipped with a rotating anode X-ray generator and a position sensitive proportional counter (PSPC). The SAXS instrument has been described in detail elsewhere.[13]

Methanol and toluene (extra pure grade) were used without further purification. Methanol/toluene solvent mixtures with different mixing ratios in volume were prepared. Polymer solutions were prepared by direct dissolution of the copolymer into methanol or solvent mixtures. In all cases, the polymer concentration was 1 wt % and measurement was performed at room temperature. Sample solutions were measured in glass capillaries (Mark, Berlin) with a diameter of 2 mm. In experimental data, the scattering intensity of corresponding solvent has been subtracted.

6.3. Results and Discussion

6.3.1. Micelle Formation in Methanol.

Since methanol is a good solvent for HEMA and a poor solvent for SB, the block copolymers are expected to form micelles in methanol consisting of a core composed of SB and a shell of HEMA swollen by the solvent. SAXS profiles of the copolymers in methanol

are shown in Figure 6.2. Strong scattering at small angles is observed in all cases, suggesting the micelle formation indeed. In addition, the scattering curves exhibit a well-marked secondary maximum, indicating a well-defined structure of micelles.

Model fitting of the experimental data was performed. Simple core–shell spherical model was adopted, the form factor of which is given as follows:[11]

$$P(q) = \{(\rho_c - \rho_s)V_c F_c(q) + (\rho_s - \rho_0)V_s F_s(q)\}^2 \tag{6.1}$$

$$F_c(q) = 3 (\sin(qR_c) - qR_c \cos(qR_c)) / (qR_c)^3 \tag{6.2}$$

$$F_s(q) = 3 (\sin(qR_s) - qR_s \cos(qR_s)) / (qR_s)^3 \tag{6.3}$$

R_c and R_s denote the radii of the core and the overall micelle, ρ_c, ρ_s, ρ_0 the electron densities of the core, the shell and the solvent, V_c and V_s the volumes of the core and the overall micelle, respectively. The scattering vector q is given by $q = 4\pi \sin\theta/\lambda$, where 2θ is the scattering angle and λ is the X-ray wavelength. Here, we assume homogeneous electron density distributions inside the core and the shell. Using the calculable values of the electron densities of the monomer units (ρ_{SB} and ρ_{HEMA}) and the solvent (ρ_0), ρ_c and ρ_s are given by

$$\rho_c = \rho_{SB} \tag{6.4}$$

$$\rho_s = \phi_{Sol}\rho_0 + (1 - \phi_{Sol})\rho_{HEMA} \tag{6.5}$$

where ϕ_{Sol} is the volume fraction of the solvent in the shell, which can be calculated by the following equation with the degree of polymerization of HEMA (n), and the volume of HEMA repeat units (v_{HEMA}):

$$\phi_{Sol} = 1 - N_{agg} \, n \, v_{HEMA} / (V_s - V_c) \tag{6.6}$$

N_{agg} denotes the aggregation number of the micelles, which is calculated from V_c, the degree of polymerization of SB (m), and the volume of SB repeat units (v_{SB}):

$$N_{agg} = V_C / (m \, v_{SB})$$ (6.7)

Assuming that the critical micelle concentration is negligibly low, i.e., all polymers contribute to the micelle formation, the number density n_p of the micelles is then calculated

$$n_p = \phi / (N_{agg} (m \, v_{SB} + n \, v_{HEMA}))$$ (6.8)

where ϕ is the volume fraction of copolymer in solution. The scattering intensity is finally given by the product of the form factor and the number density of the micelles. However, we introduced a shift factor f, since the intensity of the experimental data is obtained in arbitrary units because the data have not been calibrated to an absolute scale.

$$I(q) = f \, n_p \, P(q)$$ (6.9)

The values of $\rho_{SB} = 0.280$, $\rho_{HEMA} = 0.396$, and $\rho_0 = 0.268$ [Å^{-3}] were fixed, and three parameters, R_C, R_S, and f were variables in the fitting procedure, while the value of f was arranged to be the same for all data.
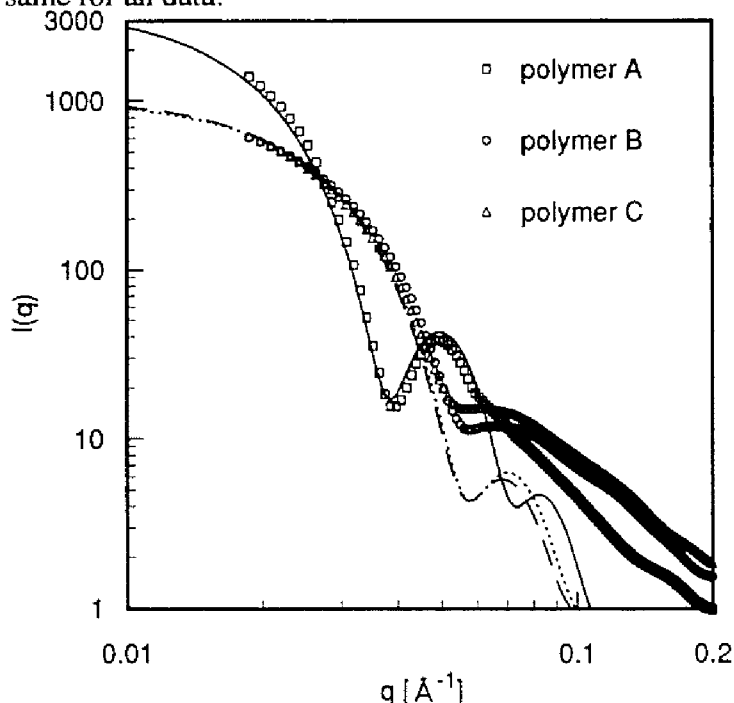
Figure 6.2. SAXS profiles of poly(SB-b-HEMA) in methanol. Solid, dotted and broken lines are theoretical curves of core-shell spherical model for polymer A, B and C, respectively.

The SAXS curves were well reproduced by the theoretical curves as shown in Figure 6.2 with the parameters listed in Table 6.1. To obtain better agreement between experimental and theoretical curves, Gaussian type distribution function was introduced for taking into account the polydispersity of micellar size. The deviation at larger angles is due to the low accuracy of the measured curves in this range, and also due to the fact that the scattering at larger angles is dominated by individual fluctuation of polymer chains in the shell (blobs), which was not considered in the present core-shell model. The resultant value of the polydispersity (σ/R_S) was about 12% in all cases. From Table 6.1, one can qualitatively understand the relationship between polymer composition and micellar structure. Increase of SB chain length (m) or reduction of HEMA length (n) enhances the aggregation number (or R_C). On the other hand, total micellar size (R_S) is almost independent of n, which is found by comparison of polymer B and C.

Table 6.1.   Characterization of Poly(SB-b-HEMA) and Their Micelles in Methanol

| polymer	$m : n^a$	M_w/M_n^b	R_C [Å]^c	R_S [Å]^c	N_{agg}^c	ϕ_{Sol}^c
A	26 : 24	1.20	64	105	164	0.82
B	12 : 22	1.20	33	76	47	0.89
C	13 : 37	1.28	28	78	27	0.91

^{a} Obtained by ^{1}H NMR before hydrolysis. ^{b} By GPC before hydrolysis. ^{c} By fitting the SAXS data. R_C and R_S are the radii of the core and the overall micelle, N_{agg} the aggregation number, ϕ_{Sol} the volume fraction of the solvent in the shell, respectively.

## 6.3.2. Relationship between Polymer Morphology and Solvent Composition.

Toluene is a good solvent for SB and poor solvent for HEMA, in contrast with methanol. Since methanol and toluene are miscible with each other, the effect of solvent selectivity on polymer morphology can be investigated by utilization of a methanol/toluene mixed solvent with changing its mixing ratio. Polymer A was used for this purpose, because polymers B and C were not soluble in toluene, which produced a turbid suspension with a small amount of precipitate due to the shorter nonpolar chain. Seven solvent mixtures of different mixing ratios and two pure solvents (methanol:toluene = 8:0, 7:1, 6:2, 5:3, 4:4, 3:5, 2:6, 1:7, 0:8) were prepared. SAXS profiles of polymer A in these solvents are shown in Figures 3–5. The scattering profile clearly depends on the mixing ratio. With increase of the volume fraction of toluene, the intensity at small angles decreases and secondary maximum shifts to a larger q and becomes broader first (Figure 6.3), then the intensity increases again when the amount of toluene exceeds that of methanol. However, the secondary maximum is not observed (Figures 6.4 and 6.5). The morphology of the copolymer in the solutions studied here can be classified into three regimes:

Micelle Region (methanol:toluene = 8:0, 7:1, 6:2, 5:3). The solutions under methanol-rich conditions show SAXS profiles similar to that in pure methanol, providing a clear secondary maximum peak as shown in Figure 6.3. These profiles suggest the micelle formation, and were fitted by theoretical curves of a core–shell model assuming a solid core composed by pure SB and a solvent-swollen shell of HEMA. The fitting curves are shown by lines in Figure 6.3. The fitting curves convoluted the distribution function of R_s as described above. The scattering at smaller angles and the secondary maximum are well reproduced by fitting curves. Only the case of methanol:toluene = 5:3, the height of secondary maximum could not coincide, which is probably due to the fact that unimers, which will be described later, also exist in the micellar solution to some extent.
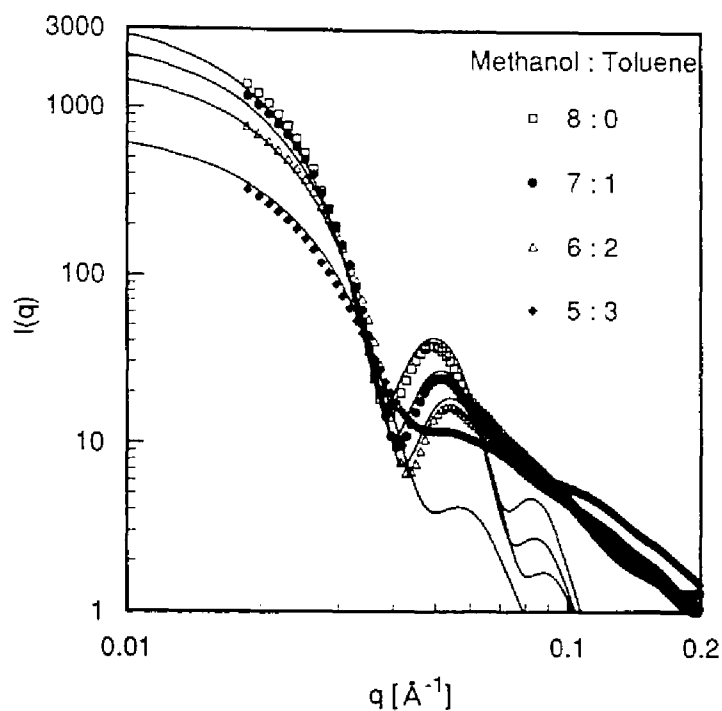
Figure 6.3. SAXS profiles of polymer A ($m : n = 26 : 24$) in methanol/toluene solvent mixtures. The polymers are suggested to form micelles under methanol-rich conditions.
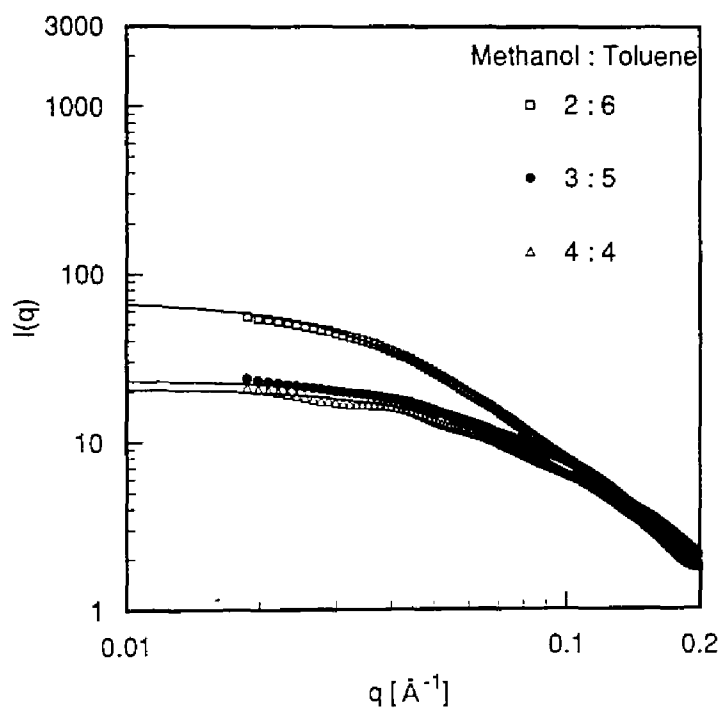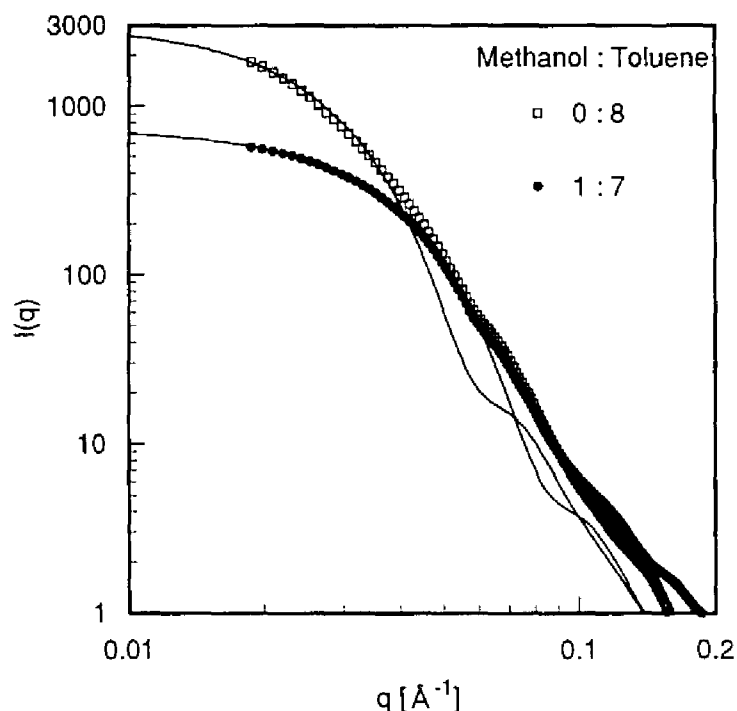

Figure 6.4. SAXS profiles of polymer A ($m : n = 26 : 24$) in methanol/toluene solvent mixtures. The polymers are suggested to exist in an unimer state at intermediate mixing ratios.

Unimer Region (methanol:toluene = 4:4, 3:5, 2:6). The scattering from the solution at intermediate mixing ratios is weak and shows a monotonic decrease against q, as can be seen Figure 6.4. The scattering profiles could be fitted by Debye formula[14] which is applied for Gaussian chains with the radius of gyration R_G:

$$P(q) = 2\{x - 1 + \exp(-x)\}/x^2 \qquad (6.10)$$

$$x = q^2 R_G^2 \qquad (6.11)$$

The good agreement between experimental and theoretical curves indicates that the polymers exist in an unimer state in these solutions. Obtained R_G values were small enough for 4:4 (22 Å) and 3:5 solutions (23 Å), which also suggests the unimer state. In the case of 2:6 solution, however, both the scattering intensity at smaller angles and the radius of gyration (40 Å) were larger than the others, implying a possibility of the formation of small aggregates. If the aggregation number is assumed to be proportional to the forward scattering intensity, it can be approximately calculated to be 3 by comparison with 3:5 solution.

Figure 6.5. SAXS profiles of polymer A ($m : n = 26 : 24$) in methanol/toluene solvent mixtures. The polymers are suggested to form reversed micelles under toluene-rich conditions.

Reversed Micelle[15] **Region (methanol:toluene = 1:7, 0:8).** Under toluene-rich conditions, the copolymers can be assumed to form reversed micelles, since the strong scattering was observed at smaller angles as shown in Figure 6.5 and the scattering profile could not be fitted by Debye function. In these conditions, the electron density of SB ($\rho_{SB} = 0.280$ [$Å^{-3}$]) is almost identical to that of solvent ($\rho_0 = 0.281$ and 0.283 for 1:7 and 0:8, respectively), then the swollen shell of SB is "invisible" and only the core composed by HEMA is observed by X-ray. It should be noticed that the scattering intensity at wider angles obeys the Porod law,[16] i.e., it follows the power law of q^{-4}. This relation is satisfied if the boundary between the scattering objects and the matrix is sharp. Hence this observation means that the micelle has the smooth interface between the core and the shell, since only the core is observed in these conditions. Assuming $\rho_S = \rho_0$ in eq (6.1), the scattering data were fitted by the form factor of homogeneous sphere, and here the distribution function of R_C was convoluted. The fitting curves are also shown in Figure 6.5. The good agreement with experimental data was observed at smaller angles. However, a small discrepancy arises at larger angles where a "shoulder" is observed in theoretical curves in spite of high polydispersity introduced ($\sigma/R_S \sim 20\%$) to smear the secondary maximum. It is probably due to the oversimplification of the model. It may indicate the formation of anisotropic micelles, which will be mentioned below. However, we have not performed precise fitting using complicated models.

All the fitting results are shown in Table 6.2. The obtained aggregation number was plotted against the volume fraction of toluene in solvent ($\phi_{toluene}$) in Figure 6.6 with schematic representation of the aggregation style. On the plot, the aggregation number of 2:6 solution was assumed to be 3. The copolymer forms relatively large micelles in methanol ($\phi_{toluene} = 0$). With an increase of $\phi_{toluene}$, the solubility of the nonpolar chain (SB) increases,

then the aggregation number decreases. At $\phi_{toluene} \sim 0.5$, no aggregate is formed since both

HEMA and SB are soluble. A further increase of $\phi_{toluene}$ reduces the solubility of the polar

chain (HEMA), induces the formation of the reversed micelles, and enhances the aggrega-

tion number. Similar behavior has been reported for polystyrene-b-poly(ethylene/propylene)

block copolymer in n-dodecane/1,4-dioxane mixtures.[17] In pure toluene ($\phi_{toluene} = 1$), quite

Table 6.2.   SAXS Results of Polymer A in Methanol/Toluene Mixture

$\phi_{toluene}$[a]	shape	R_C [Å]	R_S [Å]	R_G [Å]	N_{agg}	ϕ_{Sol}
0	micelle[b]	64	105	—	164	0.82
0.125	micelle[b]	58	103	—	122	0.86
0.25	micelle[b]	53	98	—	93	0.88
0.375	micelle[b]	39	89	—	37	0.94
0.5	unimer[c]	—	—	22	—	—
0.625	unimer[c]	—	—	23	—	—
0.75	unimer[c]	—	—	40	—	—
0.875	reversed micelle[d]	48	—	—	113	—
1	reversed micelle[d]	69	—	—	332	—

[a] The volume fraction of methanol in solvent. [b] SAXS data was fitted by core–shell model

with parameters R_C and R_S. [c] SAXS data was fitted by Debye function with a parameter R_G.

[d] SAXS data was fitted by homogeneous sphere model with a parameter R_C.

large aggregates are formed, and in fact, the obtained value of $R_C = 69$ Å is larger than the contour length of the HEMA block of the copolymer (60 Å). It implies the possibility of a formation of anisotropic micelles of which one or two dimensions are less than the contour length. Indeed, the scattering curve at $\phi_{toluene} = 1$ could be fitted by the theoretical curve of prolate ellipsoid whose half length of the minor axes corresponds to the contour length, and the ratio of major and minor axes is 3:1. However, we cannot conclude here about the micellar shape, since the scattering profile is hardly distinguishable between ellipsoids and polydisperse spheres, moreover, making sure of an existence of large dimensional aggregates (cylinder, for example) needs the information at smaller angles than that covered in this experiment.
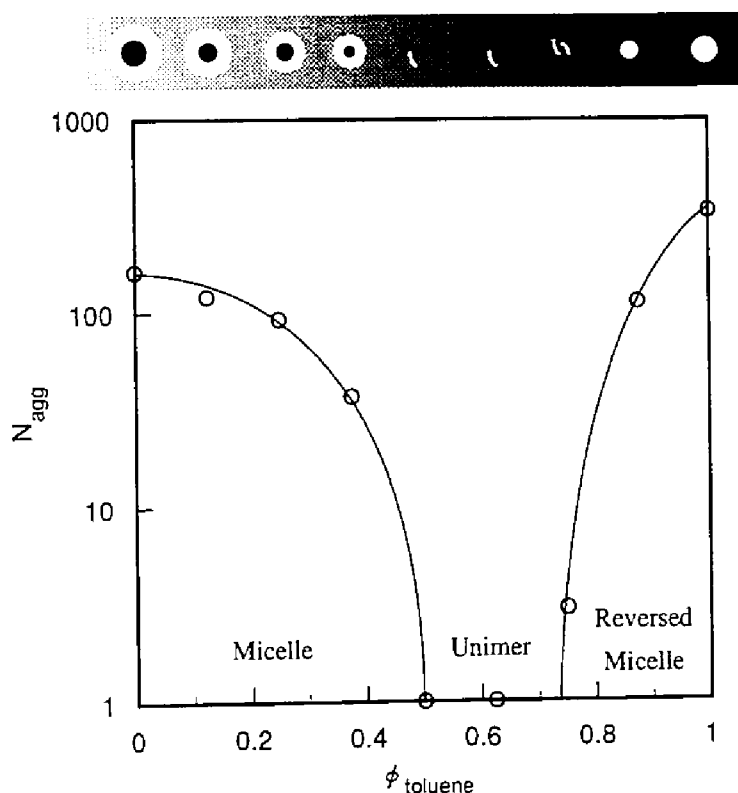
Figure 6.6. The aggregation number of polymer A ($m : n = 26 : 24$) as a function of the volume fraction of toluene in solvent.

6.4. Conclusions

Amphiphilic block polymers of poly(SB-*b*-HEMA) were synthesized by living anionic polymerization. SAXS measurements were performed for these copolymers in methanol and in methanol/toluene mixtures. They formed spherical micelles in methanol, whose aggregation numbers were dependent on the polymer composition as follows: increase of SB chain length or reduction of HEMA length enhances the aggregation number, while the total micellar size (R_s) is almost independent of the degree of polymerization of HEMA. In the solvent mixtures, three different morphologies of the polymer, i.e., continuous change from micelle to reversed micelle via unimer with increasing volume fraction of toluene were observed. We have also found that the copolymer forms a quite stable monolayer at air/water interface, which will be described in Chapter 7.

References and Notes

(1) Halperin, A.; Tirrell, M.; Lodge, T. P. *Adv. Polym. Sci.* **1992**, *100*, 31.

(2) Chu, B. *Langmuir* **1995**, *11*, 414.

(3) Tuzar, Z.; Kratochvil, P. *Advances in Colloid and Interface Science*; Elsevier: Amsterdam, 1976.

(4) Zana, R. *Colloid and Surfaces A: Physicochem. Eng. Aspects* **1997**, *123–124*, 27.

(5) Yamaoka, H.; Matsuoka, H.; Sumaru, K.; Hanada, S.; Imai, M.; Wignall, G. D. *Physica B* **1995**, *213&214*, 700.

(6) Nakano, M.; Matsuoka, H.; Yamaoka, H.; Poppe, A.; Richter, D. *Physica B* **1998**, *241–243*, 1038.

(7) Nakano, M.; Matsuoka, H.; Yamaoka, H.; Poppe, A.; Richter, D. *Macromolecules*, in press.

(8) Nakano, M.; Matsumoto, K.; Matsuoka, H.; Yamaoka, H. *Macromolecules*, submitted.

(9) Matsumoto, K.; Deguchi, M.; Nakano, M.; Yamaoka, H. *J. Polym. Sci., Part A: Polym. Chem.* **1998**, *36*, 2699.

(10) Senshu, K.; Yamashita, S.; Ito, M.; Hirao, A.; Nakahama, S. *Langmuir*, **1995**, *11*, 2293.

(11) Guinier, A.; Fournet, G. *Small-Angle Scattering of X-rays*; John Wiley: New York, 1955.

(12) Glatter, O.; Kratky, O. *Small Angle X-ray Scattering*; Academic Press: London, 1982.

(13) Ise, N.; Okubo, T.; Kunugi, S.; Matsuoka, H.; Yamamoto, K.; Ishii, Y. *J. Chem. Phys.* **1984**, *81*, 3294.

(14) Debye, P. *J. Chem. Phys.* **1946**, *14*, 636.

(15) we use the term "reversed micelle" to indicate the aggregate formed in nonpolar solvent, while "micelle" is used when the aggregates are formed in polar solvent.

(16) Porod, G. *Kolloid-Zeitschrift* **1951**, *124*, 83.

(17) Quintana, J. R.; Villacampa, M.; Katime, I. A. *Macromolecules* **1993**, *26*, 601.

Chapter 7

Self-Assembly of Poly(1,1-diethylsilabutane)-*block*-poly(2-hydroxyethyl methacrylate) Block Copolymer.

2.   Monolayer at Air–Water Interface

Abstract

Spread monolayer of the amphiphilic block polymer poly(1,1-diethylsilabutane)-*block*-poly(2-hydroxyethyl methacrylate) (poly(SB-*b*-HEMA)) on the water surface was investigated by X-ray reflectivity (XR) measurements. Clear Kiessig fringes were observed up to the third order in the XR curve, indicating the smooth-faced monolayer with high uniformity of thickness. The thickness of the monolayer increased with increasing surface pressure. Model fitting with the two-layer model revealed that the upper layer is formed by the melt of the SB chains and lower layer consists of hydrated HEMA chains.

7.1. Introduction

Adsorption of polymers at the interface plays a very important role in the stabilization and flocculation of colloidal dispersions.[1] In the case of block copolymers in solution, they adsorb at the surface when insoluble segments favorably interact to the surface, which is quite different in style from homopolymer adsorption.[1,2]

Despite the many reports on the copolymer adsorption to solid–liquid interface,[3,4] and for the lipid monolayers at the air–water interface,[5] block copolymers at the air–water interface have not been studied in detail. This may be due to the complicacy of the polymer conformation and lack of experimental methods to understand it.

Recently, we constructed a compact air–water interface X-ray reflectivity apparatus for laboratory use.[6-8] This can be a powerful method to investigate the nano-structure at the air–water interface, from the point of view that the structure of the monolayer can be analyzed precisely *in situ*.

In Chapter 6, micelle formation of poly(1,1-diethylsilabutane)-*block*-poly(2-hydroxyethyl methacrylate) in selective solvent (methanol and toluene) was described by means of small-angle X-ray scattering,[9] which showed the spherical micelle formation of the copolymer in methanol and the micelle–unimer–reversed micelle transition with increasing toluene content of methanol/toluene mixed solvents. Although the polymer is insoluble in water, it is expected to form a stable monolayer at the air–water interface. Here, we examined the spread monolayer of the copolymer on the water surface by X-ray reflectivity (XR) measurements. This block copolymer forms an uniform-thickness monolayer with a rather smooth surface.

7.2. Experimental Section

7.2.1. Sample.

Poly(1,1-diethylsilabutane)-*block*-poly(2-hydroxyethyl methacrylate) (poly(SB-*b*-HEMA), see Figure 7.1) was synthesized as described in Chapter 5.[10]
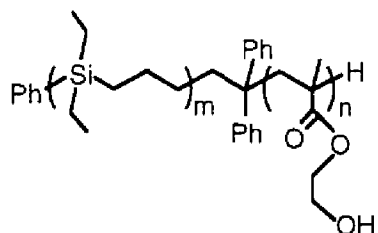
Figure 7.1. Chemical structure of poly(SB-*b*-HEMA) block copolymer.

The number-averaged degrees of polymerization of SB (m) and HEMA (n) of the copolymer were determined by ^{1}H NMR to be 26 and 24, respectively. Polydispersity index M_w/M_n obtained by GPC with $CHCl_3$ as an eluent was 1.20, where M_w and M_n are the weight- and number-averaged molecular weights, respectively. The copolymer was finally given as a white precipitate by dialysis with deionized water, which was filtered out, and lyophilized.

7.2.2. Film Balance Measurement.

Surface pressure (π)–surface area (A) isotherm of a spread monolayer was obtained by an LB trough (length 600 mm × width 150 mm) equipped with a Film Balance Controller FSD–220 (USI System, Fukuoka, Japan). The copolymer was first dissolved in chloroform to make a 1.1 mg/ml solution, and then spread on the water surface by a micro-syringe to prepare a monolayer. The measurement was performed at 29°C. The surface area was compressed by moving a barrier at the rate of 0.1 mm/sec.

7.2.3. X-ray Reflectivity (XR) Measurement.

The XR measurements were performed by a RINT–TTR–MA (Rigaku Corporation, Tokyo, Japan) which was constructed by a modification of the RINT–TTR theta–theta rotating anode X-ray system for reflectivity measurement. The details of the XR apparatus and data treatment have been fully described previously.[7,8] The advantage of this apparatus is that in situ measurement of the monolayer at the air–water interface is possible since the sample stage does not move and is kept horizontal during measurement. In addition, an LB trough (length 80 mm × width 60 mm) made of Teflon® (USI System, Fukuoka, Japan) is mounted on the sample stage, which makes possible the XR measurements of a monolayer while changing the surface pressure as schematically shown in Figure 7.2.

The chloroform solution of the copolymer which was used for π–A measurement was spread on the water surface to prepare a monolayer. The XR profiles were obtained at 29°C at the surface pressures of 25, 35, and 45 mN/m. During XR measurement, the barrier position was automatically controlled to keep the constant surface pressure required.
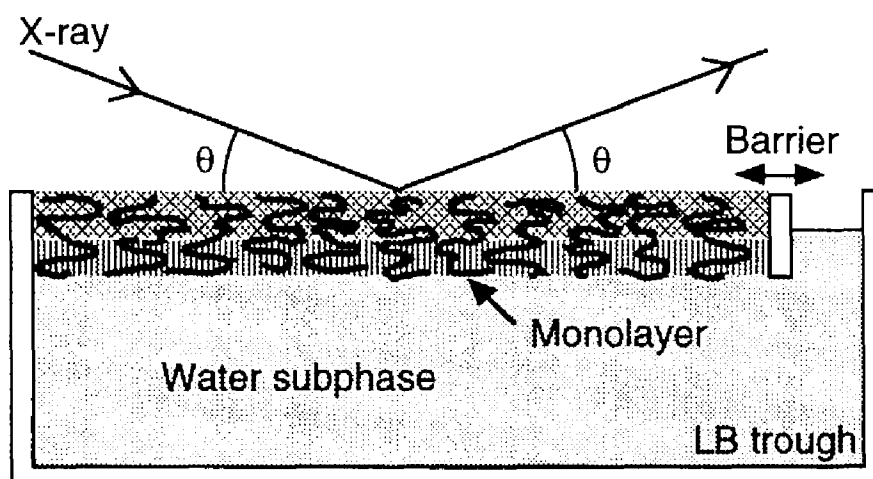

Figure 7.2. Schematic representation of XR measurement of monolayer at air–water interface. LB trough mounted on the sample stage of XR apparatus makes possible the XR measurements of monolayer with a change of the surface pressure.

7.3. Results and Discussion

The copolymers are insoluble in water since even the polar segment of HEMA itself is insoluble in water. On the other hand, copolymers that have water-soluble segments and form micelles in water cannot form a stable monolayer, because the polymer molecules on the surface easily move into solution under thermodynamic equilibrium. An "appropriate" affinity of HEMA to water, which is enough to make the molecules homogeneously spread on the water surface but not enough to be dissolved or form micelles, gives rise to a possibility of the formation of a stable monolayer on a water surface.

π–A isotherm of the monolayer of the copolymer is shown in Figure 7.3. Indeed, the monolayer was stable and was not broken down until the surface pressure reached 42 mN/m. From the isotherm, conformational information of the polymer could be extracted: At low surface pressures (<15 mN/m), a liquid-expanded monolayer is formed. In this low coverage region, both the SB segment and HEMA segment of the copolymer are adsorbed at the interface, and the copolymers form a two-dimensional structure (pancake), consisting of insoluble SB globule and HEMA segments of flattened conformation. At high surface pressures (>25 mN/m), the polymers form a three-dimensional structure (brush), where HEMA chains are stretched and packed inside the water subphase, tethered at the surface by the SB block. Between both pancake and brush regime, quasi-brush regime and transition region from pancake to quasi-brush are considered to exist. At the pancake to quasi-brush transition region (~15 mN/m), HEMA chains start to move into the water subphase because of the overlap of the chains at interface. However, this transition could not be clearly observed compared with the case of poly(styrene)–poly(ethylene oxide) diblock copolymers, which showed a pseudoplateau regime in the π–A isotherms corresponding to the pancake to quasi-brush transition.[11] At quasi-brush regime, surface pressure gradualy increases with compression, where some type of organization of HEMA chains is considered to take place.
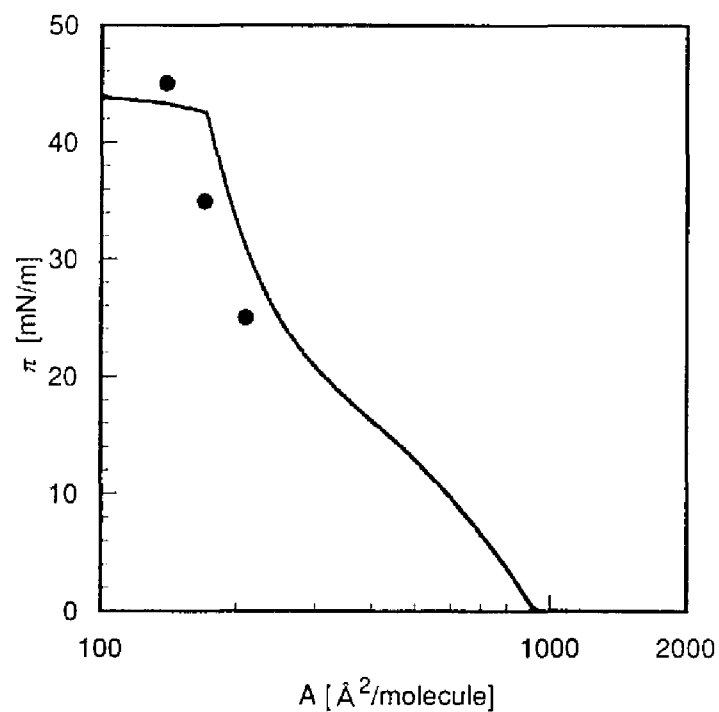
Figure 7.3. Isotherm of surface pressure versus mean molecular area for spread monolayer of the copolymer ($m : n = 26 : 24$). Open circles indicate the conditions where XR measurements were performed.
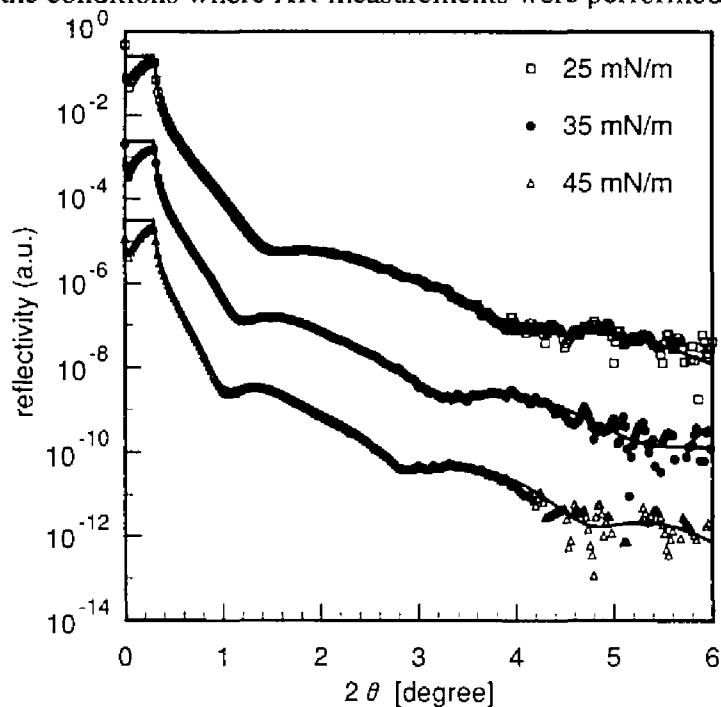
Figure 7.4. XR profiles of spread monolayer of the copolymer ($m : n = 26 : 24$) at different surface pressures. Solid lines are fitting curves with the parameters listed in Table 7.1.

The XR measurements were performed for the copolymer monolayer at the surface pressures of 25, 35, and 45 mN/m, which corresponds to the surface areas per molecule of 210, 170, 140 Å^2, respectively. In this measurement region, the copolymers are considered to have a brush conformation. The XR profiles are shown in Figure 7.4. For clarity, the curves are shifted down by 2 with respect to each other. Clear Kiessig fringes[12] were observed up to third orders, which represents uniform thickness and smooth surface of the monolayer. With increasing surface pressure, these fringes shifted toward smaller angles, indicating the increase of the thickness of the monolayer. XR data give the structural information normal to the surface, i.e., we can obtain the electron density profile of the measured layers by model fitting of XR data. Theoretical function of the reflectivity has been shown elsewhere.[8,13,14] We applied the two-layer model in which the upper layer (1st layer) is composed of SB and the lower layer (2nd layer) consists of hydrated HEMA. The electron density of the 1st layer was fixed to 0.280 Å^{-3} which corresponds to that of SB, and that of the 2nd layer was varied during fitting which must be between 0.396 (HEMA) and 0.334 (H_2O). The thickness of the 1st (d_1) and the 2nd layers (d_2), the surface roughness of air-1st layer (σ_1), 1st layer-2nd layer (σ_{12}) and 2nd layer-water (σ_2) interfaces were adjustable parameters, where roughness is introduced as a standard deviation of Gaussian distribution function to take into account the density smearing at the interface.[14] XR profiles were well fitted as can be seen in Figure 7.4 using the parameters listed in Table 7.1. The electron density profiles at different surface pressures are shown in Figure 7.5. Both d_1 and d_2 increased with the increase of the surface pressure. From a thermodynamic aspect, the surface roughness should be small to reduce the surface free energy. Indeed, the obtained σ_1 and σ_{12} were small enough compared with d_1 and d_2. In addition, the clear interface between two layers suggests the high incompatibility between SB and HEMA. On the other hand, σ_2 was relatively larger than σ_1 or σ_{12}, which may indicate that the interface is diffused by the penetra-

tion of water due to the hydration.

Actually, π–A values of these three conditions did not correspond to π–A isotherm as shown in Figure 7.3, and π = 45 mN/m could not be achieved in the π–A isotherm. It is considered that a kind of "rearrangement" of the polymer took place under the constant surface pressure condition, which reduced the surface area and made the monolayer more stable which did not break down even at 45 mN/m. In the case of lipid monolayer, the surface area is reduced while the surface pressure is kept constant which is known as "creep". The inco-incidence of π–A values could be reflecting viscoelastic character of the monolayer.[5,15,16]

The use of many adjustable parameters during the fitting procedure often causes a serious problem, that is, different values of the parameters reproduce a similar profile. However, we obtained good fitting results because the clear fringes in experimental curves enhance the reliability of the fitting. We used the obtained values for the quantitative evaluation as follows:

In all cases, the product of $A \times d_1$ was 6810 ± 130 [Å^3], which was in agreement with the volume of an SB chain ($m \ v_{SB} = 6680$, where m and v_{SB} denote the volume of repeat unit and the degree of polymerization of SB, respectively) within the experimental error. From this fact, it can be concluded that the 1st layer is formed by the melt of SB chains, and no density change or transition such as crystallization on increasing surface pressure takes place. The liquid-like state of the 1st layer is also confirmed from the fact that d_1 is much smaller than the contour length of SB chain (ca. 130 Å), indicating that SB chains are not highly oriented. Another line of evidence was obtained by differential scanning calorimetry measurement of a poly(SB) homopolymer with the same molecular weight as the SB segment of the block copolymer, which showed that the poly(SB) was in a melted state at room temperature, and had no crystallization point in the temperature range from −100 to 100°C.

Table 7.1. XR Results of Monolayer of the Copolymer ($m : n = 26 : 24$) at Air–Water Interface

π [mN/m]	A [Å²]	d_1 [Å]	d_2 [Å]	σ_1 [Å]	σ_{12} [Å]	σ_2 [Å]
25	210	33	27	3.2	4.1	6.0
35	170	42	35	3.3	4.1	7.5
45	140	47	43	4.0	4.0	8.5
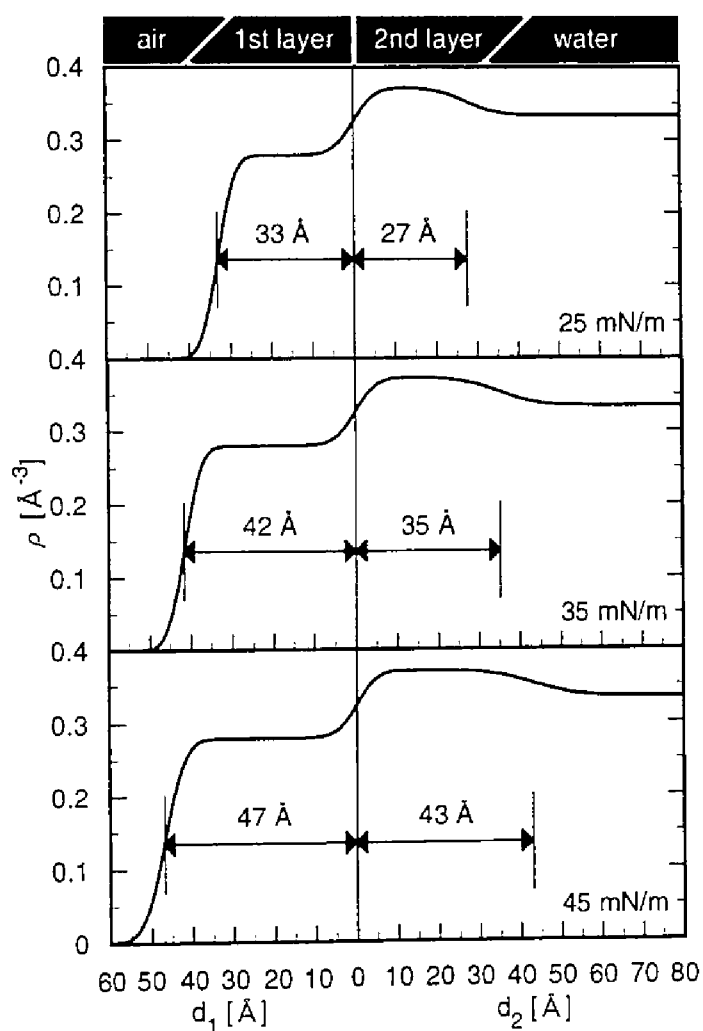
Figure 7.5   The electron density profiles of monolayer at different surface pressures obtained by fitting of XR data.

As for the 2nd layer, $A \times d_2 = 5880 \pm 260$, which was almost independent of surface pressure, was larger than the volume of a HEMA chain ($n\ v_{HEMA} = 4180$, where n and v_{HEMA} denote the volume of repeat unit and the degree of polymerization of HEMA, respectively), from which the volume fraction of water in the 2nd layer was calculated to be $29 \pm 3\%$. From the obtained electron density of the 2nd layer by fitting, the volume fraction of water in the 2nd layer was estimated to be $40 \pm 3\%$. Although there is a small difference in the volume fraction of water calculated by the two methods, the value calculated from the volume could be more reliable since the effect of the length is more sensitive on a theoretical curve than that of the electron density. In the case of micelles formed by the same copolymer in methanol,[9] much higher solvation of HEMA (82% of the volume fraction of solvent) was observed. Thus, it can be concluded that HEMA chains in the monolayer are "appropriately" hydrated.

7.4. Conclusions

The monolayer of poly(SB-*b*-HEMA) amphiphilic block polymer spread on the water surface was investigated by the XR technique. The XR curves showed excellent agreement with theoretical curves obtained by a two-layer model, the upper layer of which is formed by the melt of SB chains and the lower layer of which consists of hydrated HEMA chains. The thickness of the monolayer increased with increasing surface pressure. The product of $A \times d_1$ was constant and in agreement with the volume of an SB chain. The lower layer was estimated to contain 29% of water by comparison of $A \times d_2$ and the volume of the HEMA chain. This novel amphiphilic copolymers are expected to provide valuable information for theoretical approaches[17-21] in the surface chemistry as an example which showed various types of self-assembly systems.

References

(1) Fleer, G. J.; Cohen Stuart, M. A.; Scheutjens, J. M. H. M.; Cosgrove, T.; Vincent, B. *Polymers at Interfaces*; Chapman and Hall: London, 1993.

(2) Buscall, R., Corner, T., Stageman, J. F., Eds. *Polymer Colloids*; Elsevier Applied Science: London, 1985.

(3) Guzonas, D.; Boils, D.; Hair, M. L.; Tripp, C. *Macromolecules* **1992**, *25*, 2434.

(4) d'Oliveira, J. M. R.; Xu, R.; Jensma, T.; Winnik, M. A.; Hruska, Z.; Hurtrez, G.; Riess, G.; Martinho, J. M. G.; Croucher, M. D. *Langmuir* **1993**, *9*, 1092.

(5) Shah, D. O., Ed. *Micelles, Microemulsions, and Monolayers: Science and Technology*; Marcel Dekker: New York, 1998.

(6) Matsuoka, H.; Yamaoka, H. *Proceedings of Risø International Symposium on Material Science* **1997**, *18*, 437.

(7) Yamaoka, H.; Matsuoka, H.; Kago, K.; Endo, H.; Eckelt, J. *Physica B* **1998**, *248*, 280.

(8) Kago, K.; Matsuoka, H.; Endo, H.; Eckelt, J.; Yamaoka, H. *Supramolecular Sci.* in press.

(9) Nakano, M.; Deguchi, M.; Matsumoto, K.; Matsuoka, H.; Yamaoka, H. *Macromolecules*, submitted.

(10) Matsumoto, K.; Deguchi, M.; Nakano, M.; Yamaoka, H. *J. Polym. Sci., Part A: Polym. Chem.* **1998**, *36*, 2699.

(11) Gonçalves da Silva, A. M.; Filipe, E. J. M.; d'Oliveila, J. M. R.; Martinho, J. M. G. *Langmuir*, **1996**, *12*, 6547.

(12) Kiessig, H. *Ann. Phys.* **1931**, *10*, 769.

(13) Parrat, L. G. *Phys. Rev.*, **1954**, *95*, 359.

(14) Sinha, S. K.; Sirota, E. B.; Garoff, S.; Stanley, H. B. *Phys. Rev. B* **1988**, *38*, 2297.

(15) Kato, T. *Langmuir* **1990**, *6*, 870.

(16) Kato, T.; Hirobe, Y.; Kato, M. *Langmuir* **1991**, *7*, 2208.

(17) Alexander, S. *J. Phys. (Paris)* **1977**, *38*, 977.

(18) de Gennes, P. G. *Macromolecules* **1980**, *13*, 1069.

(19) Halperin, A.; Tirrell, M.; Lodge, T. P. *Adv. Polym. Sci.* **1992**, *100*, 31.

(20) Munch, M. R.; Gast, A. P. *Macromolecules* **1988**, *21*, 1360.

(21) Munch, M. R.; Gast, A. P. *Macromolecules* **1988**, *21*, 1366.

List of Publications

Parts of the present thesis have been or are to be published in the following journals.

Chapter 2.

Nakano, M.; Matsuoka, H.; Yamaoka, H.; Poppe, A.; Richter, D. *Physica B* **1998**, *241–243*, 1038–1040.

Chapter 3.

Nakano, M.; Matsuoka, H.; Yamaoka, H.; Poppe, A.; Richter, D. *Macromolecules*, in press.

Chapter 4.

Nakano, M.; Matsumoto, K.; Matsuoka, H.; Yamaoka, H. *Macromolecules*, submitted.

Chapter 5.

Matsumoto, K.; Deguchi, M.; Nakano, M.; Yamaoka, H. *Journal of Polymer Science: Part A: Polymer Chemistry* **1998**, *36*, 2699–2706.

Chapter 6.

Nakano, M.; Deguchi, M.; Matsumoto, K.; Matsuoka, H.; Yamaoka, H. *Macromolecules*, submitted.

Chapter 7.

Nakano, M.; Deguchi, M.; Endo, H.; Matsumoto, K.; Matsuoka, H.; Yamaoka, H. *Macromolecules*, submitted.

Acknowledgments

November 1998

Minoru Nakano